

Are Type Ia Supernovae in Restframe H Brighter in More Massive Galaxies?

KARA A. PONDER,^{1,2,3} W. MICHAEL WOOD-VASEY,¹ ANJA WEYANT,¹ NATHAN T. BARTON,^{1,4} LLUÍS GALBANY,^{1,5}
 PETER GARNAVICH,⁶ AND THOMAS MATHESON⁷

¹PITT PACC, Department of Physics and Astronomy, University of Pittsburgh, Pittsburgh, PA 15260, USA

²Berkeley Center for Cosmological Physics, University of California Berkeley, 341 Campbell Hall, Berkeley, CA 94720, USA

³Physics Division, Lawrence Berkeley National Laboratory, 1 Cyclotron Road, Berkeley, CA, 94720, USA

⁴Department of Mechanical and Civil Engineering, California Institute of Technology, Pasadena, CA 91126, USA

⁵Departamento de Física Teórica y del Cosmos, Universidad de Granada, E-18071 Granada, Spain

⁶Physics Department, University of Notre Dame, Notre Dame, IN, 46556, USA

⁷NSF's National Optical-Infrared Astronomy Research Laboratory, 950 North Cherry Avenue, Tucson, AZ 85719, USA

ABSTRACT

We analyze 99 Type Ia supernovae (SNeIa) observed in H band ($1.6\text{--}1.8 \mu\text{m}$) and find that SNeIa are intrinsically brighter in H -band with increasing host galaxy stellar mass. We find that SNeIa in galaxies more massive than $10^{10.44} M_{\odot}$ are brighter in H than SNeIa in less massive galaxies by 0.18 ± 0.05 mag. The same set of SNeIa observed at optical wavelengths, after width-color-luminosity corrections, exhibit a 0.17 ± 0.05 mag offset in the Hubble residuals. Removing two significant outliers reduces the step in H band to 0.10 ± 0.04 mag but has no effect on the optical mass step size. An analysis based on information criteria supports a step function with a break at $10^{10.44} M_{\odot}$ over a constant model with and without outliers for NIR and optical residuals. Less massive galaxies preferentially host more higher-stretch SNeIa, which are intrinsically brighter and bluer. It is only after correction for width-luminosity and color-luminosity relationships that SNeIa have brighter optical Hubble residuals in more massive galaxies. Thus the finding that SNeIa are intrinsically brighter in H in more massive galaxies is a significant and opposite correlation as the intrinsic optical brightness. If dust and the treatment of intrinsic color variation were the main driver of the host galaxy mass correlation, we would not expect a correlation of brighter H -band SNeIa in more massive galaxies. The correlation we find thus suggests that dust is not the main explanation of the observed correlation between Hubble residual and host galaxy stellar mass.

Keywords: supernova: general, cosmology: dark energy

1. INTRODUCTION

Since the late 1990s, Type Ia supernovae (SNeIa) have been used as standard candles to measure the accelerating expansion of the Universe (Riess et al. 1998; Perlmutter et al. 1999). Much work has gone into further standardizing inferred optical brightness of SNeIa by including corrections based on the stretch (Phillips 1993) and color (Riess et al. 1996; Tripp 1998) of the lightcurve. More recent work has started including an additional correction term associated with the stellar mass¹ of the host galaxy of the SNeIa (Betoule et al. 2014; Scolnic et al. 2018; Brout et al. 2019; Smith et al. 2020).

Lightcurves observed at near infrared (NIR) wavelengths ($1 \mu\text{m} < \lambda < 2.5 \mu\text{m}$) are more standard and require no or smaller corrections to their lightcurves to yield the same precision as optical lightcurves (Kasen 2006; Wood-Vasey et al. 2008; Folatelli et al. 2010; Kattner et al. 2012; Barone-Nugent et al. 2012; Dhawan et al. 2018; Burns et al. 2018). We here compile one of the largest publicly available NIR SN Ia data sets to further test the standard nature of SNeIa. We explore different possible correlations between global host galaxy properties and H -band luminosity.

Corresponding author: Kara Ponder
 kap146@pitt.edu; kponder@berkeley.edu

¹ Throughout this paper the term “mass” will always refer to the stellar mass of the galaxy.

The past decade has seen an extensive history of looking for correlations between the standardized optical luminosity of SNeIa and the properties of their host galaxies. Many papers have studied relationships with global host galaxy properties such as stellar mass, metallicity, star formation rates, and age using galaxy photometry and stellar population synthesis codes (Sullivan et al. 2006; Gallagher et al. 2008; Kelly et al. 2010; Sullivan et al. 2010; Lampeitl et al. 2010; Gupta et al. 2011; D’Andrea et al. 2011; Hayden et al. 2013; Johansson et al. 2013; Childress et al. 2013a,b; Moreno-Raya et al. 2016; Campbell et al. 2016; Roman et al. 2018; Jones et al. 2018; Rose et al. 2019). These papers have found several correlations between standardized brightness and host galaxy properties with the most significant one being host galaxy stellar mass. Some interpret this as a result of a correlation between galaxy stellar mass and things more physically related to the SN Ia explosion, such as progenitor metallicity, progenitor age, or dust (Kelly et al. 2010; Hayden et al. 2013; Childress et al. 2013b; Brout & Scolnic 2020). These analyses show that the standardized brightness of SNeIa hosted in higher-mass galaxies is brighter by ~ 0.08 mag (Childress et al. 2013b) than SNeIa hosted in galaxies with stellar mass less than $10^{10} M_{\odot}$. The mass “step” was also implemented in one of the recent studies to produce cosmological constraints: the Joint Lightcurve Analysis (JLA; Betoule et al. 2014), where they independently measured a correlation with host galaxy stellar mass and implemented a step function to account for it. Others have focused on local properties of host galaxies such as recent star formation rates within 1–5 kpc of the supernova position using spectroscopy or ultraviolet (UV) photometry (Rigault et al. 2013, 2015, 2018; Kelly et al. 2015; Uddin et al. 2017). These local property studies find that the standardized brightness of SNeIa in locally passive regions is ~ 0.094 mag (Rigault et al. 2015) brighter than those in locally star forming regions. Furthermore, Kelly et al. (2015) showed that SNeIa in locally star forming regions were more standard than those in non-star forming ones.

However, not every analysis suggests that there is a correlation with host galaxy properties. Kim et al. (2014) used an updated lightcurve analysis that is more flexible to intrinsic variations in SNeIa (introduced in Kim et al. 2013) and found any potential correlations with host galaxy stellar mass, specific star formation rates, and metallicity to be consistent with zero. Jones et al. (2015) found no evidence of a correlation between host galaxy local star formation rates derived from UV photometry by using a larger sample size than previous studies and using different selection criteria. Scolnic et al. (2014) described the systematics utilized in the Pan-STARRS SN Ia cosmology analysis (Rest et al. 2014) and found a correlation with host galaxy stellar mass with a step size of 0.037 ± 0.032 mag, which is consistent with 0 and is 2σ inconsistent with the previously reported sizes in the literature of ~ 0.1 mag. With twice as many SNeIa, the subsequent Pan-STARRS analysis (Scolnic et al. 2018) recovered a very similar small step size of 0.039 ± 0.016 mag, but now with a clear deviation from 0. Scolnic et al. (2018) noted that if they didn’t apply the BEAMS with Bias Correction (BBC Kessler & Scolnic 2017) method in their analysis they would have found a mass step of 0.064 ± 0.018 mag. The Dark Energy Survey (DES; Dark Energy Survey Collaboration et al. 2016; Abbott et al. 2019; Brout et al. 2019) originally found no evidence of a host galaxy stellar mass step for 329 SNeIa with 207 observed in the first three years of DES and the rest from low-redshift samples. However, Smith et al. (2020) showed that the DES data do exhibit a mass step if a JLA-like analysis is run, which strongly suggests that such a mass step was being corrected for by the BBC method used in the DES SN cosmology papers to date.

We see much evidence to warrant continued exploration of this parameter space to understand whether we are searching for a real correlation or if we need to improve the analysis of SNeIa lightcurves.

The majority of the previous analyses of host galaxy properties versus SN Ia corrected brightness have examined correlations using only optical lightcurves. Doing a similar analysis using NIR lightcurves will help shed light on physical mechanisms and color-dependent intrinsic dispersions. In the restframe NIR there have been far fewer studies of host galaxy correlations. Dhawan et al. (2018) looked at the J -band and, with a small sample of 30 SNeIa, found low dispersion (~ 0.10 mag) and no obvious trend with host galaxy morphology. A more in-depth study was done by Burns et al. (2018), which compared H -band brightnesses to host galaxy stellar mass estimates from K -band photometry following the mass-to-light ratio method of McGaugh & Schombert (2014). Burns et al. (2018) found a small ($\sim 1\sigma$) linear correlation between the restframe H -band and host galaxy stellar mass for their sample of ~ 115 SNeIa with host galaxy photometry. We here analyze a data set with significantly more SN Ia in low-mass host galaxies, $M < 10^{10} M_{\odot}$, the canonical break point for the mass step.

SNeIa in the H -band have been shown to be standard to 0.15–0.2 mag without lightcurve corrections (Wood-Vasey et al. 2008; Folatelli et al. 2010; Barone-Nugent et al. 2012; Kattner et al. 2012; Weyant et al. 2014; Stanishev et al. 2018; Avelino et al. 2019) whereas optical lightcurves before brightness standardization have significantly larger scatter of ~ 0.8 mag (Hamuy et al. 1995). However, there are only ~ 231 NIR lightcurves publicly available compared to the over $> 1,000$ available for optically observed SNeIa.

The improved ability to determine standard distances, together with the reduced sensitivity to dust extinction, have motivated several recent projects to pursue larger samples of SNeIa observed in the restframe NIR: CSP-I, II (Contreras et al. 2010; Stritzinger et al. 2011; Kattner et al. 2012; Krisciunas et al. 2017; Phillips et al. 2019); CfA (Wood-Vasey et al. 2008; Friedman et al. 2015); RAISINS (Kirshner 2012); SweetSpot (Weyant et al. 2014, 2018); and SIRAH (Jha et al. 2019).

To gather host galaxy properties, we used publicly available galaxy catalogs from Sloan Digital Sky Survey (SDSS), Galaxy Evolution Explorer (GALEX), and Two Micron All-Sky Survey (2MASS). We used `kcorrect` (Blanton & Roweis 2007) to estimate estimate galaxy properties including the stellar mass of the host galaxies.

We use SNooPy (Burns et al. 2011, 2014) for lightcurve fits as it is has the most developed treatment of NIR templates. We combine optical and NIR lightcurves to improve fits with the s_{BV} parameter from Burns et al. (2014). Using optical lightcurves only, we expand on the work of Burns et al. (2018) by also testing for a mass step using optical lightcurves only on this larger sample of SNeIa. Most previous analyses have explored host galaxy correlations with standardized brightnesses calculated from SALT2 (Guy et al. 2007) and/or MLCS2k2 (Jha et al. 2007) fitters (e.g., Kelly et al. 2010).

This paper is organized as follows: Section 2 explains the supernova sample we use and how we collected optical, UV, and NIR photometry of the host galaxies. Section 3 details how we fit lightcurves and created the restframe H -band and optical Hubble diagrams. Section 4 examines the host galaxy stellar mass correlation and shows that the H -band Hubble residuals and the optical width-luminosity corrected Hubble residuals are both more negative in higher-mass galaxies. Section 5 explores the statistical significance of these correlations. We find sufficient evidence for a correlation in both NIR residuals and optical residuals with host galaxy stellar mass at 3σ . We present our conclusions and recommendations for future work in Section 6.

2. SN Ia AND HOST GALAXY SAMPLE

2.1. SNeIa

We start with the compilation of literature SNeIa gathered in Weyant et al. (2014). We assigned each SN Ia to “belong” to a given survey to be able to examine properties as a function of survey. If an SN Ia was found in multiple surveys, we labeled that object with the survey name containing the most lightcurve points in H ; however, lightcurve points from all surveys were included when running the lightcurve fits. We used the following survey codes: K+, CSP, BN12, F15, W18.

- K+ is the miscellaneous early sample (Jha et al. 1999; Hernandez et al. 2000; Krisciunas et al. 2000, 2003, 2004a,b, 2007; Valentini et al. 2003; Phillips et al. 2006; Pastorello et al. 2007a,b; Stanishev et al. 2007; Pignata et al. 2008) and named for extensive early work by Kevin Krisciunas. In the full sample, we counted objects that are highly-reddened such as SN 2002cv (Elias-Rosa et al. 2008) and SN 2003cg (Elias-Rosa et al. 2006) but that will not have a lightcurve fit due to the reddening. For completeness, we added other supernovae that are peculiar (Cuadra et al. 2002; Candia et al. 2003; Sollerman et al. 2004; Krisciunas et al. 2004c, 2009; Leloudas et al. 2009; Stritzinger et al. 2014, 2015; Yamanaka et al. 2016; Magee et al. 2016) to the full sample that also will not be included in our lightcurve fits.
- CSP refers to the lightcurves released from Contreras et al. (2010, C10) and Stritzinger et al. (2011, S11). There were NIR observations of 71 SNeIa in the C10+S11 samples. One of these, SN 2004eo, is placed in the K+ sample and 11 are placed in the CfA sample.
- BN12 covers the SNeIa from Barone-Nugent et al. (2012).
- We renamed the CfA sample from WV08 (Wood-Vasey et al. 2008) to F15 due to the 74 additional SNeIa from the final data release (Friedman et al. 2015). We do not use any of the peculiar Iax supernovae (Foley et al. 2013) from Friedman et al. (2015). 5 of the F15 SNeIa overlap with and are placed in the CSP sample and 1 object is placed in the BN12 sample.
- The SweetSpot W14 sample is replaced by W18 due to the addition of 34² SNeIa from SweetSpot’s first data release (Weyant et al. 2018).

² Though Weyant et al. (2018) states that 33 lightcurves were released, 34 lightcurves were actually provided for download.

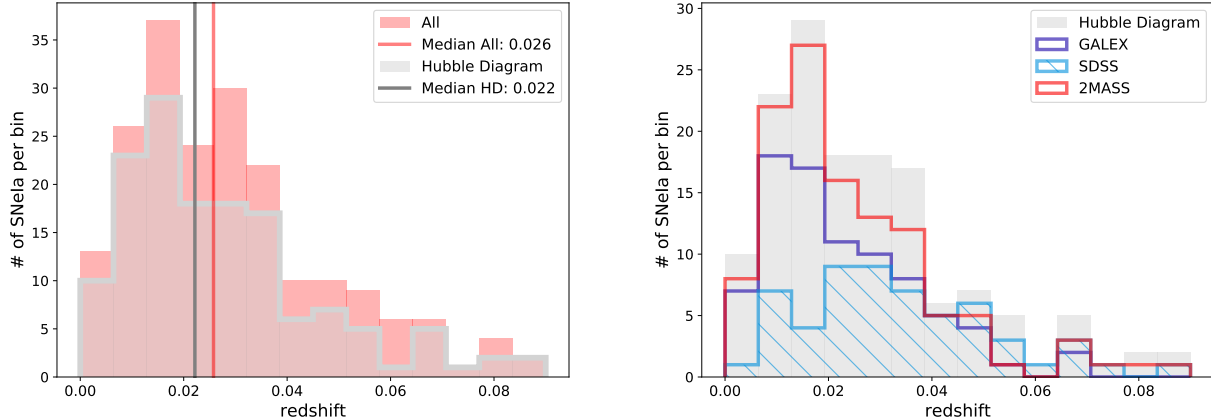


Figure 1. *Left:* Redshift distribution of the publicly available NIR sample of 231 SNeIa and the Hubble Diagram sample of 144 SNeIa. *Right:* Redshift distribution of galaxy with data from GALEX, SDSS, and 2MASS for the final sample of 144 SNeIa used in the Hubble residual analysis.

Our full sample of SNeIa *H*-band lightcurves consists of 231 SNeIa. Table 1 gives the breakdown per survey. We used the Open Supernova Catalog³ (OSC; Guillochon et al. 2017) to retrieve all lightcurve data.

Out of 231 SNeIa, 185 SNeIa could be successfully fit by SNoPy (see Section 3). In order to be included on the Hubble diagram, a supernova was required to have at least 3 observations with a signal-to-noise greater than 3, have a fit with a chi-square per degree of freedom less than 3, and not be a known peculiar supernova such as 91bg- or 02cx-like. These cuts removed 41 SNeIa nominally successful SNoPy fits. Table 1 shows how many SNeIa have fit lightcurves (“NIR LC”) and how many pass the quality cuts (“Hubble LC”). Figure 1 shows the redshift distribution of the full sample compared to the distribution of the Hubble diagram sample used for the analysis below. The full sample has a median redshift of 0.026 while the Hubble diagram sample has a slightly lower median redshift of 0.022.

Of the 144 SNeIa in the *H*-band Hubble diagram analysis, 99 have sufficient host galaxy photometry to derive stellar masses (see Section 2.2). Table 1 details how many SNeIa each sample have a successful SNoPy lightcurve fit, pass the quality cuts, and have sufficient information to calculate a host stellar mass (“Hubble LC + Host Mass”). 104 of the 144 SNeIa with NIR lightcurves used for the Hubble residual analysis also have usable optical lightcurves. 71 of those optical lightcurves were for SNeIa with enough host galaxy information to determine a stellar mass.

2.2. Host Galaxies

The host galaxy for all 231 SNeIa was identified from the IAU list of supernovae⁴ and the NASA Extragalactic Database (NED)⁵. We used the heliocentric redshift for each galaxy recorded in NED. If NED did not have a spectroscopic redshift, we recorded the redshift from the hosted supernova from the classification spectrum.

We obtained optical photometry from the SDSS Data Release 13 (SDSS Collaboration et al. 2016) via the CasJobs⁶ website. We used the *ugriz* “modelMag” magnitudes, which are based on the best fit “de Vaucouleurs” or “Exponential” profile in the *r*-band. Though “cmodelMag” magnitudes give a more accurate description of the total flux in each filter, “modelMag” magnitudes are better for color studies because the flux is measured consistently across all filters (Stoughton et al. 2002). We applied the SDSS “clean photometry requirements” that all objects are from the Primary table, are not marked as having deblending issues, cosmic rays, or other interpolation problems. 17 host galaxies had photometry that we did not include because they did not meet these “clean photometry requirements” quality cuts.

We obtained GALEX GR6/GR7⁷ (Bianchi et al. 2014) far ultraviolet (FUV/*F*) and near ultraviolet (NUV/*N*) information where available from the MAST data archive.⁸ We used the photometry that is the result of the elliptical

³ <https://sne.space/>

⁴ <http://www.cbat.eps.harvard.edu/lists/Supernovae.html>

⁵ <http://ned.ipac.caltech.edu/>

⁶ <http://skyserver.sdss.org/CasJobs/>

⁷ <http://galex.stsci.edu/GR6/>

⁸ <https://galex.stsci.edu/casjobs>

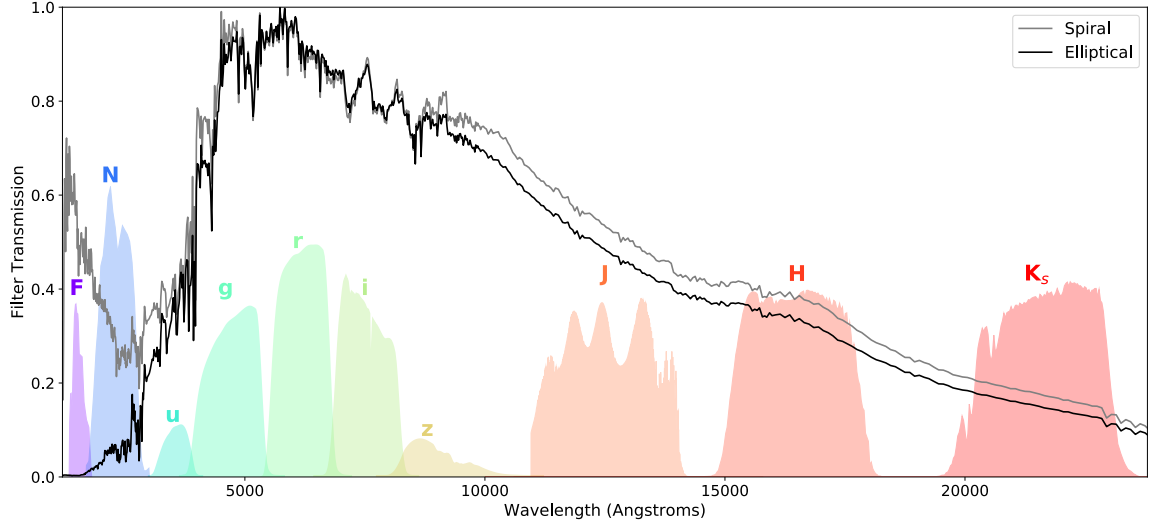


Figure 2. System transmission functions for GALEX (F, N), SDSS ($ugriz$), and 2MASS (JHK_s). These transmission functions accounts for the detector, optics, filter, and atmosphere. Over-plotted is the normalized spectral energy distribution (SED) for a Sc spiral galaxy in grey and an elliptical galaxy in black from the SWIRE Template Library (Polletta et al. 2007). For both spiral and elliptical galaxies, the majority of their flux is emitted at restframe optical wavelengths peaking in SDSS gri bands. The Sc spiral galaxies have a small bulge and obvious spiral arms containing young stars emitting heavily in the UV. Though having optical photometry observes most of the flux, observing UV and NIR can help constrain the spectrum.

aperture method “MAG_AUTO” in Source Extractor (Bertin & Arnouts 1996). GALEX often reported detections in only one of FUV or NUV magnitudes, but we only required one of these to mark an object as having UV data.

We also gathered JHK_s magnitudes from the 2MASS All-Sky Extended Source Catalog (XSC; Skrutskie et al. 2006) using the NASA/IPAC Infrared Science Archive (IRSA).⁹ We used the total magnitude calculated from the extrapolated radial surface brightness profile. One object (PGC 1361264, host of SN 2010ho) had an H -band uncertainty of zero and a magnitude significantly inconsistent with its JK_s magnitudes, so that H -band photometric point was not used to determine the mass of PGC 1361264.

We use `kcorrect` (Blanton et al. 2003; Blanton & Roweis 2007) to transform the photometry to the restframe and infer physical parameters¹⁰ such as stellar mass. `kcorrect` fits galaxy spectral energy distributions from the UV to NIR and relies on Bruzual & Charlot (2003) stellar evolution synthesis models using the Chabrier (2003) stellar initial mass function (IMF). The physical parameters that `kcorrect` reports are based on those of the galaxy templates from these models. Adding the UV and NIR photometry to the SDSS optical photometry gives sharper constraints on dust absorption and thus help distinguish the different galaxy models that overlap at optical wavelengths. Figure 2 shows an example where a spiral and elliptical galaxy larger agree in optical wavelengths, but are clearly distinguished with the addition of UV and NIR measurements. All magnitudes are converted to the AB magnitude system and are extinction corrected for Milky Way dust before being input into `kcorrect`. We derive K -corrections and host galaxy stellar mass by combining optical photometry plus GALEX and 2MASS for each host galaxy, with the requirement that there been photometric measurements for at least four filters in the set of $FNugrizJHK_s$. This requirement means that we restrict our sample to having more observations than only 2MASS but having three 2MASS observations and one GALEX observation would be acceptable. We remove 32 galaxies that are only observed by 2MASS and 1 galaxy that was only observed by GALEX. Table 2 lists how many SNe Ia host galaxies have photometry for each of the surveys that are in our analysis.

Figure 2 illustrates the wavelength coverage from these surveys. 131 SNeIa of the subset of 144 lightcurves have host galaxy photometry available in at least one of these catalogs but only 99 galaxies meet our requirement for a robust host galaxy stellar mass measurement. Even if we were able to obtain sufficient lightcurve data to have reliable lightcurve fits for the full sample of 231 SNeIa, we would only have 130 host galaxy masses to test any Hubble residual

⁹ <http://irsa.ipac.caltech.edu/frontpage/>

¹⁰ `kcorrect` does not return uncertainties on the physical parameters.

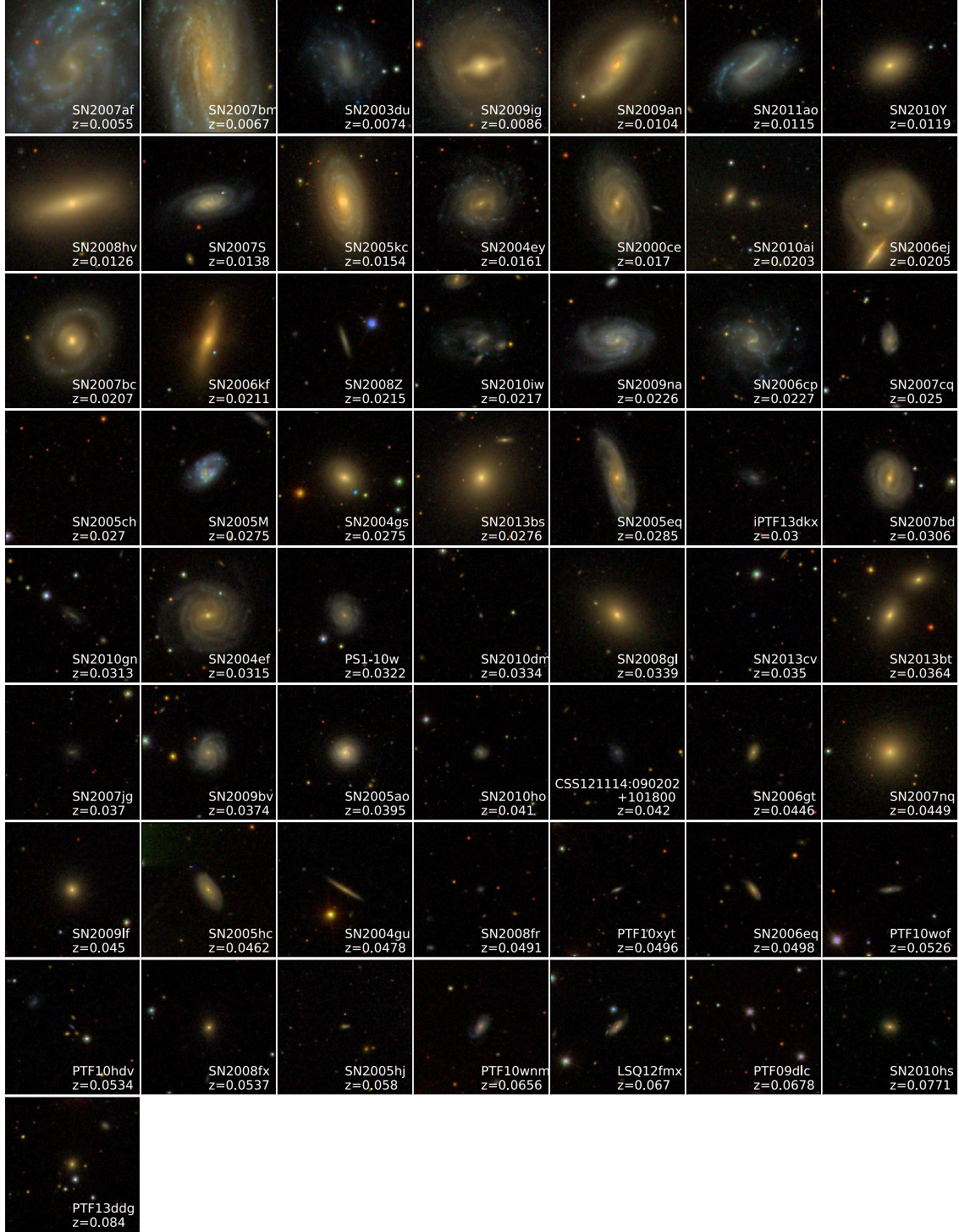


Figure 3. SDSS color postage stamps ordered by redshift. $\sim 2'$ by $2'$. North is up and East is left. The stamps are centered on the host galaxy and not the supernova. The name and redshift of the hosted supernova is in the bottom right corner of each stamp.

vs. host galaxy stellar mass correlation. Figure 3 shows color postage stamps for galaxies used from SDSS. The redshift distribution of our final sample per survey is presented in Figure 1. We summarize the photometric data in Table 3 for all 231 SNeIa.

2.2.1. Active SNeIa in Host Galaxy Observations

If any of the surveys observed a host galaxy when the respective SN Ia was active, the SN Ia could contaminate the measured flux. We cross matched the years that SDSS, GALEX, and 2MASS were observed with the time of maximum light of our supernovae and examined the respective galaxy images if there was an overlap in time. We only looked for SN Ia flux contamination from the SNeIa used in the Hubble residual analysis.

SDSS observed from 1999–2009, but no SDSS observations occurred while the respective SN Ia was active. The closest possible supernova was SN 2008gl. SN 2008gl was discovered on UT 2008-10-20 (Pignata et al. 2008) and SDSS observed its host galaxy UGC 881 on UT 2008-10-03. Friedman et al. (2015) reports a $T_{B_{\max}}$ at UT 2008-10-29, so the SDSS observation was taken a few days before the SN Ia exploded. We examined the galaxy in all *ugriz* filters and found no obvious point source to indicate additional flux at the SN Ia location.

GALEX started observations in 2003 and continued FUV observations through 2009 and NUV through 2012. Three supernovae were observed within 4 weeks of the time of maximum B-band light: SN 2006eq, SN 2007af, SN 2010kg. All other GALEX observations were at least 6 weeks before or after $T_{B_{\max}}$. The host galaxy for SN 2010kg, NGC 1633, was observed in the NUV by GALEX on UT 2010-12-27 while the supernova had $T_{B_{\max}}$ around UT 2010-12-14 (Friedman et al. 2015). NGC 1633 was also observed in 2005 and comparing these two observations showed significant UV emission from the galaxy in each image, but no obvious point source in the image from 2010. SDSS J12837.60+011348.6, host of SN 2006eq, was observed 16 days after $T_{B_{\max}}$ and NGC 5584, host of SN 2007af, was observed 24 days after $T_{B_{\max}}$. We see no additional flux from the SNeIa in these images. SN Ia are intrinsically faint in the UV. The SN UV emission could potentially be detectable if observed at the time of shock breakout, but is otherwise negligible for a star-forming galaxy such as NGC 1633.

2MASS operated between 1997 and 2001, which overlapped with very few of our SNeIa observations. Only 7 objects were observed at the same time and all events except one had at least a one year separation between $T_{B_{\max}}$ and the 2MASS observation. The one object observed in the same year was observed with 2MASS 4 months before $T_{B_{\max}}$ and was not at risk for contamination.

2.2.2. Comparing Masses Derived using Different Surveys

Figure 4 compares `kcorrect`-derived properties from just optical photometry from SDSS versus SDSS+UV, SDSS+NIR, or SDSS+UV+NIR for the 44 galaxies that had GALEX, SDSS, and 2MASS photometry. The high-mass galaxies agree with the optical-only measurements, because they have less dust and star formation and so the mass-age degeneracy that is broken by adding UV and/or NIR information is less relevant. At masses $< 10^{10} M_{\odot}$, there are differences between the SDSS-only and SDSS+ results with additional discrepancies between SDSS+UV versus SDSS+NIR in the derived mass. Adding UV and NIR wavelength coverage improves estimates of low mass galaxies.

There are 48 galaxies that have GALEX and 2MASS observations but are missing the optical data points. To check the robustness of `kcorrect` without the optical data points, we used the 44 galaxies that had photometry in all three surveys to examine the effect of missing optical data. There is larger scatter in these derived masses especially at the low mass end.

Figure 5 shows the histograms of the different mass calculations compared to the SDSS-only measurement. Of our Hubble diagram sample, 49 galaxies have SDSS plus additional photometry, 8 have only SDSS data, and 42 have GALEX+2MASS photometry. Masses derived using GALEX+SDSS, SDSS+2MASS, and GALEX+SDSS+2MASS have a median offset of 0.05 dex and a standard deviation of 0.05 dex. This bias and scatter would spread out the best location of a step function break but is much smaller than typical uncertainties on mass estimates (~ 0.5 dex). The scatter is still only 0.19 dex, while the overall range of galaxy stellar masses we are considering is $8.5\text{--}11.5 M_{\odot}$.

The masses from the GALEX+2MASS photometry show a much larger spread than if optical data was included. The median offset is 0.06 dex and the standard deviation is 0.17 dex. In Figure 5 the one large (difference > 0.5 dex) outlier corresponds to UGC 272 (SN 2005hk), which is a large blue spiral at redshift 0.013. If we examine the masses calculated from any combination of GALEX and 2MASS (possibly missing *F*, *N*, or *H*), there are 66 galaxies to compare. The median offset is 0.05 dex and the standard deviation is 0.19 dex and there is an additional 1 dex outlier of UGC 4570 (SN 2010iw) at $z=0.021$. Though this large spread is concerning, the major outliers are limited to the low masses and including optical data would not move the objects from the low mass to the high mass sample (if the high mass sample is defined as $> 10^{10} M_{\odot}$).

2.2.3. Bias in Calculated Host Galaxy Mass

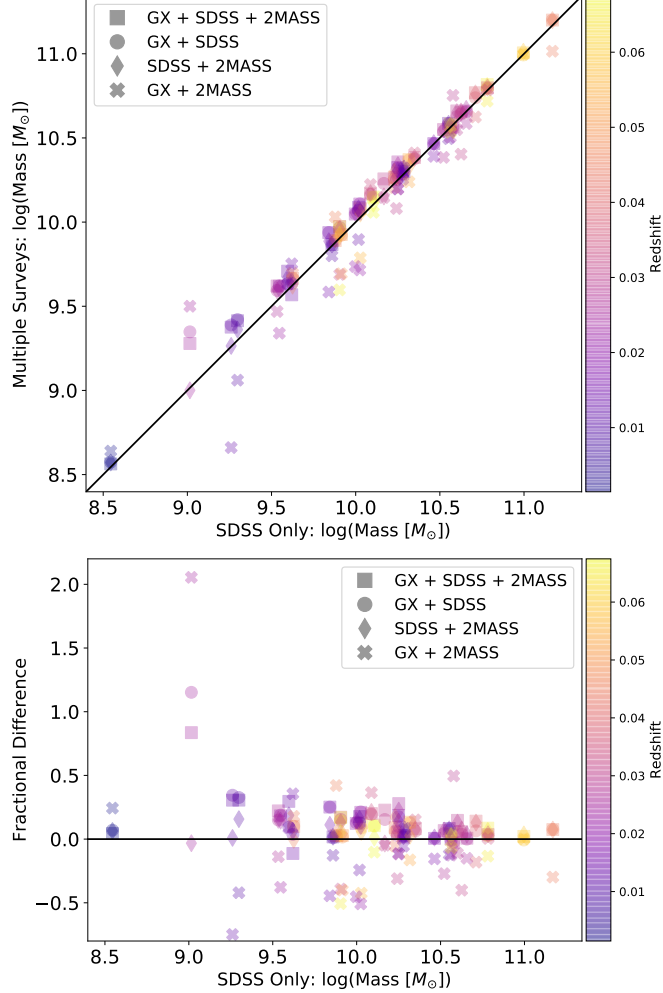


Figure 4. Comparison of the derived mass from `kcorrect` when only optical SDSS data is used versus GALEX+SDSS+2MASS (squares), GALEX+SDSS (circles), SDSS+2MASS (diamonds), and GALEX+2MASS (x). These points are for the 44 galaxies that had photometry from all three sources. *Top:* One-to-one mass comparisons. *Bottom:* Fractional difference between the SDSS-only derived masses and the masses derived from other or additional sources. The color map indicates the redshift of the host galaxy. Most high mass galaxies are in agreement with the optical only measurements; however, low mass galaxies show more variation.

Twelve of our SNeIa with SDSS photometry overlapped with those used in the Kelly et al. (2010) analysis. Kelly et al. (2010) fit *ugriz* photometry to different spectral energy distributions from PEGASE2 (Fioc & Rocca-Volmerange 1997, 1999) stellar population synthesis models using LePhare (Arnouts et al. 1999; Ilbert et al. 2006) using the IMF from Rana & Basu (1992). We found that our host galaxy masses using SDSS-only photometry are consistently lower than those reported in Kelly et al. (2010) by a median value of 0.38 dex. However, with the large uncertainties on host mass, we are consistent within 1–3 σ .

The `kcorrect` approach derives lower masses because it calculates the current mass of the stars in a galaxy instead of the mass from integrating the total star formation rate over time which includes stars that died before we observed the galaxy. To explore the bias in our data, we compared our `kcorrect`-derived masses to the photometric mass estimates from the MPA/JHU¹¹ originally presented in Kauffmann et al. (2003) for SDSS DR4 (Adelman-McCarthy et al. 2006) and updated for SDSS DR7 (Abazajian et al. 2009). The original Kauffmann et al. (2003) analysis used the Kroupa (2001) IMF, but the updated version used the Chabrier (2003) IMF which matches the IMF used in `kcorrect`. Kelly

¹¹ <http://home.strw.leidenuniv.nl/~jarle/SDSS/>

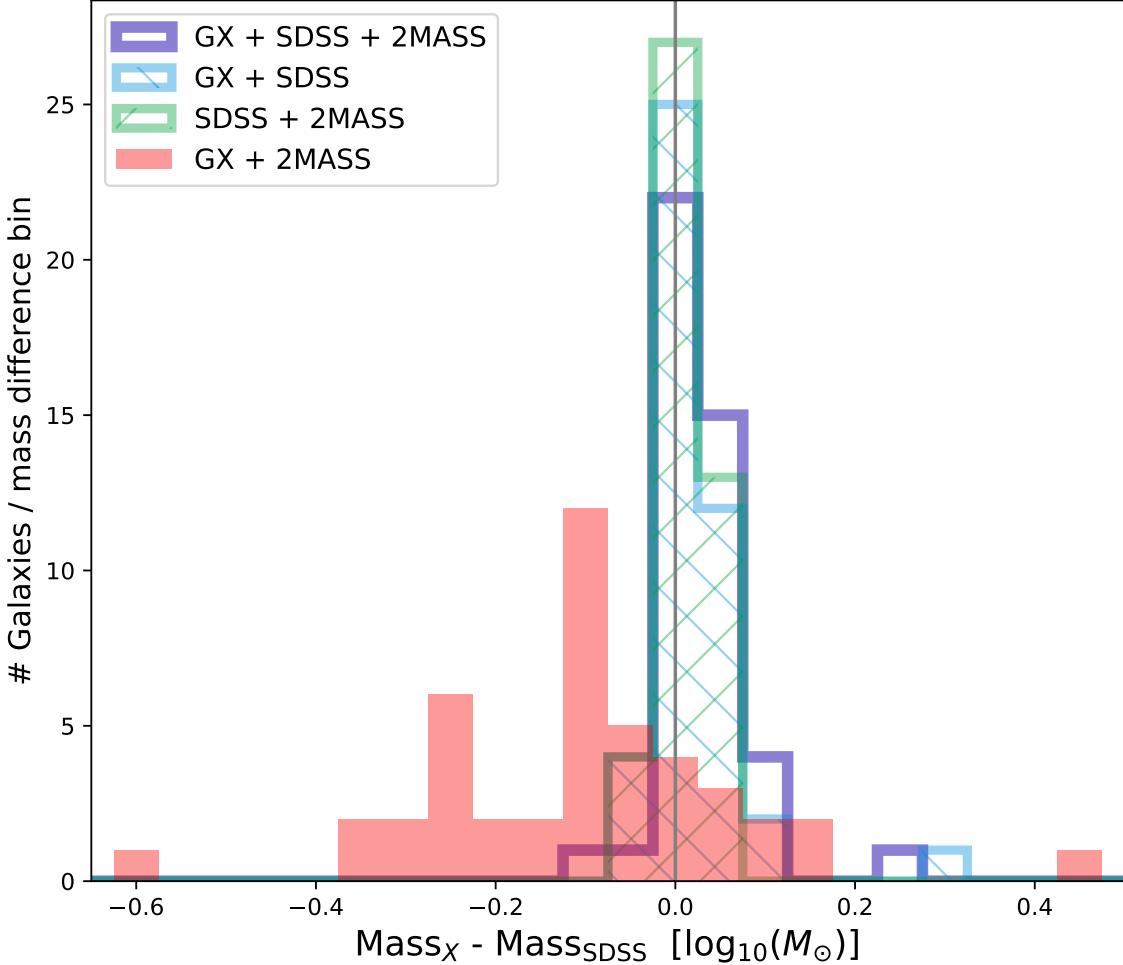


Figure 5. Difference between the different combinations of host galaxy photometry used to generate host galaxy masses compared to masses from only optical data. The purple unfilled histogram uses UV, optical, and NIR (GALEX+SDSS+2MASS) data. The blue histogram with the left hatching is the difference with respect to GALEX+SDSS. The green histogram with the right hatching is the difference with respect to SDSS+2MASS only. The filled red histogram does not use optical data at all (GALEX+2MASS). Adding GALEX or 2MASS to SDSS results in mass estimates that agree with the SDSS-derived mass. If we compare GALEX+2MASS to SDSS-only the mean mass offset is -0.06 dex, median=-0.05 dex, std deviation=0.19 dex. When we do not use the optical data, the scatter is much higher, but the mass offset and even scatter is still relatively small on the scale of the analysis we present in this paper.

et al. (2010) compared their derived masses with Kauffmann et al. (2003) as well and found a mean bias of 0.033 dex with a dispersion of 0.15 dex, which is consistent with the Kauffmann et al. (2003) data. In our sample, 41 of our host galaxies have overlapping information in MPA/JHU. Figure 6 plots the MPA/JHU DR7 masses versus our `kcorrect` masses and it is clear `kcorrect` systematically underestimates masses. This offset is linear in log mass with a slope of 1.03 and an intercept of $-0.134 \log(M_\odot)$ such that the effect increases as mass increases. Both Bernardi et al. (2010) and Moustakas et al. (2013) have previously reported that `kcorrect` produces lower masses for high mass, elliptical galaxies. Blanton & Roweis (2007) compared their `kcorrect`-derived masses to those calculated in Kauffmann et al. (2003) (on which MPA/JHU DR7 is based) and showed that the results agreed to within 0.2 dex with a 0.1 dex scatter, which roughly agrees with our findings with a mean bias of 0.27 dex and a dispersion of 0.11 dex. If we assume that the error in `kcorrect` can be estimated by the root-mean-square of the difference between `kcorrect` and MPA/JHU, then the error is ~ 0.29 dex. With this estimate of the mass error, we can confirm that our derived masses are systematically lower than those seen in Kelly et al. (2010). But these differences are not significant on the scale of the mass range of the host galaxies, and most importantly, do not preferentially change the ordering of galaxies in mass.

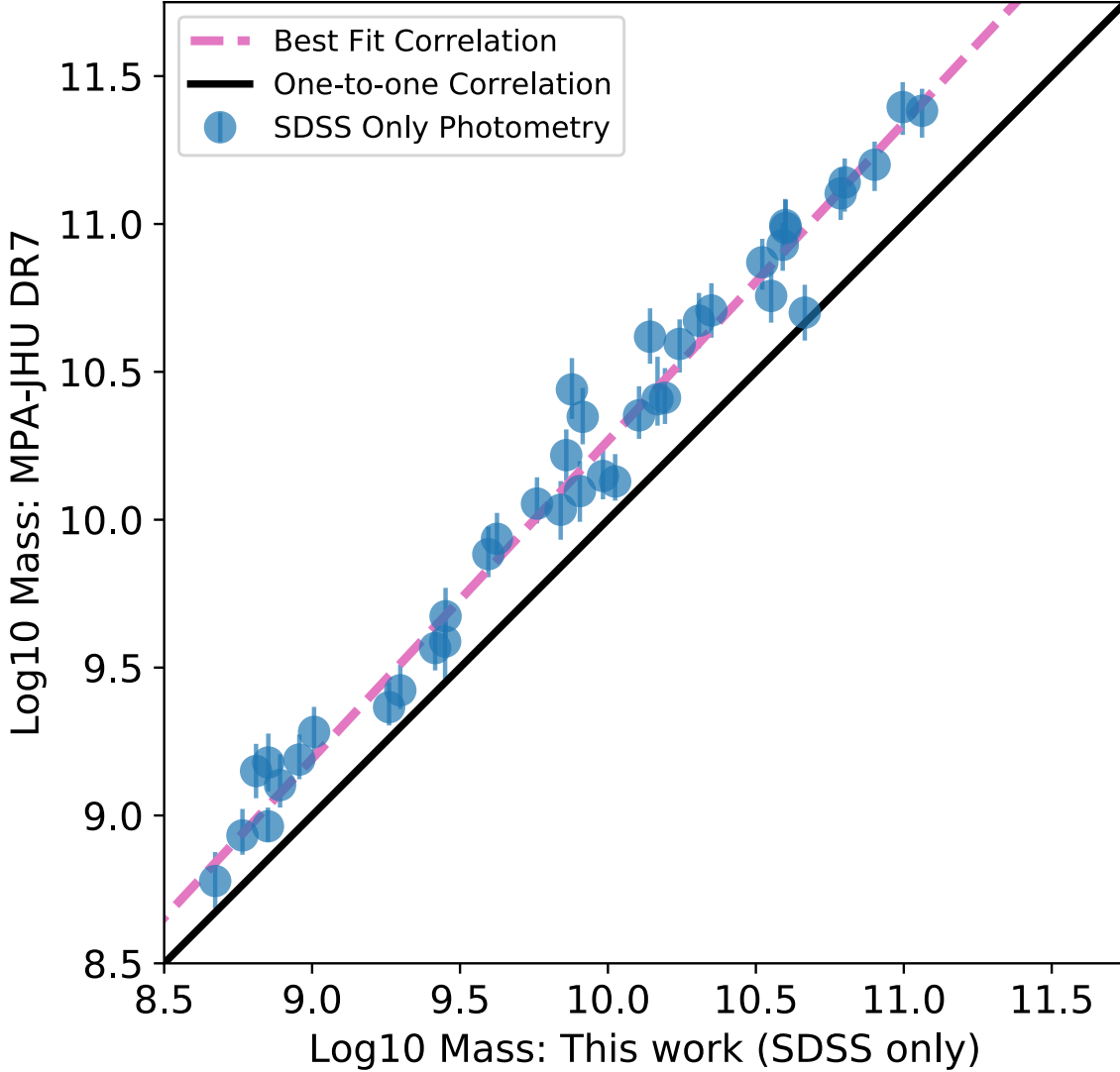


Figure 6. Comparison of `kcorrect`-derived host galaxy masses and the masses from the MPA-JHU sample originally presented in Kauffmann et al. (2003) with DR4 data and updated for DR7. The fit slope is 1.04 with offset -0.139 dex.

3. HUBBLE DIAGRAM

We here present the NIR and optical Hubble diagram from the current global collection of literature data on SNeIa observed in restframe H .

We used the SNooPy¹² fitter of Burns et al. (2011) to estimate maximum magnitudes in H with the “max_model” for the collected sample of supernovae. We fit the optical lightcurves with the SNooPy “EBV_model2”. For both models, we use the parameterization based on the updated s_{BV} width parameter introduced in Burns et al. (2014).

We adopted the same approach as in Weyant et al. (2014) of fitting separately in each band using the “max_model” SNooPy model. Unlike in Weyant et al. (2014), where we held $\Delta m_{15} = 1.1$ fixed, we here fit for the width parameter s_{BV} . We first fit with the reported time of maximum B-band light, $T_{B_{\max}}$, from the original spectroscopic confirmation announcement (generally ATel or CBET). Where we had constraining lightcurve information in the optical or NIR that started before peak brightness, we generated an updated $T_{B_{\max}}$ from a fit. We then recorded these updated $T_{B_{\max}}$ values along with the original estimates for those not updated and ran the final fits with $T_{B_{\max}}$ fixed.

¹² Version 2.0, <https://github.com/obscode/snpy>

The sample of SNeIa came from several surveys and the different transmission curves were accounted for in SNooPy using the corresponding CSP transmission curves, WHIRC transmission curves, and 2MASS (for PAIRTEL) transmission curves.

We used the default SNooPy K -corrections using the [Hsiao et al. \(2007\)](#) spectral templates, but we did not warp the spectral templates to match the observed color (“mangle=False”). We do not apply any color-luminosity correction as we do not assume a relationship between the different filters in our “max_model” fitting.

We did not use lightcurves that were observed before 1990, had no known optical $T_{B_{\max}}$, or were known to be SN 1991bg-like or other peculiar types (although we include 91T-like events). We excluded from the Hubble residual analysis any SNeIa that had fewer than three lightcurve points in the H -band. After these quality cuts, we have a sample of 144 SNeIa.

The lightcurve fits to SNe Ia presented here are shown in Figures 7–7.2.

The H -band magnitudes are reported as the fit apparent magnitude based on the “max_model” template for the given s_{BV} – there is no correction to the apparent magnitude based on s_{BV} . For the optical fits, we do include the s_{BV} correction to the apparent brightness. To emphasize this distinction we quote the H -band fits in terms of apparent magnitude and the optical fit results in terms of distance modulus (μ).

3.1. Hubble Diagram

We compare our measured SN Ia apparent brightness to that predicted by a flat LCDM model with $H_0 = 72 \text{ km s}^{-1} \text{ Mpc}^{-1}$ and $\Omega_M = 0.28$ ([Perlmutter et al. 1999](#); [Freedman et al. 2001](#)). We calculated the weighted best fit value of the absolute magnitude, after adding both an intrinsic dispersion of 0.08 mag (as reported in [Barone-Nugent et al. 2012](#)) and the equivalent magnitude uncertainty from a peculiar velocity of 300 km s^{-1} in quadrature to the reported statistical fit uncertainty from SNooPy. We redid the full analysis at 150 km s^{-1} and found minimal differences. These additions to the uncertainty were used in computing the weighted average, but are not included in the errors plotted on the residual plots or reported in Table 4. While SNooPy “max_model” reports apparent brightness and “EBV_model2” returns distance modulus, the actual calculation of residuals follows the same process. The absolute magnitude is entirely degenerate with the chosen value for H_0 . As we are here looking at residual relative brightness, the absolute brightness and value of H_0 are not directly relevant. This model was then subtracted from the data points to yield the residuals that were used to compare against properties of the host galaxies.

The results from these fits are tabulated in Table 4 and the resulting Hubble diagram with residuals is shown in Figure 8.

3.2. A Caveat on K -corrections

We note that the state of K-corrections in NIR SNeIa photometry remains in its beginning stages and we express concern that the K-corrections used here are not the final word. The two significant previously explicitly published K-corrections are those of [Kosciunas et al. \(2004b\)](#) and [Hsiao et al. \(2007\)](#). The community has continued to gather NIR spectra, but these have not yet been compiled into a new set of spectral templates. [Stanishev et al. \(2018\)](#) presented their own K-correction methodology, but do not provide an updated set of spectral templates. If SNeIa were all the same in the NIR, then the excellent NIR spectral series on SN 2011fe ([Hsiao et al. 2013](#)) or SN 2014J ([Marion et al. 2015](#)) would provide sufficient data for good K-corrections. But while SNeIa NIR exhibit less scatter in the H -band than the optical, there is still clear evidence for some variation: single- vs. double-hump (e.g., the dromedarian SN 2005hk detailed in [Phillips et al. 2007](#)), and bridge objects such as iPTF13ebh ([Hsiao et al. 2015](#)). We remain of the opinion that a new effort in K-corrections for SNeIa in the NIR would be a worthwhile endeavor with a clear benefit to the community.

4. ANALYSIS

In this section, we examine the host galaxy stellar mass correlations with the restframe H -band residuals and the optical width-luminosity-corrected distance modulus residuals. Though we present an in-depth study of host galaxy stellar mass since it is the largest trend seen in the literature with optical lightcurves, we have done the same studies examining restframe K -corrected absolute r -band magnitude as well as briefly exploring other properties of the supernova environment ($g - r$ color, host galaxy morphology, Hubble flow, NUV colors, and distance from center of host galaxy). These studies are summarized in Appendix A.

4.1. Statistical Properties of the Distributions

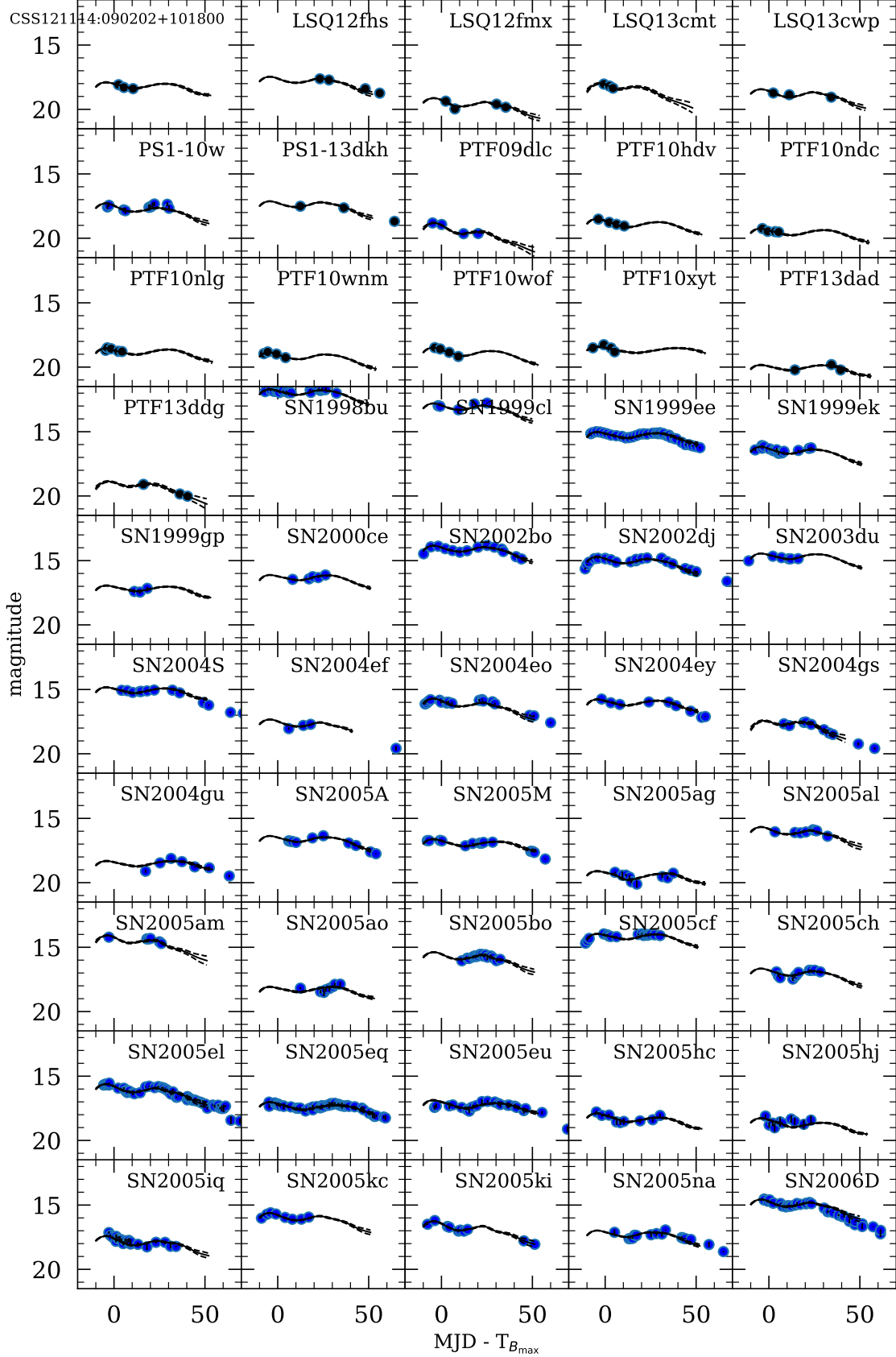


Figure 7. The SNoPy H_{\max} lightcurve fits to 144 SNeIa.

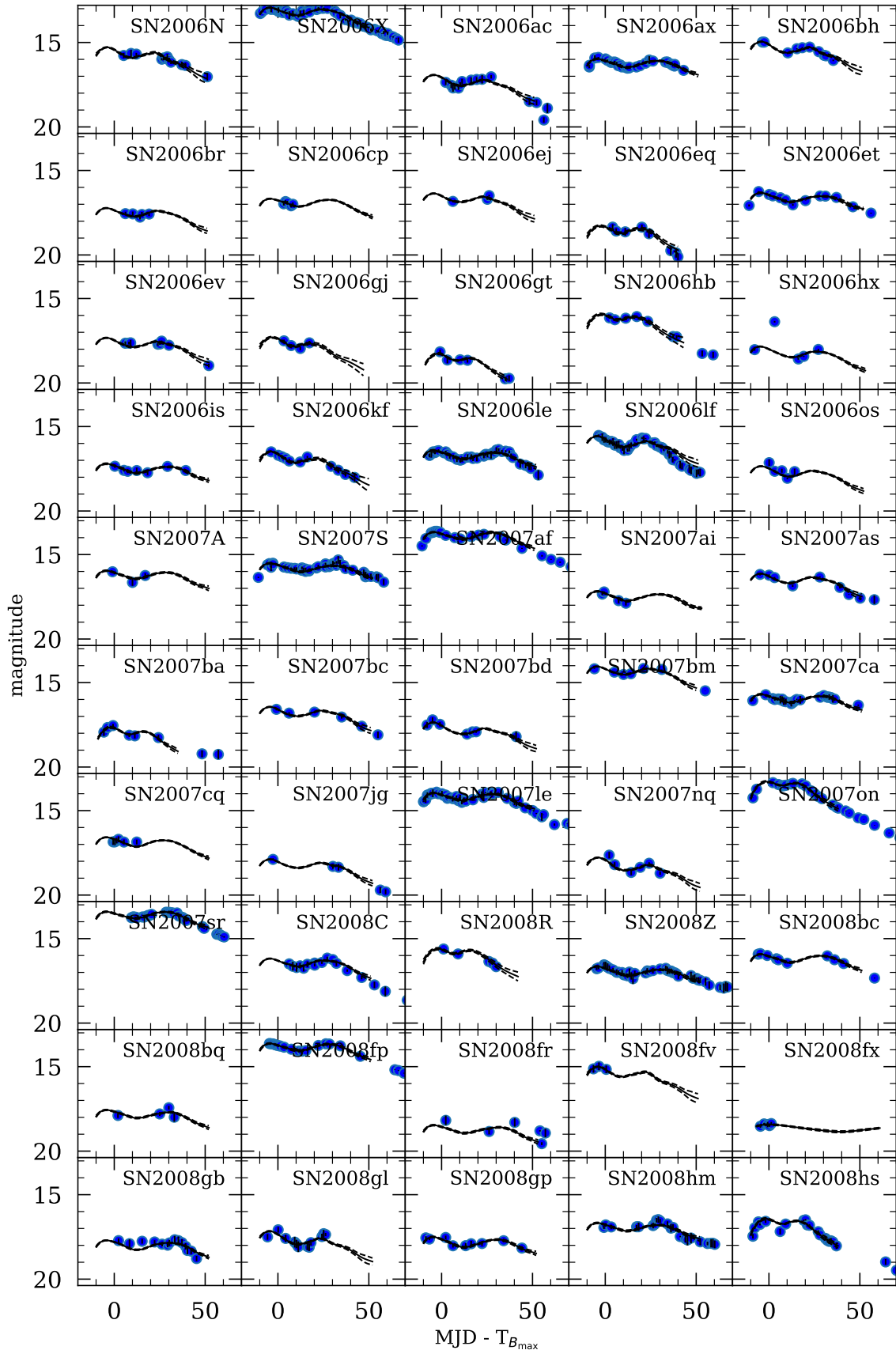


Figure 7.1. The SNoPy H_{\max} lightcurve fits to 144 SNeIa.

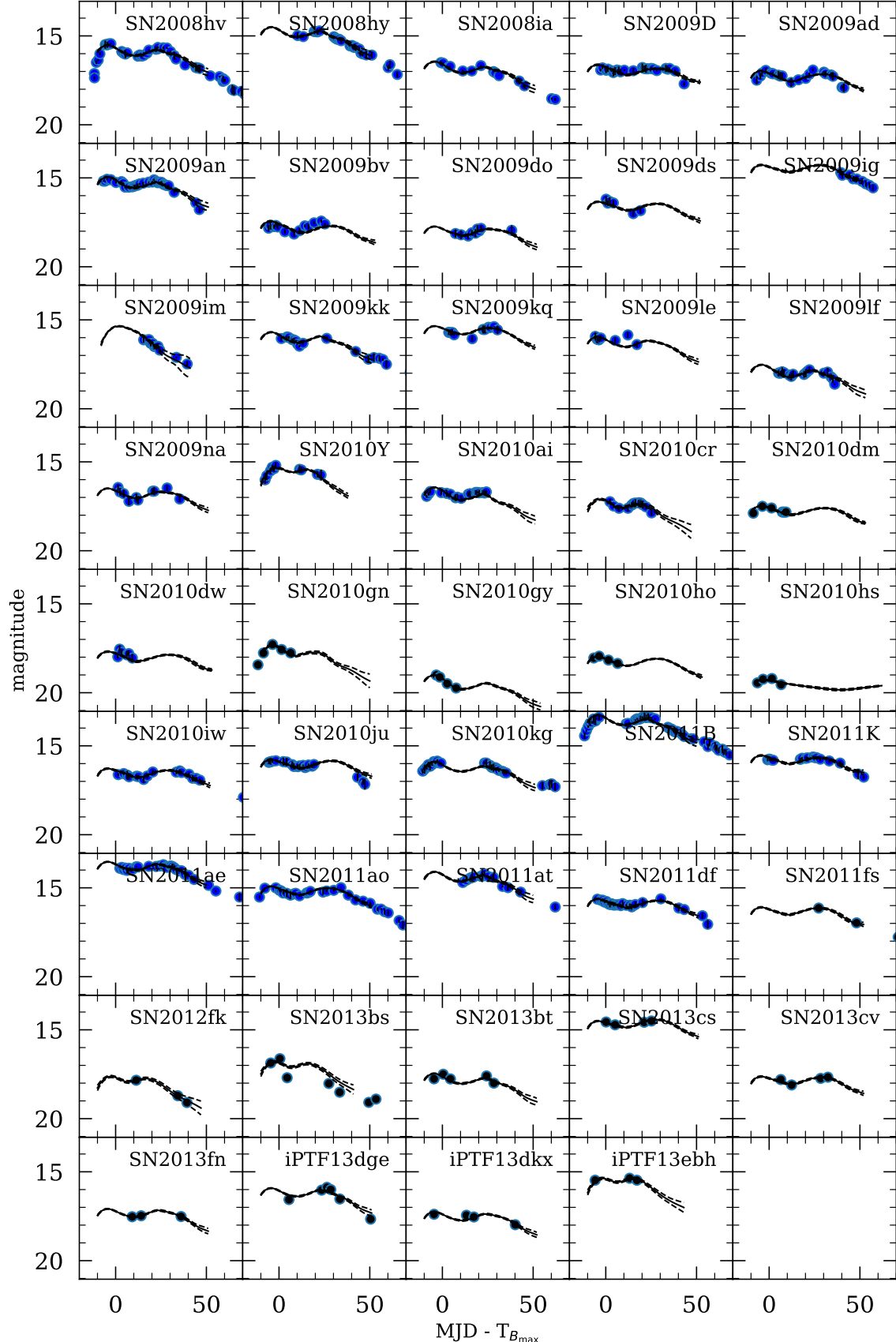


Figure 7.2. The SNoPy H_{\max} lightcurve fits to 144 SNeIa.

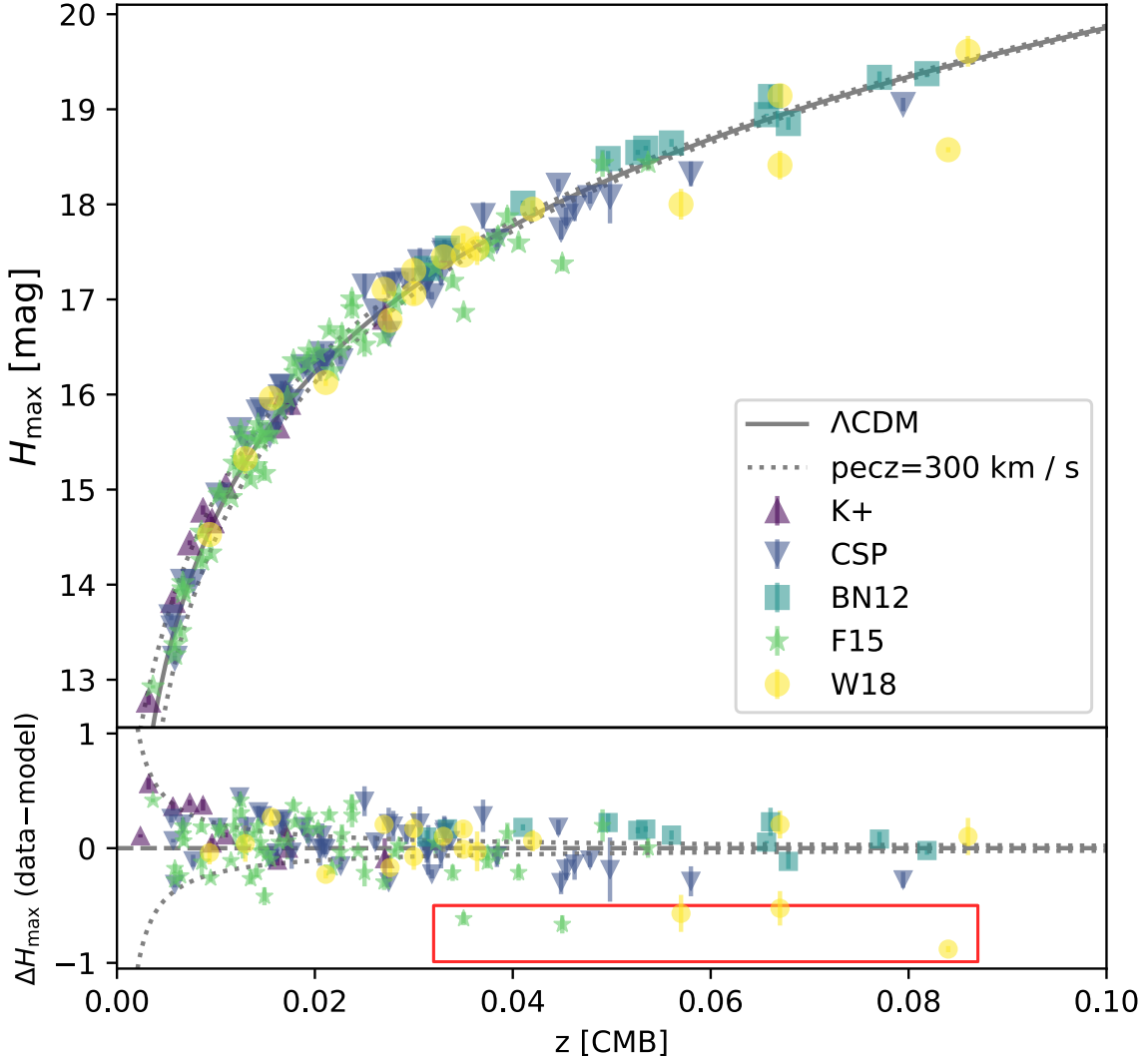


Figure 8. *Top:* SN Ia H -band Hubble diagram for the sample considered in this paper. *Bottom:* The residuals from the apparent H magnitude at maximum light (data–model) for the best-fit Λ CDM cosmology. The points are coded in different shapes to indicate the source of the SN Ia lightcurve data. The five outliers referred to in Section 5.2 are highlighted in the red box.

Having collected UV, optical, and/or NIR data allows us to estimate stellar masses for 99 out of 144 host galaxies. We separate this sample by mass where the “Light” population corresponds to galaxies with masses less than $10^{10} M_\odot$ and the “Heavy” population corresponds to galaxies with masses greater than $10^{10} M_\odot$. Figure 9 shows the Hubble residuals as a function of redshift with Light and Heavy galaxies highlighted. Those with no indicator do not have sufficient host galaxy photometry to estimate mass. We observe a population of bright (residual < -0.5 mag) SNeIa at $z > 0.03$. We see no clear trend in host galaxy mass versus redshift.

The top left plot of Figure 10 shows the H_{\max} Hubble residuals (ΔH_{\max}) versus host galaxy mass and the top right plot shows a histogram of the Hubble residuals grouped by mass with the full sample included in grey for comparison. Table 5 shows the full details of the fits for the different populations including their peak residual magnitude, weighted peak residual magnitude, χ^2 , χ^2/DoF , standard deviation, interquartile range (IQR), the standard error on the mean (SEM), and the intrinsic standard deviation that would result in a reduced $\chi^2 = 1$.

We find that the measured unweighted standard deviation of the whole sample is 0.229 mag and the IQR equivalent to 1σ assuming a Gaussian distribution is 0.211 mag. The standard deviation (IQR) of SN Ia residuals in Light hosts

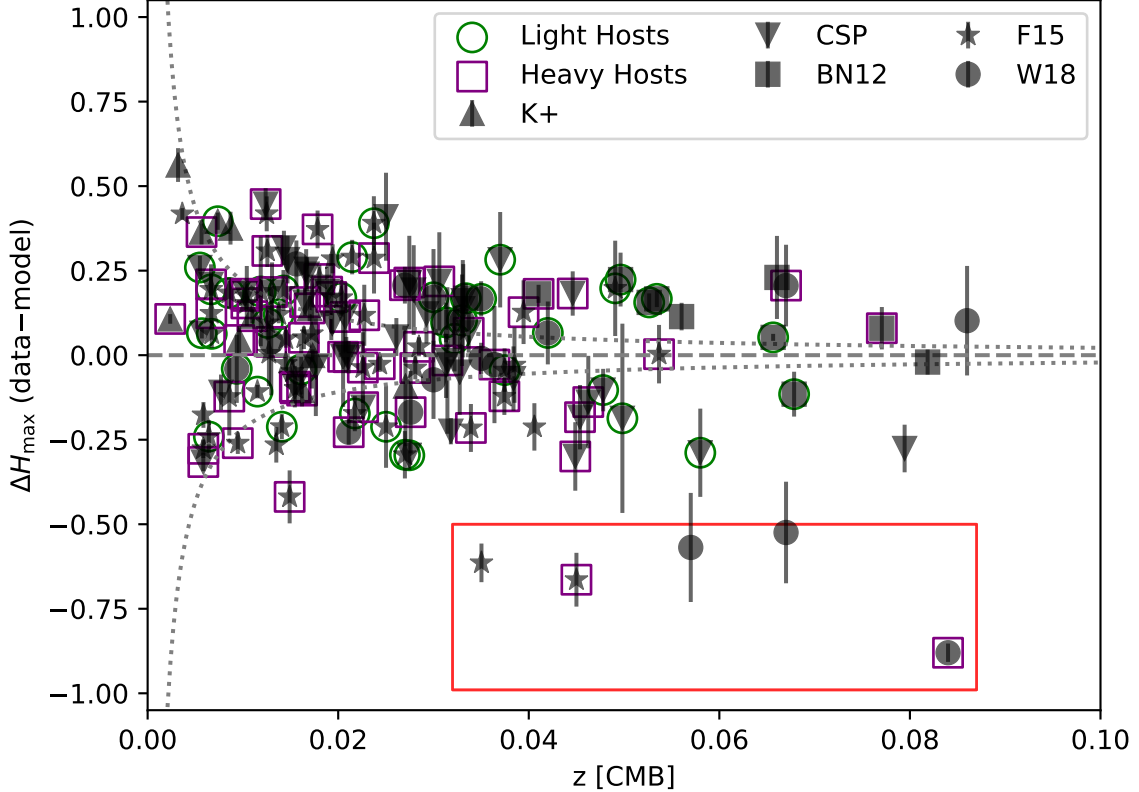


Figure 9. The residuals from the apparent H magnitude at maximum light (data–model) for the best-fit Λ CDM cosmology. The points are coded in different shapes to indicate the source of the SN Ia lightcurve data. If no host galaxy mass was calculated, the point does not have a circle or square around it. Overlaid on the points are the classification of their host galaxy: green circles are galaxies with mass $< 10^{10} M_{\odot}$ and purple squares are galaxies with mass $> 10^{10} M_{\odot}$. The five outliers referred to in Section 5.2 are highlighted in the red box.

is 0.187 (0.215) mag, while the standard deviation (IQR) of SNeIa residuals in Heavy hosts is 0.237 (0.219) mag. The SNeIa in lighter hosts produce a tighter scatter in their distribution.

The weighted average residual of the Light population is 0.050 ± 0.030 mag and the weighted average residual of the Heavy population is -0.031 ± 0.031 mag. The difference in average weighted residuals is 0.081 ± 0.043 mag with more massive galaxies hosting brighter SNeIa, which is a $\sim 1.88\sigma$ detection and with an amplitude in agreement with the literature.

If we remove the outlier population at $\Delta H_{\max} \leq -0.5$ mag, the separation between the peaks drops to 0.013 ± 0.039 mag, a 0.33σ significance (Table 5) indicating these outliers may be driving the $\sim 2\sigma$ correlation seen in the full sample. Though we see that SNeIa hosted in lighter galaxies have lower standard deviation than SNeIa hosted in heavier galaxies, the scatter in the heavy sample is dominated by the bright ($\Delta H_{\max} \leq -0.5$ mag) SNeIa at redshifts of $0.03 < z < 0.09$. If we remove the outliers, the standard deviations for both populations are equivalent. We will explore this “outlier population” further in Section 5.2.

4.1.1. Correlations with Corresponding Optical Lightcurves

Host galaxy correlations have been well studied in the optical wavelengths. To compare our results to these studies, we repeated the analysis with optical lightcurves of SNeIa observed in the H -band. The optical data set is only 104 SNeIa in total, 38 with optical host galaxy photometry, and 71 with host galaxy mass estimates. The bottom panels in Figure 10 shows the distributions from host galaxy stellar mass compared with the optical distance modulus (μ) residuals. Table 6 presents the resulting weighted residuals and standard deviations. Here we see no difference in the Light and Heavy host galaxies with a difference in average weighted residuals 0.069 ± 0.056 mag, which is less than 1σ .

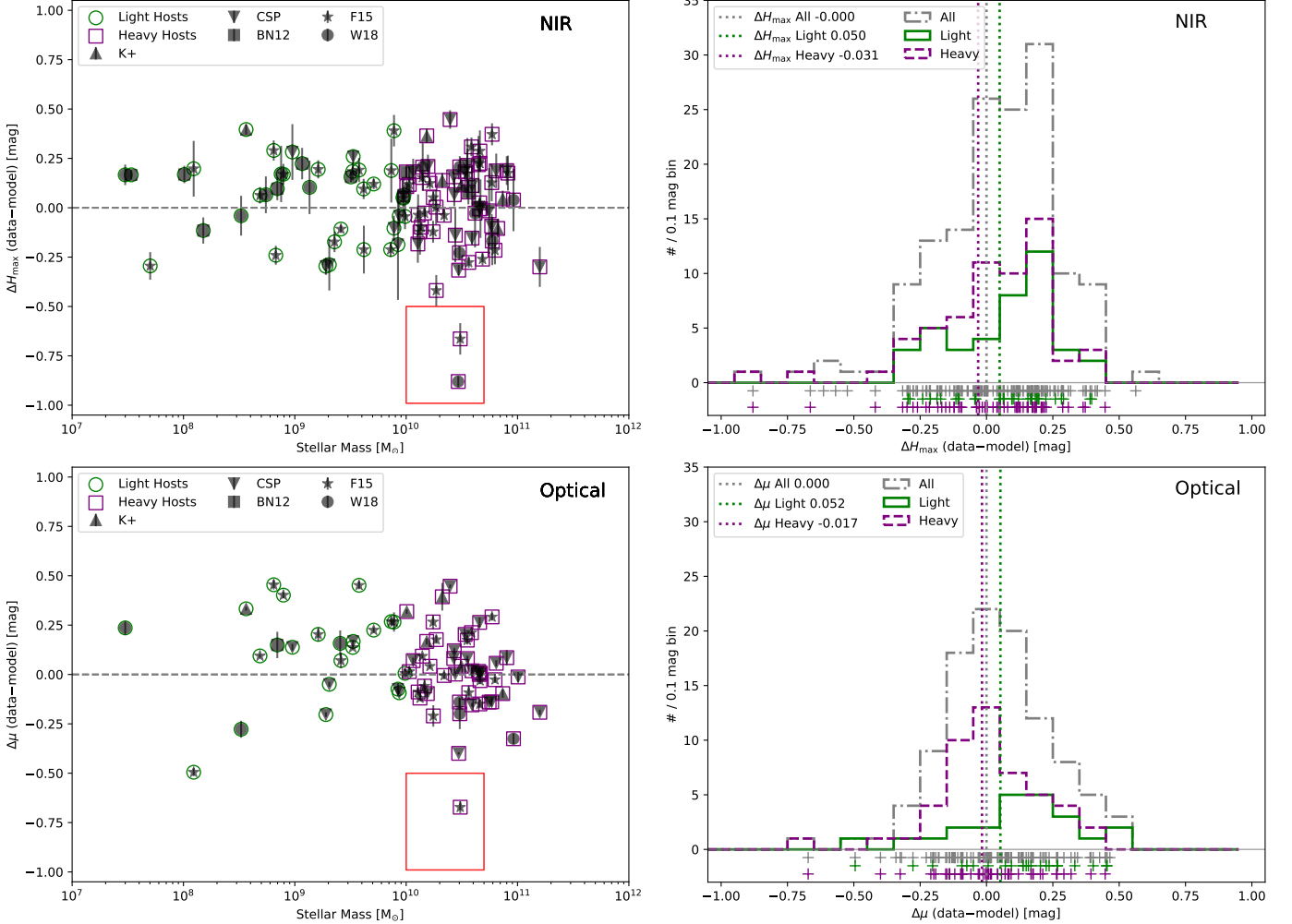


Figure 10. *Top Left:* SN Ia Hubble residuals vs host galaxy mass. The points are coded in different shapes to indicate the source of the SN Ia lightcurve data. Overlaid on the points are the classification of their host galaxy: green circles are galaxies with mass $< 10^{10} M_{\odot}$ and purple squares are galaxies with mass $> 10^{10} M_{\odot}$. *Bottom Left:* Same as top left but for the distance modulus from optical lightcurves. *Top Right:* Histogram of Hubble residuals (data–model) for the SNeIa of the full sample (grey dotted). *Bottom Right:* Same as top right but for the distance modulus from optical lightcurves.

In this histogram analysis, we found no statistically significant trends between restframe H or optical SN Ia brightness and host galaxy properties.

4.2. Functional Form of Correlation

In the previous section, we compared the weighted mean residuals of SNeIa separated by different host galaxy properties and found a $\sim 2\sigma$ result supporting a 0.081 mag shift in NIR Hubble residual with increasing mass. Though this is in agreement with the results in the literature from optical studies, we showed that it is a result of a bright SN Ia population. However, there is no strong reason to model any host-galaxy brightness dependence by a simple step function. To further test the significance of this correlation, we explore different function forms for the relationship between SN Ia Hubble diagram residuals and the host galaxy stellar mass.

4.2.1. Different Models to Fit

We fit 7 different models using `scipy.optimize.curve_fit`: a constant function corresponding to a single population and no correlation, a linear function, a step function with a break corresponding to the threshold used in the previous section ($10^{10} M_{\odot}$), a step function that fits for the location of the break as well as the amplitude and y-intercept,

and several logistic functions. We fit three logistic functions: one where the threshold was held constant at $10^{10} M_{\odot}$, one where it was allowed to float, and the generalized logistic equation. The error on the fitted model parameters corresponds to the diagonal elements of the resulting covariance matrix.

4.2.2. Information Criteria

After fitting the different functions to our data, we compare which model describes the data better using two different information criteria (ICs): the Akaike Information Criterion (AIC; [Akaike 1974](#)) and the Bayesian/Schwartz Information Criterion (BIC; [Schwarz 1978](#)). We use the updated AIC_c ([Sugiura 1978](#)), which is more suitable for smaller samples.

Information criteria allow for a comparison of different models by balancing an improved χ^2 versus an increase in the number of fit parameters. However, AIC_c and BIC cannot be used to determine the absolute goodness-of-fit of the model; they can only establish which model the data favor compared to another model. We calculate ΔAIC_c and ΔBIC relative to the constant model. If the difference in IC is > 2 , a constant model is preferred; > 5 , a constant model is strongly preferred; < -2 , the compared model is preferred; and < -5 the compared model is strongly preferred. When $0 < \text{IC} < 2$, there is a preference for a constant model, but not a statistically significant one. Likewise, an IC between -2 and 0 shows a preference for the compared model, but it is not significant.

4.2.3. *H*-band and Optical Results

To estimate the best site of the break (step function) or midpoint (logistic function), we fixed the position at a range of values between $7 < \log_{10}(\text{mass}/M_{\odot}) < 12$ and fit for the other parameters in the respective models. We then use the ICs to compare the model at each transition location versus the model with the step or midpoint located at the original threshold of $10^{10.0} M_{\odot}$ and chose the location with the lowest IC. The top panels of Figure 11 show the results from doing this procedure for the step function for ΔH_{\max} and the optical distance modulus ($\Delta\mu$).

The top left panel is the result of fitting 99 H_{\max} residuals and has a global minimum at $10^{10.44} M_{\odot}$. The top right panel finds the best fit location for the 71 optical lightcurves, which similarly favors a threshold at $10^{10.44} M_{\odot}$ but shows a local minimum below $10^{10} M_{\odot}$. Below a mass of $10^{9.28} M_{\odot}$, the lower mass bin has less than 20% of the total number of SNeIa making it more susceptible to edge effects during fitting. The same is true for the higher mass bin above a mass of $10^{10.65} M_{\odot}$. Therefore, we only consider breaks in the step function between $10^{9.28} M_{\odot}$ and $10^{10.65} M_{\odot}$, which is indicated in the grey band in the top panels in Figure 11.

The ICs strongly prefer a break at $10^{10.44} M_{\odot}$ over $10^{10} M_{\odot}$ in both cases. Both the H_{\max} and μ residuals favor a mass step at $10^{10.44} M_{\odot}$, which is in between the typical number found at $10^{10} M_{\odot}$ (e.g., [Sullivan et al. 2010](#); [Lampeitl et al. 2010](#); [Gupta et al. 2011](#); [Childress et al. 2013b](#)) and $10^{10.8} M_{\odot}$ found in [Kelly et al. \(2010\)](#).

The bottom panels of Figure 11 show the models from the best fits: constant, linear, the best-fit step function, the modified logistic using the threshold value, and the best-fit midpoint location for the modified logistic. Table 7 summarizes the best fit models using ICs and Table 8 outlines the significance in the slope of the linear function, the step size of the best-fit step function, and the step size of the step function with a break at the original threshold. The H_{\max} residuals prefer a linear function and strongly prefer a step function at the best-fit break over a constant model. The slope of the linear function is found at 2.67σ but the best-fit step at $10^{10.44} M_{\odot}$ finds a 0.18 ± 0.05 mag step at 3.6σ .

The ICs from distance modulus residuals behave similarly to the H_{\max} residuals with a slightly lower preference for a linear model but a similarly strong preference for the best-fit step function. The best-fit step function was found at a $> 3\sigma$ significance level and is a detection. We report a step size of 0.10 ± 0.05 mag at $10^{10} M_{\odot}$ which is similar to what was found previously in the literature. By using the updated best-fit location of $10^{10.44} M_{\odot}$, this step size increases to 0.17 ± 0.05 mag.

The modified logistic provides a smooth transition between two populations unlike a step function which is an abrupt change; however, this model introduces more free parameters. For the H_{\max} residuals, the modified logistic function with the best-fit midpoint essentially replicates the best-fit break step function with a smooth transition between the two groups and a midpoint at $10^{10.38} M_{\odot}$. With the additional free parameters, the ICs do not clearly prefer this function over a constant model with the AIC_c preferring the logistic function and the BIC preferring a constant function. The modified logistic function at the $10^{10} M_{\odot}$ midpoint has a weaker preference for the logistic function with the AIC_c, but the BIC also shows a weaker preference for the constant model. The optical distance modulus residuals for the modified logistic at the $10^{10} M_{\odot}$ midpoint behaves the same as for the H_{\max} residuals. When we allow the midpoint to float, the best midpoint is at the edge of our parameter space towards the high mass ($10^{11.60} M_{\odot}$) and

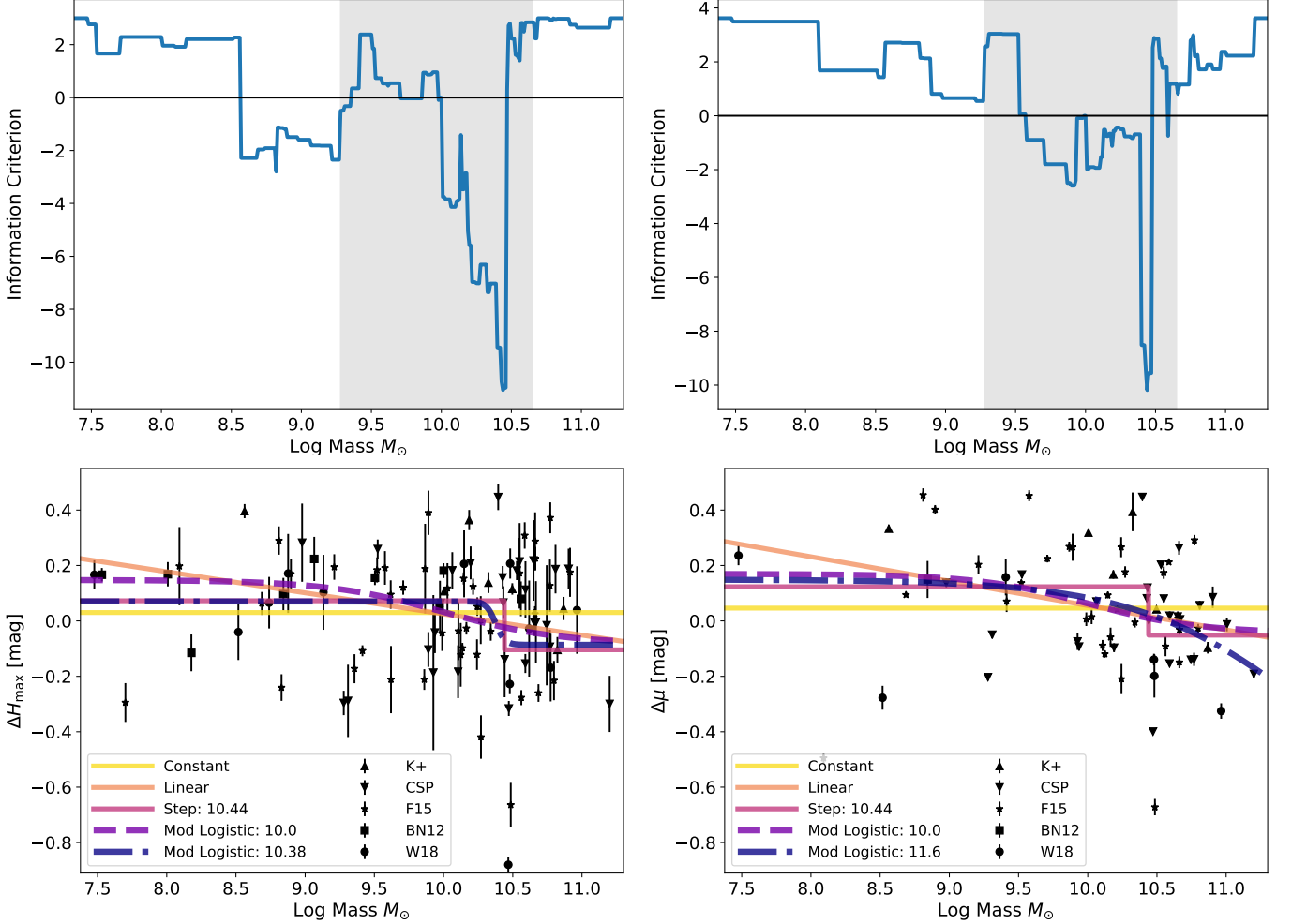


Figure 11. Results from finding the best fit step location and fitting several functions to the residuals versus host galaxy mass. *Top:* Best fit location of the step function threshold shown using the AIC_c . The grey band highlights the area that we consider for the step function break such that the lower or higher mass bin has at least 20% of the total SNeIa. *Bottom:* Various functions fit to the host galaxy mass versus Hubble residuals. *Left:* Results from using the H_{\max} Hubble residuals. *Right:* Results from using the distance modulus (μ) optical lightcurve Hubble residuals.

neither of the ICs prefer this model. Given the IC inconsistencies and the poor fit with $\Delta\mu$, we show the curves in Figure 11 but do not include any of the fit parameters.

The generalized logistic function for the H_{\max} residuals behaves similarly to the modified logistic function with a midpoint at $10^{10} M_\odot$, but the ICs do not support this model. For the optical residuals, the generalized logistic function returned a straight line around 0.05 mag which completely overlaps with the constant model; however, the ICs do not prefer this model due to the additional parameters it introduced. Since the ICs were strongly against these models in every scenario, we do not include the fit on the plots.

We showed here that there is a significant correlation between host galaxy mass and the H_{\max} NIR lightcurves in which more massive galaxies host SNeIa that are brighter than those hosted in lower mass galaxies by 0.18 ± 0.05 mag. We also confirmed a significant correlation between host galaxy mass and optical lightcurves in which more massive galaxies host SNeIa that have more negative width-luminosity corrected optical brightnesses by 0.17 ± 0.05 mag. Our results also agree with the literature (Childress et al. 2013b) in that a step function is more preferred over a linear function to describe the correlation between residuals and host galaxy mass.

5. DISCUSSION

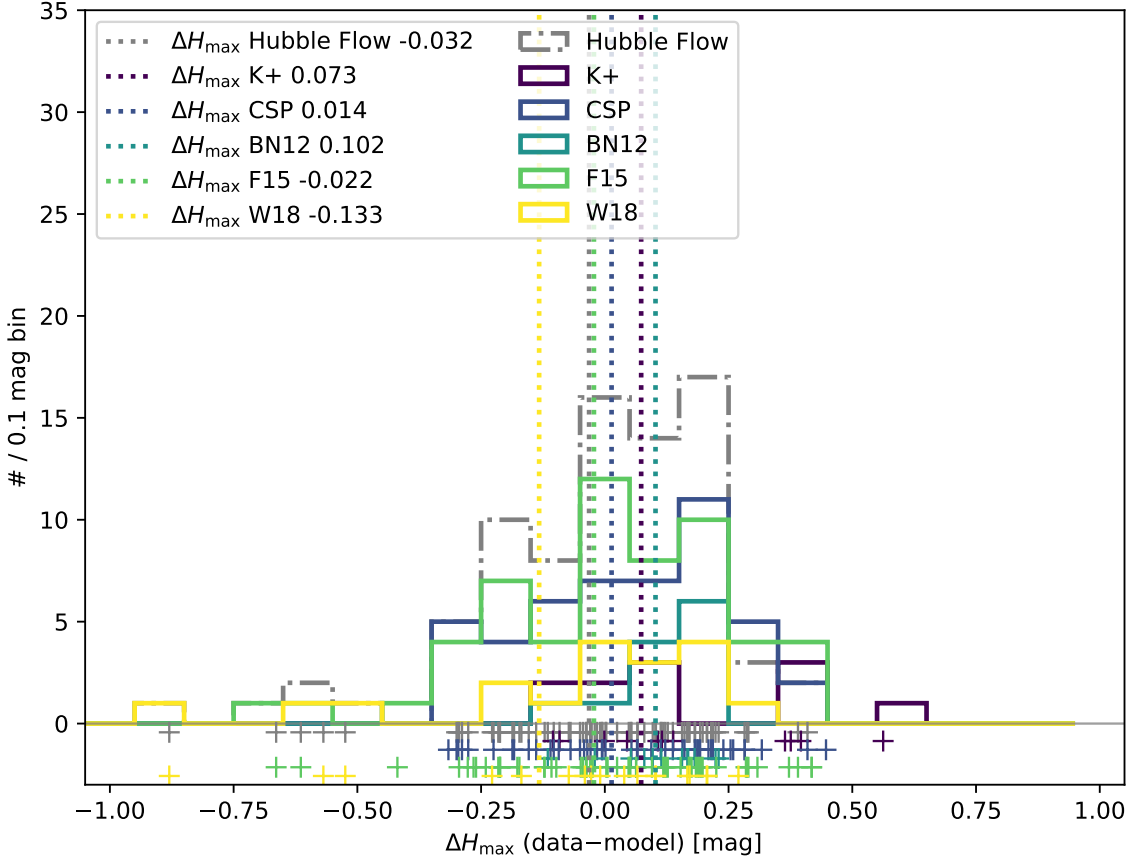


Figure 12. The H -band residuals for all Hubble flow SNeIa (grey dashed) and for each sample. The individual points are shown below the $y = 0$ axis for ease of reference to the original data.

In this section we will further explore the statistical significance of our analysis by studying effects from using a heterogeneous set of SNeIa, the outlier population, joint data samples, errors on lightcurve fits, and finally whether we are adding new information by including the NIR.

5.1. Comparison of Residuals per Sample

Here we look at the statistical properties of the residuals if we separate them per sample, which are summarized in Table 9. Figure 12 shows the H_{\max} residuals colored by SN lightcurve source (Sample). The difference in weighted mean residuals between the brightest (W18) and dimmest (BN12) samples is 0.24 mag and 0.20 mag for the H_{\max} and μ residuals, respectively (see Table 9). This difference between surveys is larger than any step size we see based on any host-galaxy feature. However, the brightest population comes from W18 which features 3 of the bright outlier SNeIa. These 3 SNeIa also factor into the larger standard deviation and intrinsic dispersion seen in W18. BN12, the dimmest sample, has the tightest standard deviation. We note that BN12 reported a small range in B -band stretch for their lightcurves indicating a data set lacking in intrinsic variation of SNeIa and 8 out of 9 BN12 SNeIa with host galaxy photometry are in blue galaxies.

However, while the surveys have different mean properties in their residuals, they overall appear to form a continuous distribution. We thus assert that using SNeIa from different samples is not greatly biasing our results. A possible exception is BN12, which shows little variation in host galaxy type and may contain an intrinsically different distribution of SNeIa.

In Table 9, the K+ sample does not have a reported intrinsic dispersion for the H_{\max} residuals. To determine the intrinsic dispersion, we set the χ^2/DoF equal to one and solve for the intrinsic dispersion. For K+, this dispersion would have to be imaginary since the χ^2/DoF is less than one. The K+ sample has a lower redshift distribution than the other surveys (see the purple triangles in Figure 8). The imaginary implied intrinsic dispersion is a manifestation

of the high peculiar velocity choice of 300 km s^{-1} . The K+ sample is the lowest redshift collection (you can piece this out of Figure 8) and is thus most sensitive to the peculiar velocity assumed. If the assumed peculiar velocity is reduced to 150 km s^{-1} , the implied intrinsic dispersion for H_{\max} residuals is 0.166 mag. For all other surveys, the intrinsic dispersion increases by $\sim 0.01\text{--}0.03$ mag if the peculiar velocity is 150 km s^{-1} . We see a similar response to the change in peculiar velocities from the μ residuals. Though we do see small differences noted in Table 9, reducing the peculiar velocity has no affect on the outcome of this analysis.

5.2. Removing NIR Outlier Population

As noted in Section 4.1, there is a small outlier population of 5 SNeIa with very negative (≤ -0.5 mag) Hubble residuals. The outlier SNeIa are LSQ13cmt (W18), LSQ13cwp (W18), PTF13ddg (W18), SN 2005eu (F15), and SN 2009lf (F15). Only PTF13ddg and SN 2009lf have host galaxy mass measurements and so figured in the host-galaxy mass analyses. We examined each lightcurve closely and found nothing unusual for LSQ13cmt, SN 2005eu, and SN 2009lf. Though LSQ13cwp helped to discover a lensed galaxy system due to its coincidental projected spatial proximity to it, this supernova is removed enough from the system to not be affected by the lens (Galbany et al. 2018). PTF13ddg is notable because it is the largest outlier but it is at a redshift of 0.084 and only has 3 data points in the H -band. The two SNeIa from F15 have 16 and 23 lightcurve points in the H -band while the W18 SNeIa all have only 3 data points per lightcurve.

We excluded the 2 outliers that had host galaxy information, PTF13ddg and SN 2009lf, and repeated the ΔH_{\max} fits versus host galaxy mass from Section 4.2. Table 10 presents the number of supernovae, the step size, and the best fit (BF) step location for the original sample and for the sample without the large outliers. We find that the significance of the slope drops very little to 2.5σ and the step size also drops to 2.5σ with a size of 0.10 ± 0.04 mag, but the location of the best-fit step remains the same at $10^{10.44} M_{\odot}$. The AIC_c prefers a linear function or step function at $10^{10.44} M_{\odot}$ over a constant model, but the BIC has no preference compared to a linear model and prefers a constant model when compared to the step function.

One out of those 5 SNeIa was also present in the optical data set with host galaxy mass, and this SN Ia is also an outlier in that sample with $\Delta\mu \sim 0.6$ mag. The correlation with mass for the linear model and step function at $10^{10} M_{\odot}$ remain at the same amplitude and significance. The best-fit break is still at $10^{10.44} M_{\odot}$ and magnitude of the step the same with a drop in the dispersion to 0.17 ± 0.05 mag (3.4σ). The ICs decreased very little and still strongly favor a non-constant model.

In the NIR, removing these large H -band outliers reduced the significance of the step reported above to 2.5σ but kept the location of the step at $10^{10.44} M_{\odot}$. The correlation is still partially preferred over a constant model providing support that some of this correlation is not driven by the outliers. The optical lightcurve mass step significance was only slightly affected by removing this supernova. Our results thus further indicate strong support for a host galaxy stellar mass correlation with optical width-luminosity corrected Hubble residuals.

5.3. SNeIa with Both H -band and Optical Lightcurves

We here explore the results from limiting the data set to only the SNeIa that have both H -band and optical lightcurves. A summary of the results is presented in Table 10 under “Joint”.

66 SNeIa with host galaxy stellar masses measured have both NIR and optical lightcurves that satisfy our quality cuts for inclusion in the Hubble analysis. The H -band brightness residuals continue to favor the best-fit step function at $10^{10.44} M_{\odot}$ with a reduced step of 0.11 ± 0.05 mag. We calculate a null detection at $10^{10} M_{\odot}$ and find a low significance correlation of 2.6σ with a linear model. All of the ICs are inconclusive with the AIC_c favoring a linear model over a constant model but all other comparisons do not clearly favor one model over another. The BIC for the linear model does not prefer a model and the constant model is favored over the two step functions. The optical correlation step size increased by 0.01 mag increasing the significance to 3.6σ and the ICs are equivalent to those for the full sample. The ICs very strongly favor a mass-dependent model.

The same SNeIa that show a mass dependence in optical wavelengths show some evidence for a correlation with the H -band brightness.

5.4. Difference in Optical and NIR Error Bars

The quoted uncertainties on the H -band residuals are larger than those for the optical distance modulus for two main reasons. First, the model for NIR lightcurves is more uncertain than optical lightcurves and that uncertainty

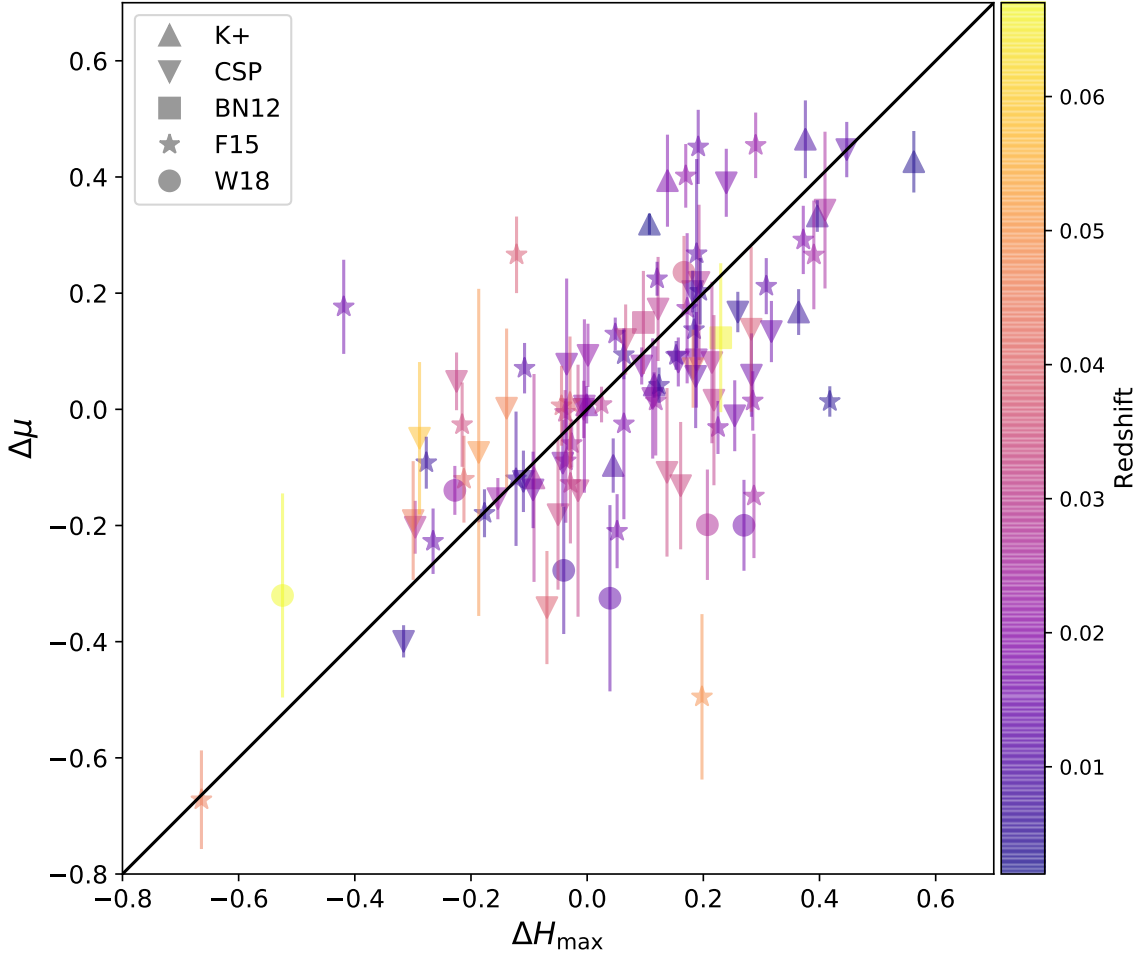


Figure 13. Optical Hubble residuals (μ) vs. H_{\max} residuals. As in previous figures, the different shapes indicate the source of the SN Ia lightcurve data. The color map indicates the redshift of the host galaxy. The black line illustrates a one-to-one relationship to guide the eye. The Pearson r-coefficient is 0.63.

gets propagated to the quoted error in fit brightness. Second, there are fewer NIR lightcurve points used to fit the H_{\max} model. This model only uses lightcurve points from the H -band, and typically NIR lightcurves are less densely sampled than optical lightcurves. The EBV_model2 uses lightcurve points from all of the optical lightcurves instead of just one band.

We added in quadrature an additional scatter of 0.08 mag to approximate the intrinsic scatter and refit the models for dependence of Hubble residual versus host-galaxy mass. For the ΔH_{\max} comparisons, we continue to see some evidence for a host galaxy mass correlation with a $\sim 2.20\sigma$ detection for the best-fit step function that has a break at $10^{10.44} M_{\odot}$ and an amplitude of 0.11 ± 0.05 . All the information criteria prefer a constant model. The correlation with host galaxy mass in the optical is degraded with this addition showing a reduced 0.14 ± 0.05 mag for the best fit step, whose location has not changed. The AIC_c prefers the step function while the BIC is inconclusive but close to preferring the constant model. Adding additional intrinsic error removes the significance for both NIR and optical lightcurves but does not affect the location of the break in the NIR or optical.

5.5. Are the NIR Residuals Adding More Information to the Optical Residuals?

Is the NIR analysis an independent test of host galaxy correlations or degenerate with the tests done at optical wavelengths? Figure 13 presents the H_{\max} residuals plotted against the μ residuals.

One source of potential correlation is a mis-estimate of the cosmological redshift for a supernova. If we use the wrong cosmological redshift for an object, we would expect to see strong correlations between the optical and NIR

brightnesses due to using the wrong cosmological redshift rather than due to any intrinsic physics about the supernova. In particular, the lower redshift supernovae ($z < 0.02$) are affected by larger peculiar velocities. In Table 11, we present the mean, weighted mean, standard error on the mean, standard deviation and Pearson correlation coefficient (r) for the full sample and if the sample was split at $z = 0.02$. The samples of $z < 0.02$ and > 0.02 show the same properties and similar correlation coefficients, which indicates that the correlation between optical and NIR supernovae are not driven by peculiar velocities.

The optical and H Hubble residuals are clearly and strongly correlated. This is not a surprise as effectively similar relationships are found when considering large sets of lightcurves in training lightcurve fitters. But we here we have answered the question from a data-driven exploration with Hubble residuals directly from a significant selection of supernovae not involved in the construction of the SNooPy templates.

5.6. Direction of the H versus Optical Correlation

The trend we observed in the H -band peak magnitudes is that larger galaxies, which are also more red and more likely to be ellipticals, host brighter supernova than lower mass galaxies, which are bluer and more likely spirals. This correlation is the opposite of the trend observed in uncorrected optical brightness. Hamuy et al. (1995) first found that galaxies with a younger stellar population hosted brighter supernova. Continued works such as Hamuy et al. (1996) and Sullivan et al. (2006) found correlations with the lightcurve shape parameters Δm_B and stretch s , respectively, where faster declining (dimmer) SNeIa were hosted in elliptical and higher-mass galaxies whereas slower declining (brighter) SNeIa were hosted in spiral and lower-mass galaxies. All subsequent analyses have found a correlation between host galaxy properties and the shape of the width of the lightcurve. However, after width-luminosity standardization, the correlation with host galaxy properties for optical SNeIa switches such that larger mass galaxies have brighter residuals than lower mass galaxies.

We find an H -band correlation with host galaxy stellar mass opposite to the that in the optical.

5.7. Comparison to Burns et al. (2018)

We measured a 3.6σ correlation between H_{\max} residuals and host galaxy mass which dropped to 2.5σ (at the best-fit step break) when removing the outliers. These results are in contrast to Burns et al. (2018) who found a smaller 2σ correlation between B -band lightcurves and host galaxy mass and a $\sim 1\sigma$ correlation in H -band. However, they fit a straight line to the Hubble residuals versus host galaxy mass which we showed here produce a less significant result and is less preferred compared to using a step function. But a key difference is that the sample considered in Burns et al. (2018) had substantially fewer lower-mass galaxies, and was thus inherently less sensitive to any mass step. Our linear correlation has a slope of 0.08 ± 0.03 mag ($\log M_\odot$) $^{-1}$ which is in agreement with the linear correlation they found of 0.04 ± 0.03 mag ($\log M_\odot$) $^{-1}$. If we reduce our sample size to only CSP SNeIa, we recover a linear relationship consistent with zero and none of the ICs prefer a non-constant model.

Brout & Scolnic (2020) claim that the host galaxy stellar mass dependence seen at optical wavelengths is due to the correlation of dust in different galaxies. Because NIR is less sensitive to dust, we should not see any significant correlations between the NIR residuals and host galaxy mass if the correlation is driven by dust. The Burns et al. (2018) results support this finding; however, our results do not support this hypothesis. Without the outlier population, the H band residual step is 0.11 mag compared to the 0.17 mag in the optical (at the best fit step break) indicating that some of the correlation may be due to dust but not all of the correlation.

6. CONCLUSION

We have collected and analyzed a data sample of 231 SNeIa with observations in the restframe H -band. We fit the lightcurves using SNooPy, and found 144 of the SNeIa had lightcurve fits suitable for inclusion in a Hubble diagram. We combined measurements from SDSS, 2MASS, and GALEX to determine photometric stellar masses for the host galaxies of 99 of these 144 SNeIa.

We explored possible correlations between H_{\max} residuals from the SNooPy fitter and host galaxy properties. Though we only presented the results from host galaxy stellar mass in the main text, further studies are presented in Appendix A. Using the 99 SNeIa with host galaxy stellar mass measurements, we report a 0.18 ± 0.05 mag step at $10^{10.44} M_\odot$ in agreement with the step seen at optical wavelengths. The AIC_c and BIC also prefer this step function over a constant model. By further investigating the sample, we have shown that the correlation with H -band brightnesses is partially driven by outliers and removing these from the sample lowers the significance of the step to 2.5σ at

$10^{10.44} M_{\odot}$, but the ICs do not have a strong preference the step function over a constant model. SNeIa are intrinsically brighter in H in more massive galaxies.

Using the optical lightcurves corresponding to the sample of NIR lightcurves, we have confirmed a host galaxy mass step of ~ 0.1 mag around $10^{10} M_{\odot}$. We have further shown that the observed step in standardized optical brightness as a function of host galaxy stellar mass persists after removing the outlier population. Showing this trend using a third lightcurve fitter provides further evidence of either a physical phenomenon or that there is some intrinsic property that is not well understood in optical wavelengths.

The correlation found between H -band residuals and host galaxy mass is the opposite correlation seen with optical residuals. In the NIR, high-mass galaxies host brighter SNeIa than low-mass galaxies, but in optical wavelengths the *uncorrected* residuals show that brighter SNeIa are hosted in lower-mass galaxies. But after correction for stretch and color, the correlation of optical Hubble residuals goes the other way, with more negative Hubble residuals in more massive galaxies.

If the cause of the host galaxy mass trend is dust, metallicity (Tremonti et al. 2004), or stellar population age, then we would expect to see no correlation in the NIR since SNeIa in the NIR are less sensitive to dust, progenitor metallicity (Kasen 2006), and progenitor age¹³. Because we do recover a significant correlation in the NIR, we disagree that dust is a favored driver of the optical host-galaxy mass correlation as previously reported in Burns et al. (2018) and Brout & Scolnic (2020). We suggest that is more likely that the step in host galaxy stellar mass is due to differences in the nature of progenitor systems in different environments.

This analysis has concluded that SNeIa in the H -band currently show convincing evidence of correlations with host galaxy stellar mass. With more data from ground based studies imminent (CSP II and SweetSpot), we will be able to increase the sample size to test for the correlations again and to determine if there is a correlation or if there is a persistent outlier population. Now is the time to examine these relationships in low redshift NIR lightcurve data to improve our NIR models in preparation for the $\sim 2,500$ high-redshift NIR SNeIa that will be observed by Nancy Grace Roman Space Telescope (Spergel et al. 2015).

ACKNOWLEDGMENTS

K.A.P., M.W.-V., and L.G. were supported in part by the US National Science Foundation under Grant AST-1311862. K.A.P. additionally acknowledges support from PITT PACC. K.A.P. was also supported in part by the Berkeley Center for Cosmological Physics and the Director, Office of Science, Office of High Energy Physics of the U.S. Department of Energy under Contract No. DE-AC02-05CH11231. L.G. was additionally funded in part by the European Union’s Horizon 2020 research and innovation programme under the Marie Skłodowska-Curie grant agreement No. 839090.

We thank Saurabh Jha, Kyle Boone, and Ravi Gupta for useful conversations.

This research has made use of the The NASA/IPAC Extragalactic Database (NED) which is funded by the National Aeronautics and Space Administration and operated by the California Institute of Technology.

Funding for the Sloan Digital Sky Survey IV has been provided by the Alfred P. Sloan Foundation, the U.S. Department of Energy Office of Science, and the Participating Institutions. SDSS-IV acknowledges support and resources from the Center for High-Performance Computing at the University of Utah. The SDSS web site is www.sdss.org.

SDSS-IV is managed by the Astrophysical Research Consortium for the Participating Institutions of the SDSS Collaboration including the Brazilian Participation Group, the Carnegie Institution for Science, Carnegie Mellon University, the Chilean Participation Group, the French Participation Group, Harvard-Smithsonian Center for Astrophysics, Instituto de Astrofísica de Canarias, The Johns Hopkins University, Kavli Institute for the Physics and Mathematics of the Universe (IPMU) / University of Tokyo, Lawrence Berkeley National Laboratory, Leibniz Institut für Astrophysik Potsdam (AIP), Max-Planck-Institut für Astronomie (MPIA Heidelberg), Max-Planck-Institut für Astrophysik (MPA Garching), Max-Planck-Institut für Extraterrestrische Physik (MPE), National Astronomical Observatories of China, New Mexico State University, New York University, University of Notre Dame, Observatório Nacional / MCTI, The Ohio State University, Pennsylvania State University, Shanghai Astronomical Observatory, United Kingdom Participation Group, Universidad Nacional Autónoma de México, University of Arizona, University of Colorado Boulder,

¹³ Initial mass of ^{56}Ni is linked to progenitor age (Howell et al. 2009) and SNeIa in the NIR are less affected by ^{56}Ni mass (Kasen 2006).

University of Oxford, University of Portsmouth, University of Utah, University of Virginia, University of Washington, University of Wisconsin, Vanderbilt University, and Yale University.

This publication makes use of data products from the Two Micron All Sky Survey, which is a joint project of the University of Massachusetts and the Infrared Processing and Analysis Center/California Institute of Technology, funded by the National Aeronautics and Space Administration and the National Science Foundation.

This research has made use of the NASA/IPAC Infrared Science Archive, which is operated by the Jet Propulsion Laboratory, California Institute of Technology, under contract with the National Aeronautics and Space Administration.

Some of the data presented in this paper were obtained from the Mikulski Archive for Space Telescopes (MAST). STScI is operated by the Association of Universities for Research in Astronomy, Inc., under NASA contract NAS5-26555. Support for MAST for non-HST data is provided by the NASA Office of Space Science via grant NNX09AF08G and by other grants and contracts.

Software: Python¹⁴, NumPy¹⁵, SciPy¹⁶, matplotlib (Hunter 2007)¹⁷, AstroPy (Astropy Collaboration et al. 2013)¹⁸, IDL¹⁹

APPENDIX

A. OTHER EXPLORED CORRELATIONS

We ran the same analysis from Section 4.1 on many different host properties including absolute r -band magnitude (M_r), $g-r$ color, galaxy morphology, NUV colors, smooth Hubble flow, and distance from the host galaxy. The M_r and $g-r$ color properties exhibited $\sim 2 - 3 \sigma$ correlations with the Hubble residuals, so we continued those two properties through every analysis step. However, no significant correlation was found with these host galaxy properties, but we include summaries of the findings here for completeness.

A.1. Absolute r -band Magnitude

The restframe absolute r -band magnitude shows a similar correlation as with host galaxy mass for the distributions. We define a “bright” and “dim” population with a threshold at between them at $r = -21.0$ mag, which was chosen to correspond with the typical brightness of a galaxy with mass $\sim 10^{10} M_\odot$. The outlier population found in mostly high mass and red galaxies is present here as well in the bright population. The weighted means of the distributions for NIR result in $< 3 \sigma$ detection and the optical residuals result in $< 1 \sigma$ detection.

We used 57 H_{\max} and 38 μ residuals to test the functional form of correlations with the restframe, absolute r -band magnitude, M_r . When fitting the step function with a floating break, we limited the range to $-21.9 < M_r < -18.4$ mag to ensure each bin had at least 20% of the total SNeIa. The model that most favors a correlation with the H_{\max} residuals is the best-fit step function with a break at -21.2 mag. The size of the best-fit step is 0.32 ± 0.08 mag, a 4σ detection, with the ICs both exhibiting a large preference for the step function. The distance modulus residuals show a large preference towards a break at -20.25 mag with an amplitude of 0.15 ± 0.05 mag. The AIC_c is around -2 and the BIC around 1 showing some preference for this step but not a large one.

We then ran the same sample changes presented in Section 5. If the outlier population is removed, H_{\max} correlations are degraded with the best-fit step function retaining a $\sim 3 \sigma$ detection but the break is moved to $M_r = -18.85$ mag. The location of the break is shifted to the edge of our parameter space indicating the outlier SNeIa had a large effect on the M_r fits and we do not have a correlation in M_r . Without the outliers, the μ residuals still prefer a step at -20.25 mag with a slight degradation of the significance of the step down to 2.8σ . For the joint sample, the H_{\max} residuals move the break down to -18.85 mag with a $> 3 \sigma$ step indicating there most likely is not a step in this sample. The joint sample for optical residuals showed a 2.8σ step function correlation with a break at -20.25 mag, but the ICs showed no model preference. We do not recover a correlation for either NIR or optical residuals in the joint sample. When adding intrinsic error the step location for H_{\max} residuals is again at -21.2 mag with a $\sim 2.7 \sigma$

¹⁴ <http://python.org>

¹⁵ <http://www.numpy.org>

¹⁶ <http://www.scipy.org>

¹⁷ <http://matplotlib.org>

¹⁸ <http://www.astropy.org>

¹⁹ <http://www.harrisgeospatial.com/ProductsandSolutions/GeospatialProducts/IDL.aspx>

step but the ICs are split between a preference for the step function and a constant model. Adding additional error to the optical sample moves the best fit step location to -18.85 mag, has a $< 2 \sigma$ correlation, and the ICs favor a constant model resulting there is no correlation in this sample.

The results for the H -band are driven by the outlier population and the optical SNeIa do not conclusively support a M_r correlation.

A.2. Other Correlations

Other correlations that we tested are:

- **Restframe $g - r$ Color:** No significant correlation was found in either the NIR or optical using 57 and 37 objects, respectively. Our initial study of $g - r$ color returned a $\sim 3 \sigma$ correlation when comparing the distribution parameters from Section 4.1. Once we ran the full analysis with this property, we found that this correlation was driven by the outlier SNeIa. There were two objects from the outlier population with $g - r$ colors and both were in red galaxies with $g - r > 0.6$ mag. We found no correlations when running the analysis from Section 4.2.
- **Galaxy Morphology:** We use two methods to separate galaxies based on their morphology: the inverse concentration index (Strateva et al. 2001; Shimasaku et al. 2001) and the ratio of the likelihoods for a de Vaucouleurs versus Exponential profile fit to the surface brightness. Using 47 galaxies, we recovered no correlation with galaxy morphology.
- **Smooth Hubble Flow:** We tested the effects of using SNe with $z > 0.02$ corresponding to the smooth Hubble Flow. This cut reduced our sample size by half and produced the same results as the full sample. Table 5 includes the results of using only Hubble flow SNeIa for three different host galaxy properties, and they are all labeled starting with “Hubble”. The distributions of residuals of SNeIa with $z < 0.02$ in mass, color, and M_r are the same as the distributions of SNeIa residuals with $z > 0.02$. Therefore, we find no evidence for evolution with redshift. The one exception is the outlier group of SNeIa hosted in red, bright, high mass galaxies which only appear at $z > 0.03$, but there are so few of them it is unclear if this is a real trend or a coincidence of small sample size.
- **NUV colors:** By using $NUV - H$, we are picking out young, blue stars versus old, red stars, which should act as a tracer for recent star formation. We found that the SN Ia Hubble residuals versus $NUV - H$ color histograms are mostly identical in scatter with a negligible offset. $NUV - g$ exhibits the same distribution.
- **Distance from host galaxy:** We found no discernible correlation in projected distances of supernovae from their host galaxies, except for the outlier population which are all very separated from their host galaxy.

REFERENCES

- Abazajian, K. N., Adelman-McCarthy, J. K., Agüeros, M. A., et al. 2009, ApJS, 182, 543, doi: [10.1088/0067-0049/182/2/543](https://doi.org/10.1088/0067-0049/182/2/543)
- Abbott, T. M. C., Allam, S., Andersen, P., et al. 2019, ApJ, 872, L30, doi: [10.3847/2041-8213/ab04fa](https://doi.org/10.3847/2041-8213/ab04fa)
- Adelman-McCarthy, J. K., Agüeros, M. A., Allam, S. S., et al. 2006, ApJS, 162, 38, doi: [10.1086/497917](https://doi.org/10.1086/497917)
- Akaike, H. 1974, IEEE Transactions on Automatic Control, 19, 716
- Arnouts, S., Cristiani, S., Moscardini, L., et al. 1999, MNRAS, 310, 540, doi: [10.1046/j.1365-8711.1999.02978.x](https://doi.org/10.1046/j.1365-8711.1999.02978.x)
- Astropy Collaboration, Robitaille, T. P., Tollerud, E. J., et al. 2013, A&A, 558, A33, doi: [10.1051/0004-6361/201322068](https://doi.org/10.1051/0004-6361/201322068)
- Avelino, A., Friedman, A. S., Mandel, K. S., et al. 2019, arXiv e-prints, arXiv:1902.03261, <https://arxiv.org/abs/1902.03261>
- Barone-Nugent, R. L., Lidman, C., Wyithe, J. S. B., et al. 2012, MNRAS, 425, 1007, doi: [10.1111/j.1365-2966.2012.21412.x](https://doi.org/10.1111/j.1365-2966.2012.21412.x)
- Bernardi, M., Shankar, F., Hyde, J. B., et al. 2010, MNRAS, 404, 2087, doi: [10.1111/j.1365-2966.2010.16425.x](https://doi.org/10.1111/j.1365-2966.2010.16425.x)
- Bertin, E., & Arnouts, S. 1996, A&AS, 117, 393, doi: [10.1051/aas:1996164](https://doi.org/10.1051/aas:1996164)
- Betoule, M., Kessler, R., Guy, J., et al. 2014, A&A, 568, A22, doi: [10.1051/0004-6361/201423413](https://doi.org/10.1051/0004-6361/201423413)

- Bianchi, L., Conti, A., & Shiao, B. 2014, Advances in Space Research, 53, 900, doi: [10.1016/j.asr.2013.07.045](https://doi.org/10.1016/j.asr.2013.07.045)
- Blanton, M. R., & Roweis, S. 2007, AJ, 133, 734, doi: [10.1086/510127](https://doi.org/10.1086/510127)
- Blanton, M. R., Brinkmann, J., Csabai, I., et al. 2003, AJ, 125, 2348, doi: [10.1086/342935](https://doi.org/10.1086/342935)
- Brout, D., & Scolnic, D. 2020, arXiv e-prints, arXiv:2004.10206. <https://arxiv.org/abs/2004.10206>
- Brout, D., Scolnic, D., Kessler, R., et al. 2019, ApJ, 874, 150, doi: [10.3847/1538-4357/ab08a0](https://doi.org/10.3847/1538-4357/ab08a0)
- Bruzual, G., & Charlot, S. 2003, MNRAS, 344, 1000, doi: [10.1046/j.1365-8711.2003.06897.x](https://doi.org/10.1046/j.1365-8711.2003.06897.x)
- Burns, C. R., Stritzinger, M., Phillips, M. M., et al. 2011, AJ, 141, 19, doi: [10.1088/0004-6256/141/1/19](https://doi.org/10.1088/0004-6256/141/1/19)
- . 2014, ApJ, 789, 32, doi: [10.1088/0004-637X/789/1/32](https://doi.org/10.1088/0004-637X/789/1/32)
- Burns, C. R., Parent, E., Phillips, M. M., et al. 2018, ApJ, 869, 56, doi: [10.3847/1538-4357/aae51c](https://doi.org/10.3847/1538-4357/aae51c)
- Campbell, H., Fraser, M., & Gilmore, G. 2016, MNRAS, 457, 3470, doi: [10.1093/mnras/stw115](https://doi.org/10.1093/mnras/stw115)
- Candia, P., Krisciunas, K., Suntzeff, N. B., et al. 2003, PASP, 115, 277, doi: [10.1086/368229](https://doi.org/10.1086/368229)
- Chabrier, G. 2003, PASP, 115, 763, doi: [10.1086/376392](https://doi.org/10.1086/376392)
- Childress, M., Aldering, G., Antilogus, P., et al. 2013a, ApJ, 770, 107, doi: [10.1088/0004-637X/770/2/107](https://doi.org/10.1088/0004-637X/770/2/107)
- . 2013b, ApJ, 770, 108, doi: [10.1088/0004-637X/770/2/108](https://doi.org/10.1088/0004-637X/770/2/108)
- Contreras, C., Hamuy, M., Phillips, M. M., et al. 2010, AJ, 139, 519, doi: [10.1088/0004-6256/139/2/519](https://doi.org/10.1088/0004-6256/139/2/519)
- Cuadra, J., Suntzeff, N. B., Candia, P., Krisciunas, K., & Phillips, M. M. 2002, in Revista Mexicana de Astronomia y Astrofisica Conference Series, Vol. 14, Revista Mexicana de Astronomia y Astrofisica Conference Series, ed. J. J. Claria, D. Garcia Lambas, & H. Levato, 121–121
- D’Andrea, C. B., Gupta, R. R., Sako, M., et al. 2011, ApJ, 743, 172, doi: [10.1088/0004-637X/743/2/172](https://doi.org/10.1088/0004-637X/743/2/172)
- Dark Energy Survey Collaboration, Abbott, T., Abdalla, F. B., et al. 2016, MNRAS, 460, 1270, doi: [10.1093/mnras/stw641](https://doi.org/10.1093/mnras/stw641)
- Dhawan, S., Jha, S. W., & Leibundgut, B. 2018, A&A, 609, A72, doi: [10.1051/0004-6361/201731501](https://doi.org/10.1051/0004-6361/201731501)
- Elias-Rosa, N., Benetti, S., Cappellaro, E., et al. 2006, MNRAS, 369, 1880, doi: [10.1111/j.1365-2966.2006.10430.x](https://doi.org/10.1111/j.1365-2966.2006.10430.x)
- Elias-Rosa, N., Benetti, S., Turatto, M., et al. 2008, MNRAS, 384, 107, doi: [10.1111/j.1365-2966.2007.12638.x](https://doi.org/10.1111/j.1365-2966.2007.12638.x)
- Fioc, M., & Rocca-Volmerange, B. 1997, A&A, 500, 507. <https://arxiv.org/abs/astro-ph/9707017>
- . 1999, arXiv e-prints, astro. <https://arxiv.org/abs/astro-ph/9912179>
- Folatelli, G., Phillips, M. M., Burns, C. R., et al. 2010, AJ, 139, 120, doi: [10.1088/0004-6256/139/1/120](https://doi.org/10.1088/0004-6256/139/1/120)
- Foley, R. J., Challis, P. J., Chornock, R., et al. 2013, ApJ, 767, 57, doi: [10.1088/0004-637X/767/1/57](https://doi.org/10.1088/0004-637X/767/1/57)
- Freedman, W. L., Madore, B. F., Gibson, B. K., et al. 2001, ApJ, 553, 47, doi: [10.1086/320638](https://doi.org/10.1086/320638)
- Friedman, A. S., Wood-Vasey, W. M., Marion, G. H., et al. 2015, ApJS, 220, 9, doi: [10.1088/0067-0049/220/1/9](https://doi.org/10.1088/0067-0049/220/1/9)
- Galbany, L., Collett, T. E., Méndez-Abreu, J., et al. 2018, MNRAS, 479, 262, doi: [10.1093/mnras/sty1448](https://doi.org/10.1093/mnras/sty1448)
- Gallagher, J. S., Garnavich, P. M., Caldwell, N., et al. 2008, ApJ, 685, 752, doi: [10.1086/590659](https://doi.org/10.1086/590659)
- Guillochon, J., Parrent, J., Kelley, L. Z., & Margutti, R. 2017, ApJ, 835, 64, doi: [10.3847/1538-4357/835/1/64](https://doi.org/10.3847/1538-4357/835/1/64)
- Gupta, R. R., D’Andrea, C. B., Sako, M., et al. 2011, ApJ, 740, 92, doi: [10.1088/0004-637X/740/2/92](https://doi.org/10.1088/0004-637X/740/2/92)
- Guy, J., Astier, P., Baumont, S., et al. 2007, A&A, 466, 11, doi: [10.1051/0004-6361:20066930](https://doi.org/10.1051/0004-6361:20066930)
- Hamuy, M., Phillips, M. M., Maza, J., et al. 1995, AJ, 109, 1, doi: [10.1086/117251](https://doi.org/10.1086/117251)
- Hamuy, M., Phillips, M. M., Suntzeff, N. B., et al. 1996, AJ, 112, 2391, doi: [10.1086/118190](https://doi.org/10.1086/118190)
- Hayden, B. T., Gupta, R. R., Garnavich, P. M., et al. 2013, ApJ, 764, 191, doi: [10.1088/0004-637X/764/2/191](https://doi.org/10.1088/0004-637X/764/2/191)
- Hernandez, M., Meikle, W. P. S., Aparicio, A., et al. 2000, MNRAS, 319, 223
- Howell, D. A., Sullivan, M., Brown, E. F., et al. 2009, ApJ, 691, 661, doi: [10.1088/0004-637X/691/1/661](https://doi.org/10.1088/0004-637X/691/1/661)
- Hsiao, E. Y., Conley, A., Howell, D. A., et al. 2007, ApJ, 663, 1187, doi: [10.1086/518232](https://doi.org/10.1086/518232)
- Hsiao, E. Y., Marion, G. H., Phillips, M. M., et al. 2013, ApJ, 766, 72, doi: [10.1088/0004-637X/766/2/72](https://doi.org/10.1088/0004-637X/766/2/72)
- Hsiao, E. Y., Burns, C. R., Contreras, C., et al. 2015, A&A, 578, A9, doi: [10.1051/0004-6361/201425297](https://doi.org/10.1051/0004-6361/201425297)
- Hunter, J. D. 2007, Computing In Science & Engineering, 9, 90
- Ilbert, O., Arnouts, S., McCracken, H. J., et al. 2006, A&A, 457, 841, doi: [10.1051/0004-6361:20065138](https://doi.org/10.1051/0004-6361:20065138)
- Jha, S., Riess, A. G., & Kirshner, R. P. 2007, ApJ, 659, 122, doi: [10.1086/512054](https://doi.org/10.1086/512054)
- Jha, S., Garnavich, P. M., Kirshner, R. P., et al. 1999, ApJS, 125, 73, doi: [10.1086/313275](https://doi.org/10.1086/313275)
- Jha, S. W., Avelino, A., Burns, C., et al. 2019, Supernovae in the Infrared avec Hubble, HST Proposal
- Johansson, J., Thomas, D., Pforr, J., et al. 2013, MNRAS, 435, 1680, doi: [10.1093/mnras/stt1408](https://doi.org/10.1093/mnras/stt1408)
- Jones, D. O., Riess, A. G., & Scolnic, D. M. 2015, ArXiv e-prints. <https://arxiv.org/abs/1506.02637>
- Jones, D. O., Riess, A. G., Scolnic, D. M., et al. 2018, ApJ, 867, 108, doi: [10.3847/1538-4357/aae2b9](https://doi.org/10.3847/1538-4357/aae2b9)

- Kasen, D. 2006, ApJ, 649, 939, doi: [10.1086/506588](https://doi.org/10.1086/506588)
- Kattner, S., Leonard, D. C., Burns, C. R., et al. 2012, PASP, 124, 114, doi: [10.1086/664734](https://doi.org/10.1086/664734)
- Kauffmann, G., Heckman, T. M., White, S. D. M., et al. 2003, MNRAS, 341, 33, doi: [10.1046/j.1365-8711.2003.06291.x](https://doi.org/10.1046/j.1365-8711.2003.06291.x)
- Kelly, P. L., Filippenko, A. V., Burke, D. L., et al. 2015, Science, 347, 1459, doi: [10.1126/science.1261475](https://doi.org/10.1126/science.1261475)
- Kelly, P. L., Hicken, M., Burke, D. L., Mandel, K. S., & Kirshner, R. P. 2010, ApJ, 715, 743, doi: [10.1088/0004-637X/715/2/743](https://doi.org/10.1088/0004-637X/715/2/743)
- Kessler, R., & Scolnic, D. 2017, ApJ, 836, 56, doi: [10.3847/1538-4357/836/1/56](https://doi.org/10.3847/1538-4357/836/1/56)
- Kim, A. G., Thomas, R. C., Aldering, G., et al. 2013, ApJ, 766, 84, doi: [10.1088/0004-637X/766/2/84](https://doi.org/10.1088/0004-637X/766/2/84)
- Kim, A. G., Aldering, G., Antilogus, P., et al. 2014, ApJ, 784, 51, doi: [10.1088/0004-637X/784/1/51](https://doi.org/10.1088/0004-637X/784/1/51)
- Kirshner, R. P. 2012, RAISIN: Tracers of cosmic expansion with SN IA in the IR HST Proposal 13046. http://archive.stsci.edu/proposal_search.php?id=13046&mission=hst
- Krisciunas, K., Hastings, N. C., Loomis, K., et al. 2000, ApJ, 539, 658, doi: [10.1086/309263](https://doi.org/10.1086/309263)
- Krisciunas, K., Phillips, M. M., & Suntzeff, N. B. 2004a, ApJL, 602, L81, doi: [10.1086/382731](https://doi.org/10.1086/382731)
- Krisciunas, K., Suntzeff, N. B., Candia, P., et al. 2003, AJ, 125, 166, doi: [10.1086/345571](https://doi.org/10.1086/345571)
- Krisciunas, K., Phillips, M. M., Suntzeff, N. B., et al. 2004b, AJ, 127, 1664
- Krisciunas, K., Suntzeff, N. B., Phillips, M. M., et al. 2004c, AJ, 128, 3034, doi: [10.1086/425629](https://doi.org/10.1086/425629)
- Krisciunas, K., Garnavich, P. M., Stanishev, V., et al. 2007, AJ, 133, 58, doi: [10.1086/509126](https://doi.org/10.1086/509126)
- Krisciunas, K., Marion, G. H., Suntzeff, N. B., et al. 2009, AJ, 138, 1584, doi: [10.1088/0004-6256/138/6/1584](https://doi.org/10.1088/0004-6256/138/6/1584)
- Krisciunas, K., Contreras, C., Burns, C. R., et al. 2017, AJ, 154, 211, doi: [10.3847/1538-3881/aa8df0](https://doi.org/10.3847/1538-3881/aa8df0)
- Kroupa, P. 2001, MNRAS, 322, 231, doi: [10.1046/j.1365-8711.2001.04022.x](https://doi.org/10.1046/j.1365-8711.2001.04022.x)
- Lampeitl, H., Smith, M., Nichol, R. C., et al. 2010, ApJ, 722, 566, doi: [10.1088/0004-637X/722/1/566](https://doi.org/10.1088/0004-637X/722/1/566)
- Leloudas, G., Stritzinger, M. D., Sollerman, J., et al. 2009, A&A, 505, 265, doi: [10.1051/0004-6361/200912364](https://doi.org/10.1051/0004-6361/200912364)
- Magee, M. R., Kotak, R., Sim, S. A., et al. 2016, A&A, 589, A89, doi: [10.1051/0004-6361/201528036](https://doi.org/10.1051/0004-6361/201528036)
- Marion, G. H., Sand, D. J., Hsiao, E. Y., et al. 2015, ApJ, 798, 39, doi: [10.1088/0004-637X/798/1/39](https://doi.org/10.1088/0004-637X/798/1/39)
- McGaugh, S. S., & Schombert, J. M. 2014, AJ, 148, 77, doi: [10.1088/0004-6256/148/5/77](https://doi.org/10.1088/0004-6256/148/5/77)
- Moreno-Raya, M. E., Mollá, M., López-Sánchez, Á. R., et al. 2016, ApJL, 818, L19, doi: [10.3847/2041-8205/818/1/L19](https://doi.org/10.3847/2041-8205/818/1/L19)
- Moustakas, J., Coil, A. L., Aird, J., et al. 2013, ApJ, 767, 50, doi: [10.1088/0004-637X/767/1/50](https://doi.org/10.1088/0004-637X/767/1/50)
- Pastorello, A., Mazzali, P. A., Pignata, G., et al. 2007a, MNRAS, 377, 1531, doi: [10.1111/j.1365-2966.2007.11700.x](https://doi.org/10.1111/j.1365-2966.2007.11700.x)
- Pastorello, A., Taubenberger, S., Elias-Rosa, N., et al. 2007b, MNRAS, 376, 1301, doi: [10.1111/j.1365-2966.2007.11527.x](https://doi.org/10.1111/j.1365-2966.2007.11527.x)
- Perlmutter, S., Aldering, G., Goldhaber, G., et al. 1999, ApJ, 517, 565, doi: [10.1086/307221](https://doi.org/10.1086/307221)
- Phillips, M. M. 1993, ApJL, 413, L105, doi: [10.1086/186970](https://doi.org/10.1086/186970)
- Phillips, M. M., Krisciunas, K., Suntzeff, N. B., et al. 2006, AJ, 131, 2615, doi: [10.1086/503108](https://doi.org/10.1086/503108)
- Phillips, M. M., Li, W., Frieman, J. A., et al. 2007, PASP, 119, 360, doi: [10.1086/518372](https://doi.org/10.1086/518372)
- Phillips, M. M., Contreras, C., Hsiao, E. Y., et al. 2019, Publications of the Astronomical Society of the Pacific, 131, 014001, doi: [10.1088/1538-3873/aae8bd](https://doi.org/10.1088/1538-3873/aae8bd)
- Pignata, G., Maza, J., Hamuy, M., et al. 2008, Central Bureau Electronic Telegrams, 1545
- Polletta, M., Tajer, M., Maraschi, L., et al. 2007, ApJ, 663, 81, doi: [10.1086/518113](https://doi.org/10.1086/518113)
- Rana, N. C., & Basu, S. 1992, A&A, 265, 499
- Rest, A., Scolnic, D., Foley, R. J., et al. 2014, ApJ, 795, 44, doi: [10.1088/0004-637X/795/1/44](https://doi.org/10.1088/0004-637X/795/1/44)
- Riess, A. G., Press, W. H., & Kirshner, R. P. 1996, ApJ, 473, 88, doi: [10.1086/178129](https://doi.org/10.1086/178129)
- Riess, A. G., Filippenko, A. V., Challis, P., et al. 1998, AJ, 116, 1009, doi: [10.1086/300499](https://doi.org/10.1086/300499)
- Rigault, M., Copin, Y., Aldering, G., et al. 2013, A&A, 560, A66, doi: [10.1051/0004-6361/201322104](https://doi.org/10.1051/0004-6361/201322104)
- Rigault, M., Aldering, G., Kowalski, M., et al. 2015, ApJ, 802, 20, doi: [10.1088/0004-637X/802/1/20](https://doi.org/10.1088/0004-637X/802/1/20)
- Rigault, M., Brinnel, V., Aldering, G., et al. 2018, arXiv e-prints, arXiv:1806.03849. <https://arxiv.org/abs/1806.03849>
- Roman, M., Hardin, D., Betoule, M., et al. 2018, A&A, 615, A68, doi: [10.1051/0004-6361/201731425](https://doi.org/10.1051/0004-6361/201731425)
- Rose, B. M., Garnavich, P. M., & Berg, M. A. 2019, ApJ, 874, 32, doi: [10.3847/1538-4357/ab0704](https://doi.org/10.3847/1538-4357/ab0704)
- Schwarz, G. 1978, Ann. Statist., 6, 461, doi: [10.1214/aos/1176344136](https://doi.org/10.1214/aos/1176344136)
- Scolnic, D., Rest, A., Riess, A., et al. 2014, ApJ, 795, 45, doi: [10.1088/0004-637X/795/1/45](https://doi.org/10.1088/0004-637X/795/1/45)
- Scolnic, D. M., Jones, D. O., Rest, A., et al. 2018, ApJ, 859, 101, doi: [10.3847/1538-4357/aab9bb](https://doi.org/10.3847/1538-4357/aab9bb)

- SDSS Collaboration, Albareti, F. D., Allende Prieto, C., et al. 2016, ArXiv e-prints.
<https://arxiv.org/abs/1608.02013>
- Shimasaku, K., Fukugita, M., Doi, M., et al. 2001, AJ, 122, 1238, doi: [10.1086/322094](https://doi.org/10.1086/322094)
- Skrutskie, M. F., Cutri, R. M., Stiening, R., et al. 2006, AJ, 131, 1163, doi: [10.1086/498708](https://doi.org/10.1086/498708)
- Smith, M., Sullivan, M., Wiseman, P., et al. 2020, MNRAS, 494, 4426, doi: [10.1093/mnras/staa946](https://doi.org/10.1093/mnras/staa946)
- Sollerman, J., Lindahl, J., Kozma, C., et al. 2004, A&A, 428, 555, doi: [10.1051/0004-6361:20041320](https://doi.org/10.1051/0004-6361:20041320)
- Spergel, D., Gehrels, N., Baltay, C., et al. 2015, ArXiv e-prints. <https://arxiv.org/abs/1503.03757>
- Stanishev, V., Goobar, A., Benetti, S., et al. 2007, A&A, 469, 645, doi: [10.1051/0004-6361:20066020](https://doi.org/10.1051/0004-6361:20066020)
- Stanishev, V., Goobar, A., Amanullah, R., et al. 2018, A&A, 615, A45, doi: [10.1051/0004-6361/201732357](https://doi.org/10.1051/0004-6361/201732357)
- Stoughton, C., Lupton, R. H., Bernardi, M., et al. 2002, AJ, 123, 485, doi: [10.1086/324741](https://doi.org/10.1086/324741)
- Strateva, I., Ivezić, Ž., Knapp, G. R., et al. 2001, AJ, 122, 1861, doi: [10.1086/323301](https://doi.org/10.1086/323301)
- Stritzinger, M. D., Phillips, M. M., Boldt, L. N., et al. 2011, AJ, 142, 156, doi: [10.1088/0004-6256/142/5/156](https://doi.org/10.1088/0004-6256/142/5/156)
- Stritzinger, M. D., Hsiao, E., Valenti, S., et al. 2014, A&A, 561, A146, doi: [10.1051/0004-6361/201322889](https://doi.org/10.1051/0004-6361/201322889)
- Stritzinger, M. D., Valenti, S., Hoeflich, P., et al. 2015, A&A, 573, A2, doi: [10.1051/0004-6361/201424168](https://doi.org/10.1051/0004-6361/201424168)
- Sugiura, N. 1978, Commun. Stat. A-Theor., 7, 13
- Sullivan, M., Le Borgne, D., Pritchett, C. J., et al. 2006, ApJ, 648, 868, doi: [10.1086/506137](https://doi.org/10.1086/506137)
- Sullivan, M., Conley, A., Howell, D. A., et al. 2010, MNRAS, 406, 782, doi: [10.1111/j.1365-2966.2010.16731.x](https://doi.org/10.1111/j.1365-2966.2010.16731.x)
- Tremonti, C. A., Heckman, T. M., Kauffmann, G., et al. 2004, ApJ, 613, 898, doi: [10.1086/423264](https://doi.org/10.1086/423264)
- Tripp, R. 1998, A&A, 331, 815
- Uddin, S. A., Mould, J., & Wang, L. 2017, ApJ, 850, 135, doi: [10.3847/1538-4357/aa93e9](https://doi.org/10.3847/1538-4357/aa93e9)
- Valentini, G., Di Carlo, E., Massi, F., et al. 2003, ApJ, 595, 779, doi: [10.1086/377448](https://doi.org/10.1086/377448)
- Weyant, A., Wood-Vasey, W. M., Allen, L., et al. 2014, ApJ, 784, 105, doi: [10.1088/0004-637X/784/2/105](https://doi.org/10.1088/0004-637X/784/2/105)
- Weyant, A., Wood-Vasey, W. M., Joyce, R., et al. 2018, AJ, 155, 201, doi: [10.3847/1538-3881/aab901](https://doi.org/10.3847/1538-3881/aab901)
- Wood-Vasey, W. M., Friedman, A. S., Bloom, J. S., et al. 2008, ApJ, 689, 377, doi: [10.1086/592374](https://doi.org/10.1086/592374)
- Yamanaka, M., Maeda, K., Tanaka, M., et al. 2016, PASJ, 68, 68, doi: [10.1093/pasj/psw047](https://doi.org/10.1093/pasj/psw047)

Table 1. Number of SNeIa from NIR Surveys

| SN Survey | Total | NIR LC | Hubble LC | Hubble LC +Host Mass |
|-----------|-------|--------|-----------|----------------------|
| K+ | 34 | 13 | 11 | 7 |
| CSP | 59 | 54 | 47 | 28 |
| BN12 | 12 | 12 | 12 | 9 |
| F15 | 92 | 78 | 56 | 43 |
| W18 | 34 | 28 | 18 | 12 |
| Total | 231 | 185 | 144 | 99 |

Table 2. Number of Host Galaxies Observed in Our Sample per Galaxy Catalog.

| Survey | All | Hubble |
|----------------------|-----|--------|
| SDSS only | 13 | 8 |
| + GALEX | 12 | 8 |
| + 2MASS | 11 | 9 |
| + GALEX + 2MASS | 46 | 32 |
| GALEX + 2MASS | 48 | 42 |
| Removed from sample: | | |
| GALEX only | 1 | 1 |
| 2MASS only | 35 | 32 |
| No Host Photometry | 15 | 12 |

NOTE—“All” corresponds to the full sample of 231 NIR SNeIa and “Hubble” corresponds to the 144 NIR SNeIa on the Hubble diagram presented here.

Table 3. Host Galaxy Summary Table

| Name | Host Galaxy | F | N | u | g | r | i | z | J | H | K | Mass a | LC |
|-------------------------|---------------------------|-------|-------|-------|-------|-------|-------|-------|-------|-------|-------|----------|-------|
| CSS121006:232854+085452 | SDSS J232854.54+085452.3 | — | — | — | — | — | — | — | — | — | — | — | N |
| CSS121009:011101-172841 | 2MASX J011105973-1728527 | — | 20.77 | — | 17.87 | 17.57 | 17.37 | 17.24 | — | 14.19 | 13.77 | 13.87 | 10.43 |
| CSS121114:090202+101800 | SDSS J090202.19+101759.7 | 19.59 | 19.35 | 18.77 | 17.87 | 17.57 | 17.37 | 17.24 | — | — | — | 8.74 | Y |
| LSQ12fhs | 2MASX J22522347+2036373 | 18.13 | 17.67 | — | — | — | — | — | 15.27 | 15.46 | 15.31 | 9.13 | Y |
| LSQ12fmx | 2MASX J031252.93-001223.8 | 18.96 | 18.58 | 17.9 | 16.77 | 16.24 | 15.93 | 15.72 | 15.41 | 15.28 | 15.28 | 10.15 | Y |
| LSQ13cmt | ESO 541- G 013 | — | — | — | — | — | — | — | — | — | — | — | Y |
| LSQ13cwp | 2MASX J04035024+0239275 | — | — | — | — | — | — | — | 13.33 | 13.13 | 13.43 | — | Y |
| PS1-10w | CGCG 290-062 | 18.33 | 17.96 | 16.92 | 15.72 | 15.13 | 14.83 | 14.64 | 14.7 | 14.65 | 14.98 | 9.97 | Y |
| PS1-13dhh | None | — | — | — | — | — | — | — | — | — | — | — | Y |
| PTF09dlc | SDSS J1214630.02+062507.1 | — | — | 21.16 | 19.82 | 19.6 | 19.35 | 19.23 | — | — | — | 8.18 | Y |
| PTF10bjjs | MCG +09- 21-83 | — | — | — | — | — | — | — | — | — | — | — | N |
| PTF10hdv | SDSS J120745.44+412928.7 | — | — | 21.01 | 20.27 | 20.34 | 20.2 | 20.6 | — | — | — | 7.53 | Y |
| PTF10icb | MCG +10-19-1 | — | — | — | — | — | — | — | — | — | — | — | N |
| PTF10ndc | SDSS J171949.85+284201.7 | — | — | — | — | — | — | — | — | — | — | — | Y |
| PTF10nlg | None | — | — | — | — | — | — | — | — | — | — | — | Y |
| PTF10wnm | SDSS J002203.68+270221.5 | 18.84 | 18.37 | 17.97 | 16.86 | 16.42 | 16.11 | 15.93 | 15.7 | 15.9 | 15.24 | 9.97 | Y |
| PTF10wof | SDSS J233241.42+152131.5 | 19.81 | 19.55 | 18.72 | 17.61 | 17.14 | 16.87 | 16.7 | — | — | — | 9.5 | Y |
| PTF10xyt | SDSS J231902.41+134726.2 | — | — | 19.54 | 18.54 | 18.06 | 17.8 | 17.64 | — | — | — | 9.07 | Y |
| PTF11moy | SDSS J170618.19+383218.5 | — | — | 22.35 | 21.27 | 20.87 | 20.71 | 21.07 | — | — | — | 7.74 | N |
| PTF11qmo | 2MASX J10064866-0741124 | 18.34 | — | — | — | — | — | — | 14.12 | 14.1 | 13.95 | 10.1 | N |
| PTF11qri | LCRS B124431.1-060321 | — | — | 18.68 | 17.56 | 17.08 | 16.83 | 16.65 | — | — | — | 9.53 | N |
| PTF13dad | None | — | — | — | — | — | — | — | — | — | — | — | Y |
| PTF13ddg | 2MASX J004753.23+314848.1 | — | — | 19.33 | 17.32 | 16.44 | 16.06 | 15.78 | 15.47 | 15.4 | 15.54 | 10.47 | Y |
| SN 1991T | NGC 4527 | — | — | — | — | — | — | — | — | — | — | — | N |
| SN 1991bg | NGC 4374 | — | — | — | — | — | — | — | — | — | — | — | N |
| SN 1998bu | NGC 3368 | — | 14.78 | — | — | — | — | — | — | 8.13 | 7.95 | 8.16 | 10.01 |
| SN 1998aa | NGC 2595 | — | — | — | — | — | — | — | — | — | — | — | N |
| SN 1998ac | NGC 6063 | 16.03 | 15.6 | — | — | — | — | — | 12.26 | 12.09 | 12.39 | 9.67 | N |
| SN 1999cl | M88 | — | — | — | — | — | — | — | — | — | — | — | Y |
| SN 1999cp | NGC 5468 | — | — | — | — | — | — | — | 11.82 | 11.71 | 12.24 | — | N |
| SN 1999ee | IC 5179 | 15.18 | 14.53 | — | — | — | — | — | 10.55 | 10.33 | 10.47 | 10.5 | Y |
| SN 1999ek | UGC 3329 | — | — | — | — | — | — | — | 12.53 | 12.43 | 12.09 | — | Y |
| SN 1999gp | UGC 1993 | — | — | — | — | — | — | — | 12.45 | 12.19 | 12.53 | — | N |
| SN 2000E | NGC 6951 | — | — | — | — | — | — | — | — | — | — | — | N |
| SN 2000bh | ESO 573-14 | — | — | — | — | — | — | — | — | — | — | — | N |
| SN 2000br | NGC 4520 | — | — | — | — | — | — | — | — | — | — | — | N |
| SN 2000ca | ESO 383-32 | — | — | — | — | — | — | — | — | — | — | — | N |
| SN 2000ce | UGC 4195 | 16.76 | 16.11 | 15.28 | 13.83 | 13.08 | 12.71 | 12.42 | 12.15 | 12.02 | 12.19 | 10.32 | Y |

Table 3 continued on next page

Table 3 (*continued*)

| Name | Host Galaxy | F | N | u | g | r | i | z | J | H | K | Mass <i>a</i> | LC |
|-----------|--------------------------------|-------|-------|-------|-------|-------|-------|-------|-------|-------|-------|---------------|-------|
| SN 2000cx | NGC 524 | — | — | — | — | — | — | — | — | — | — | — | N |
| SN 2001ba | MCG -05-28-1 | — | — | — | — | — | — | — | — | — | — | — | N |
| SN 2001bt | IC 4830 | — | — | — | — | — | — | — | — | — | — | — | N |
| SN 2001cn | IC 4758 | — | — | — | — | — | — | — | — | — | — | — | N |
| SN 2001cz | NGC 4679 | — | — | — | — | — | — | — | — | — | — | — | N |
| SN 2001el | NGC 1448 | — | — | — | — | — | — | — | — | — | — | — | N |
| SN 2002bo | NGC 3190 | 18.02 | 15.95 | — | — | — | — | — | 9.4 | 9.15 | 9.3 | 10.19 | Y |
| SN 2002cv | NGC 3190 | — | — | — | — | — | — | — | — | — | — | — | N |
| SN 2002dj | NGC 5018 | — | 15.58 | — | — | — | — | — | 9.51 | 9.38 | 9.56 | 10.87 | Y |
| SN 2003cg | NGC 3169 | — | — | — | — | — | — | — | — | — | — | — | N |
| SN 2003du | UGC 9391 | — | 15.97 | 16.68 | 15.12 | 14.67 | 14.58 | 14.57 | — | — | — | 8.56 | Y |
| SN 2003gs | NGC 936 | — | — | — | — | — | — | — | — | — | — | — | N |
| SN 2003hv | NGC 1201 | — | — | — | — | — | — | — | — | — | — | — | N |
| SN 2004S | MCG -05-16-21 | — | — | — | — | — | — | — | — | 12.72 | 12.6 | 12.79 | — |
| SN 2004ef | UGC 12158 | — | 16.41 | 15.82 | 14.19 | 13.43 | 13.08 | 12.83 | 12.82 | 12.62 | 12.71 | 10.75 | Y |
| SN 2004eo | NGC 6928 | 18.53 | 16.39 | — | — | — | — | — | — | 10.64 | 10.41 | 10.56 | 10.82 |
| SN 2004ey | UGC 11816 | 16.04 | 15.61 | 15.76 | 14.48 | 13.86 | 13.56 | 13.39 | 13.04 | 12.87 | 13.26 | 9.94 | Y |
| SN 2004gs | MCG +03-22-20 | 20.05 | 19.18 | 16.29 | 14.49 | 13.7 | 13.31 | 13.02 | 13.01 | 12.76 | 12.88 | 10.55 | Y |
| SN 2004gu | FGC 175A | 21.27 | 20.83 | 19.1 | 17.37 | 16.49 | 16.04 | 15.64 | 15.02 | 14.77 | 14.86 | 9.89 | Y |
| SN 2005A | NGC 958 | 15.92 | 15.27 | — | — | — | — | — | — | 10.76 | 10.48 | 10.64 | 10.9 |
| SN 2005M | NGC 2930 | 15.86 | 15.58 | 16.3 | 15.75 | 15.6 | 15.53 | 15.44 | 13.86 | 13.82 | 13.83 | 9.28 | Y |
| SN 2005ag | 2MASX J14564322+0919361 | — | — | — | — | — | — | — | 14.51 | 14.34 | 14.25 | — | Y |
| SN 2005al | NGC 5304 | 19.56 | 17.8 | — | — | — | — | — | 11.31 | 11.11 | 11.35 | 10.39 | Y |
| SN 2005am | NGC 2811 | — | — | — | — | — | — | — | 9.81 | 9.6 | 9.81 | — | Y |
| SN 2005ao | NGC 6462 | 17.34 | 16.61 | 16.06 | 14.45 | 13.76 | 13.42 | 13.12 | 12.93 | 12.72 | 12.86 | 10.77 | Y |
| SN 2005bl | NGC 4070 | — | 18.52 | 15.17 | 13.34 | 12.5 | 12.13 | 11.9 | 11.62 | 11.39 | 11.59 | 10.9 | N |
| SN 2005bo | NGC 4708 | 15.98 | — | — | — | — | — | — | 12.04 | 11.89 | 11.98 | 9.86 | Y |
| SN 2005cf | MCG -01-39-3 | 15.91 | 15.07 | — | — | — | — | — | — | — | — | 7.7 | Y |
| SN 2005ch | APMUKS(B1) B141934.25+021314.0 | 21.19 | 21.27 | 22.17 | 19.95 | 19.65 | 19.38 | 19.54 | — | — | — | 8.69 | Y |
| SN 2005el | NGC 1819 | — | — | — | — | — | — | — | — | — | — | — | Y |
| SN 2005eq | MCG -01-9-6 | 17.1 | 16.63 | 15.65 | 14.24 | 13.47 | 13.09 | 12.75 | 12.63 | 12.46 | 12.63 | 10.66 | Y |
| SN 2005eu | NSF J022743.32+281037.6 | — | — | — | — | — | — | — | — | — | — | — | Y |
| SN 2005hc | MCG +00-6-3 | — | 18.56 | 17.42 | 15.79 | 15.03 | 14.68 | 14.42 | 13.87 | 13.76 | 13.83 | 10.44 | Y |
| SN 2005hj | SDSS J012648.45-011417.3 | — | — | 20.15 | 18.82 | 18.15 | 17.8 | 17.54 | — | — | — | 9.31 | Y |
| SN 2005hk | UGC 272 | 16.45 | 16.14 | 16.31 | 14.84 | 14.38 | 14.18 | 14.09 | 15.08 | 14.1 | 14.83 | 9.38 | N |
| SN 2005iq | MCG -03-1-8 | 17.51 | 17.33 | — | — | — | — | — | 13.38 | 13.15 | 13.59 | 10.43 | Y |
| SN 2005kc | NGC 7311 | — | 15.77 | 14.44 | 12.61 | 11.8 | 11.42 | 11.15 | 10.77 | 10.53 | 10.75 | 10.77 | Y |
| SN 2005ke | NGC 1371 | — | — | — | — | — | — | — | — | — | — | — | N |
| SN 2005ki | NGC 3332 | — | — | — | — | — | — | — | 11.25 | 11.1 | 11.22 | — | Y |
| SN 2005ku | SDSS J225942.66-000048.8 | 19.1 | 18.56 | 17.88 | 16.74 | 16.29 | 16.03 | 15.85 | 15.32 | 15.29 | 15.5 | 9.67 | N |
| SN 2005ls | MCG +07-7-1 | 16.42 | 15.75 | 15.37 | 14.46 | 13.94 | 13.72 | 13.52 | 13.1 | 13.08 | 13.19 | 10.05 | N |

Table 3 *continued on next page*

Table 3 (*continued*)

| Name | Host Galaxy | F | N | u | g | r | i | z | J | H | K | Mass <i>a</i> | LC |
|-----------|--------------------------------|-------|-------|-------|-------|-------|-------|-------|-------|-------|-------|---------------|----|
| SN 2005na | UGC 3634 | — | — | — | — | — | — | — | 11.94 | 11.68 | 11.91 | — | Y |
| SN 2006D | MCG -01-33-34 | 15.88 | 15.49 | — | — | — | — | — | 12.34 | 12.16 | 12.33 | 9.52 | Y |
| SN 2006E | NGC 5338 | — | — | — | — | — | — | — | — | — | — | — | N |
| SN 2006N | MCG +11-8-12 | — | 18.61 | — | — | — | — | — | 11.93 | 11.76 | 11.96 | 10.27 | Y |
| SN 2006X | NGC 4321 | — | — | — | — | — | — | — | 8.35 | 8.2 | 8.43 | — | Y |
| SN 2006ac | NGC 4619 | 15.67 | 15.21 | — | — | — | — | — | 11.72 | 11.59 | 11.73 | 10.66 | Y |
| SN 2006ax | NGC 3663 | 15.99 | 15.31 | — | — | — | — | — | 11.61 | 11.39 | 11.73 | 10.43 | Y |
| SN 2006bd | UGC 6609 | 20.57 | 18.61 | 16.02 | 14.05 | 13.25 | 12.87 | 12.57 | 12.28 | 11.99 | 12.16 | 10.66 | N |
| SN 2006bh | NGC 7329 | — | 14.53 | — | — | — | — | — | 10.69 | 10.49 | 10.72 | 10.53 | Y |
| SN 2006br | NGC 5185 | — | — | — | — | — | — | — | 12.09 | 11.94 | 12.08 | — | Y |
| SN 2006bt | CGCG 108-013 | — | — | 16.02 | 14.14 | 13.37 | 13.0 | 12.74 | 12.42 | 12.24 | 12.43 | 10.82 | N |
| SN 2006cp | UGC 7357 | 16.7 | — | 15.4 | 14.33 | 13.85 | 13.65 | 13.5 | 13.99 | 13.7 | 13.98 | 10.03 | Y |
| SN 2006cz | MCG -01-38-2 | — | 16.28 | — | — | — | — | — | 12.73 | 12.51 | 12.56 | 10.86 | N |
| SN 2006ej | NGC 191 | — | 16.98 | 15.47 | 13.56 | 12.73 | 12.33 | 12.05 | 11.43 | 11.14 | 11.41 | 10.67 | Y |
| SN 2006eq | SDSS J12837.60+011348.6 | 20.97 | 20.1 | 18.78 | 17.24 | 16.47 | 16.06 | 15.76 | 15.55 | 14.98 | 15.19 | 9.93 | Y |
| SN 2006et | NGC 232 | — | 18.12 | — | — | — | — | — | 11.93 | 11.64 | 11.72 | 10.59 | Y |
| SN 2006ev | UGC 11758 | — | — | — | — | — | — | — | 12.33 | 12.07 | 12.15 | — | Y |
| SN 2006gj | UGC 2650 | — | — | — | — | — | — | — | 12.83 | 12.74 | 12.88 | — | Y |
| SN 2006gr | UGC 12071 | — | — | 15.88 | 14.55 | 13.81 | 13.41 | 13.12 | — | — | — | 10.64 | N |
| SN 2006gt | 2MASX J00561810-0137327 | — | 22.04 | 18.53 | 16.8 | 16.0 | 15.63 | 15.34 | 15.45 | 15.32 | 15.34 | 10.06 | Y |
| SN 2006hb | MCG -04-12-34 | — | — | — | — | — | — | — | 12.09 | 11.91 | 12.11 | — | Y |
| SN 2006hx | PGC 73820 | — | 20.22 | — | — | — | — | — | 14.8 | 14.36 | 14.59 | 10.1 | Y |
| SN 2006is | APMUKS(BJ) B051529.79-235009.8 | — | — | — | — | — | — | — | — | — | — | — | Y |
| SN 2006kf | UGC 2829 | — | — | 15.5 | 13.68 | 12.87 | 12.48 | 12.19 | 11.84 | 11.63 | 11.83 | 10.66 | Y |
| SN 2006le | UGC 3218 | 15.2 | 14.18 | — | — | — | — | — | 10.92 | 10.74 | 10.95 | 10.66 | Y |
| SN 2006lf | UGC 3108 | — | — | — | — | — | — | — | 11.08 | 10.95 | 11.13 | — | Y |
| SN 2006lu | 2MASX J09151727-2536001 | 18.84 | 18.52 | — | — | — | — | — | 14.91 | 14.76 | 14.99 | 10.19 | N |
| SN 2006mq | ESO 494-G26 | — | — | — | — | — | — | — | — | — | — | — | N |
| SN 2006ot | NGC 1316 | — | — | — | — | — | — | — | — | — | — | — | N |
| SN 2007A | UGC 1333 | 18.5 | 17.94 | 17.07 | 15.13 | 14.28 | 13.86 | 13.56 | 13.15 | 12.92 | 13.3 | 11.01 | N |
| SN 2006ob | UGC 2384 | — | — | — | — | — | — | — | 12.61 | 12.41 | 12.49 | — | Y |
| SN 2006os | ESO 544-G31 | — | 20.2 | — | — | — | — | — | 12.68 | 12.56 | 12.69 | 11.13 | N |
| SN 2007T | NGC 105 | — | — | — | — | — | — | — | — | — | — | — | Y |
| SN 2007N | MCG -01-33-12 | — | — | — | — | — | — | — | — | — | — | — | N |
| SN 2007S | UGC 5378 | 16.83 | 16.33 | 15.69 | 14.27 | 13.83 | 13.51 | 13.28 | 13.06 | 12.95 | 13.18 | 9.71 | Y |
| SN 2007af | NGC 5584 | — | 13.57 | 14.07 | 12.86 | 12.28 | 11.97 | 12.2 | 11.72 | 11.42 | 11.79 | 9.52 | Y |
| SN 2007ai | MCG -04-38-4 | — | — | — | — | — | — | — | 12.38 | 12.16 | 12.27 | — | Y |
| SN 2007as | ESO 18-G18 | — | — | — | — | — | — | — | 12.62 | 12.39 | 12.83 | — | Y |
| SN 2007ax | NGC 2577 | 19.34 | 18.62 | — | — | — | — | — | — | — | — | — | N |
| SN 2007ba | UGC 9798 | — | — | 15.61 | 13.79 | 12.95 | 12.58 | 12.32 | 12.06 | 11.79 | 11.96 | 10.59 | Y |
| SN 2007bc | UGC 6332 | — | — | — | — | — | — | — | — | — | — | — | N |

Table 3 *continued on next page*

Table 3 (*continued*)

| Name | Host Galaxy | <i>F</i> | <i>N</i> | <i>u</i> | <i>g</i> | <i>r</i> | <i>i</i> | <i>J</i> | <i>H</i> | <i>K</i> | Mass <i>a</i> | LC |
|-----------|---------------------------|----------|----------|----------|----------|----------|----------|----------|----------|----------|---------------|---------|
| SN 2007bd | UGC 4455 | 17.47 | 17.12 | 16.32 | 14.51 | 13.7 | 13.32 | 13.01 | 12.98 | 12.73 | 12.76 | 10.65 Y |
| SN 2007bm | NGC 3672 | — | 13.79 | 13.47 | 12.0 | 11.25 | 10.86 | 10.63 | 10.08 | 9.93 | 10.11 | 10.2 Y |
| SN 2007ca | MCG -02-34-61 | — | 16.32 | — | — | — | — | 13.4 | 13.27 | 13.41 | 13.15 | 9.58 Y |
| SN 2007co | MCG +05-43-16 | — | — | — | — | — | — | 13.06 | 12.9 | 13.15 | — | N |
| SN 2007cq | 2MASX J22144070+0504435 | 18.14 | 17.73 | 16.99 | 15.81 | 15.32 | 15.09 | 14.89 | 14.72 | 14.6 | 14.68 | 9.62 Y |
| SN 2007fb | UGC 12859 | — | 17.26 | — | — | — | — | 12.7 | 12.52 | 12.79 | 12.79 | 10.12 N |
| SN 2007hx | SDSS J020626.74-005400.4 | — | — | — | — | — | — | — | — | — | — | N |
| SN 2007if | J011051.37+152739 | — | — | — | — | — | — | — | — | — | — | N |
| SN 2007jg | SDSS J032950.83+000316.0 | 19.64 | 19.37 | 18.99 | 17.95 | 17.52 | 17.33 | 17.33 | — | — | — | 8.98 Y |
| SN 2007jh | CGCG 391-014 | — | — | — | — | — | — | — | — | — | — | N |
| SN 2007je | NGC 7721 | — | 14.04 | — | — | — | — | 10.41 | 10.25 | 10.52 | 10.21 | Y |
| SN 2007nq | UGC 595 | 20.76 | 19.48 | 15.77 | 14.04 | 13.2 | 12.82 | 12.48 | 12.54 | 12.41 | 12.39 | 11.2 Y |
| SN 2007on | NGC 1404 | — | 15.2 | — | — | — | — | 8.67 | 8.47 | 8.67 | 8.67 | 10.47 Y |
| SN 2007qe | NSF J235412.09+272432.3 | — | — | — | — | — | — | — | — | — | — | N |
| SN 2007rx | BATC J234012.05+272512.23 | — | — | — | — | — | — | — | — | — | — | N |
| SN 2007sr | NGC 4038 | — | — | — | — | — | — | — | — | — | — | Y |
| SN 2008A | NGC 634 | 18.27 | 17.29 | — | — | — | — | — | 11.63 | 11.4 | 11.57 | 10.49 N |
| SN 2008C | UGC 3611 | — | — | — | — | — | — | — | 12.38 | 12.13 | 12.3 | — Y |
| SN 2008R | NGC 1200 | 18.91 | 17.51 | — | — | — | — | — | 10.43 | 10.21 | 10.41 | 10.81 Y |
| SN 2008Z | SDSS J094315.36+361709.2 | — | — | 18.9 | 17.6 | 16.97 | 16.63 | 16.36 | — | — | — | 8.81 Y |
| SN 2008ae | IC 577 | 16.78 | 16.3 | 15.98 | 14.82 | 14.3 | 13.91 | 13.72 | 13.34 | 13.2 | 13.36 | 10.26 N |
| SN 2008af | UGC 9640 | — | — | — | — | — | — | — | — | — | — | N |
| SN 2008bc | KK 1524 | — | — | — | — | — | — | — | 13.14 | 12.93 | 13.19 | — Y |
| SN 2008bq | ESO 308-G25 | — | — | — | — | — | — | — | 12.39 | 12.27 | 12.42 | — Y |
| SN 2008fp | ESO 428-G14 | — | 16.04 | — | — | — | — | — | 10.57 | 10.36 | 10.57 | 9.98 Y |
| SN 2008fr | SDSS J011149.19+143826.5 | — | — | 20.6 | 19.4 | 19.09 | 18.92 | 19.11 | — | — | — | 8.09 Y |
| SN 2008fv | NGC 3147 | 14.31 | 13.67 | — | — | — | — | — | 9.26 | 9.14 | 9.25 | 10.91 Y |
| SN 2008fx | 2MASX J02113233+2353074 | — | — | 18.75 | 16.93 | 16.1 | 15.73 | 15.42 | 15.26 | 14.75 | 14.91 | 10.27 Y |
| SN 2008gb | UGC 2427 | — | 16.99 | — | — | — | — | — | 14.06 | 13.95 | 14.09 | 9.99 Y |
| SN 2008gl | UGC 881 | 21.15 | 19.63 | 16.28 | 14.4 | 13.57 | 13.17 | 12.88 | 12.55 | 12.43 | 12.54 | 10.8 Y |
| SN 2008gp | MCG +00-9-74 | — | — | — | — | — | — | — | 12.8 | 12.72 | 12.82 | — Y |
| SN 2008ha | UGC 12682 | — | — | — | — | — | — | — | — | — | — | N |
| SN 2008hm | 2MFGC 02845 | — | — | — | — | — | — | — | 13.52 | 13.34 | 13.39 | — Y |
| SN 2008hs | NGC 910 | — | 18.41 | — | — | — | — | — | 11.03 | 10.81 | 11.04 | 10.77 Y |
| SN 2008hv | NGC 2765 | 19.78 | 17.62 | 14.33 | 12.59 | 11.83 | 11.53 | 11.19 | 11.05 | 10.86 | 11.06 | 10.59 Y |
| SN 2008hy | IC 334 | 19.43 | — | — | — | — | — | — | 9.48 | 9.24 | 9.5 | 10.69 Y |
| SN 2008ia | ESO 125-6 | — | — | — | — | — | — | — | 11.71 | 11.52 | 11.74 | — Y |
| SN 2008s1 | UGC 8472 | — | — | — | — | — | — | — | — | — | — | N |
| SN 2009D | MCG -03-10-52 | 16.96 | 16.55 | — | — | — | — | 13.12 | 12.89 | 13.06 | 10.16 | Y |
| SN 2009F | NGC 1725 | — | — | — | — | — | — | — | — | — | — | N |
| SN 2009Y | NGC 5728 | — | — | — | — | — | — | — | — | — | — | N |

Table 3 *continued on next page*

Table 3 (*continued*)

| Name | Host Galaxy | F | N | u | g | r | i | z | J | H | K | Mass <i>a</i> | LC | |
|-----------|--------------------------|-------|-------|-------|-------|-------|-------|-------|-------|-------|---------|---------------|-------|---|
| SN 2009ad | UGC 3236 | — | 17.35 | — | — | — | — | 13.18 | 12.93 | 13.1 | 10.34 | Y | | |
| SN 2009al | NGC 3425 | 20.18 | 18.29 | 15.85 | 13.99 | 13.17 | 12.78 | 12.54 | 12.28 | 12.04 | 12.37 | 10.56 | N | |
| SN 2009an | NGC 4332 | — | 16.98 | 15.04 | 13.27 | 12.32 | 11.86 | 11.51 | 11.15 | 10.89 | 11.08 | 10.15 | Y | |
| SN 2009bv | MCG +06-29-39 | — | — | 16.62 | 15.38 | 14.79 | 14.5 | 14.28 | 14.15 | 13.96 | 14.2 | 10.24 | Y | |
| SN 2009dc | UGC 10064 | — | — | — | — | — | — | — | — | — | — | — | N | |
| SN 2009do | NGC 4537 | — | — | — | — | — | — | — | 12.63 | 12.4 | 12.47 | — | Y | |
| SN 2009ds | NGC 3905 | — | 15.24 | — | — | — | — | — | 11.83 | 11.62 | 11.72 | 10.55 | Y | |
| SN 2009fv | NGC 6173 | 19.66 | 18.19 | — | — | — | — | — | 11.16 | 10.99 | 11.21 | 11.17 | N | |
| SN 2009fw | ESO 597-6 | — | — | — | — | — | — | — | — | — | — | — | N | |
| SN 2009ig | NGC 1015 | — | — | 14.61 | 12.94 | 12.21 | 11.85 | 11.61 | 11.23 | 11.05 | 11.19 | 10.12 | Y | |
| SN 2009im | NGC 1355 | — | — | — | — | — | — | — | 11.81 | 11.64 | 11.84 | — | Y | |
| SN 2009jr | IC 1320 | 15.93 | 15.47 | — | — | — | — | — | 12.52 | 12.31 | 12.51 | 10.0 | N | |
| SN 2009kk | 2MFGC 03182 | — | — | — | — | — | — | — | 13.43 | 13.22 | 13.5 | — | Y | |
| SN 2009kq | MCG +05-21-1 | 16.49 | 15.95 | — | — | — | — | — | 12.69 | 12.58 | 12.72 | 9.62 | Y | |
| SN 2009le | ESO 478-6 | — | — | — | — | — | — | — | 11.46 | 11.27 | 11.43 | — | Y | |
| SN 2009lf | 2MASX J02014081+1519521 | — | — | 17.39 | 15.67 | 14.89 | 14.54 | 14.27 | 14.34 | 14.04 | 14.21 | 10.49 | Y | |
| SN 2009na | UGC 5884 | 16.13 | 15.68 | 15.19 | 14.08 | 13.6 | 13.39 | 13.24 | 13.12 | 12.96 | 12.92 | 10.11 | Y | |
| SN 2010Y | NGC 3392 | 20.02 | 18.67 | 15.95 | 14.15 | 13.35 | 12.96 | 12.68 | 12.47 | 12.33 | 12.59 | 9.87 | Y | |
| SN 2010ag | UGC 10679 | 18.77 | 18.05 | 16.95 | 15.34 | 14.55 | 14.15 | 13.86 | 13.35 | 13.19 | 13.37 | 10.38 | N | |
| SN 2010ai | SDSS J125925.04+275948.2 | — | 21.76 | 19.63 | 17.58 | 16.86 | 16.51 | 16.29 | — | — | — | 8.9 | Y | |
| SN 2010cr | NGC 5177 | — | 19.59 | — | — | — | — | — | 13.48 | 13.03 | 13.19 | 9.89 | Y | |
| SN 2010dl | IC 1391 | 21.93 | 19.93 | 17.13 | 15.36 | 14.58 | 14.22 | 13.98 | 13.95 | 13.8 | 14.17 | 10.27 | N | |
| SN 2010dm | SDSS J121133.31+471628.6 | — | — | 20.78 | 19.62 | 19.19 | 19.05 | 18.91 | — | — | — | 8.01 | Y | |
| SN 2010dw | 2MASX J15224062-055521.4 | — | — | — | — | — | — | — | 14.52 | 14.36 | 14.57 | — | Y | |
| SN 2010ew | CGCG 173-018 | 17.67 | — | — | — | — | — | — | 14.35 | 14.17 | 14.47 | 9.66 | N | |
| SN 2010ex | CGCG 475-019 | 17.59 | 17.02 | 16.36 | 15.33 | 14.88 | 14.7 | 14.53 | 14.42 | 14.35 | 14.61 | 9.62 | N | |
| SN 2010gn | SDSS J171750.05+405252.5 | — | 20.06 | 19.15 | 18.1 | 17.62 | 17.38 | 17.38 | — | — | — | 8.84 | Y | |
| SN 2010gy | A022712-0432 | — | — | — | — | — | — | — | — | — | — | — | Y | |
| SN 2010ho | PGC 1361264 | 18.4 | 18.08 | 17.24 | 16.06 | 15.53 | 15.25 | 15.05 | 15.35 | — | -999.02 | — | 10.0 | Y |
| SN 2010hs | 2MASX J02253767+2445579 | — | — | — | 18.06 | 16.55 | 15.81 | 15.46 | 15.21 | 15.01 | 14.64 | 15.25 | 10.56 | Y |
| SN 2010iw | UGC 4570 | 17.72 | — | 17.56 | 15.81 | 15.25 | 15.09 | 14.95 | 16.02 | 16.12 | 16.35 | 9.36 | Y | |
| SN 2010ju | UGC 3341 | — | — | — | — | — | — | — | 11.79 | 11.58 | 11.72 | — | Y | |
| SN 2010jv | NGC 2379 | — | — | — | — | — | — | — | 12.41 | 12.19 | 12.42 | — | N | |
| SN 2010kg | NGC 1633 | 16.33 | 15.71 | — | — | — | — | — | 12.07 | 11.9 | 12.14 | 10.24 | Y | |
| SN 2011B | NGC 2655 | 17.42 | 15.28 | — | — | — | — | — | 8.77 | 8.56 | 8.79 | 10.56 | Y | |
| SN 2011K | CSS J044530.38-072054.7 | — | — | — | — | — | — | — | — | — | — | — | Y | |
| SN 2011aa | UGC 3906 | — | — | — | — | — | — | — | — | — | — | — | N | |
| SN 2011ae | MCG -03-30-19 | 15.42 | 15.14 | — | — | — | — | — | 13.29 | 13.05 | 13.83 | 8.83 | Y | |
| SN 2011ao | IC 2973 | 15.94 | 15.58 | 15.09 | 14.13 | 13.71 | 13.54 | 13.39 | 13.54 | 13.31 | 13.58 | 9.41 | Y | |
| SN 2011at | MCG -02-24-27 | 16.46 | 15.92 | — | — | — | — | — | 12.49 | 12.15 | 12.46 | 9.21 | Y | |
| SN 2011by | NGC 3972 | — | — | — | — | — | — | — | — | — | — | — | N | |

Table 3 continued on next page

Table 3 (*continued*)

| Name | Host Galaxy | F | N | u | g | r | i | z | J | H | K | Mass <i>a</i> | LC |
|------------------|---------------------------|-------|-------|-------|-------|-------|-------|-------|-------|-------|-------|---------------|----|
| SN 2011de | UGC 10018 | — | 16.6 | — | — | — | — | — | 12.86 | 12.67 | 12.78 | 10.52 | N |
| SN 2011df | NGC 6801 | — | 15.21 | — | — | — | — | — | 12.02 | 11.83 | 12.21 | 10.14 | Y |
| SN 2011fe | M101 | — | — | — | — | — | — | — | — | — | — | — | N |
| SN 2011fs | UGC 11975 | 16.65 | 15.8 | — | — | — | — | — | 11.9 | 11.76 | 11.88 | 10.48 | Y |
| SN 2011gf | SDSS J211222.69-074913.9 | — | — | — | — | — | — | — | — | — | — | — | N |
| SN 2011gy | UGC 02756 | — | — | — | — | — | — | — | — | — | — | — | N |
| SN 2011io | 2MASX J23024668+0848186 | — | 20.89 | 18.18 | 16.22 | 15.34 | 14.93 | 14.61 | 14.17 | 13.95 | 14.23 | 10.24 | N |
| SN 2011iy | NGC 4984 | — | — | — | — | — | — | — | — | — | — | — | N |
| SN 2011jh | NGC 4682 | — | — | — | — | — | — | — | — | — | — | — | N |
| SN 2012Z | NGC 1309 | — | — | — | — | — | — | — | — | — | — | — | N |
| SN 2012bh | UGC 7228 | — | 17.13 | — | — | — | — | — | 13.06 | 12.78 | 12.96 | 10.24 | N |
| SN 2012bo | NGC 4726 | — | — | — | — | — | — | — | — | — | — | — | N |
| SN 2012bp | SDSS J161812.44+362902.6 | — | 18.88 | 18.12 | 16.98 | 16.57 | 16.4 | 16.3 | — | — | — | 9.03 | N |
| SN 2012dn | ESO 462-G16 | — | — | — | — | — | — | — | — | — | — | — | N |
| SN 2012em | CGCG 453-001 | — | 19.83 | 16.43 | 14.58 | 13.75 | 13.37 | 13.08 | 12.83 | 12.73 | 12.91 | 10.82 | N |
| SN 2012fk | 2MASX J023052.08+222832.6 | — | — | — | — | — | — | — | 15.02 | 14.75 | 14.67 | — | Y |
| SN 2013ar | 2MASX J083745.57+492840.0 | — | — | — | — | — | — | — | — | — | — | — | N |
| SN 2013bs | NGC 6343 | — | 15.78 | 13.95 | 13.14 | 12.76 | 12.52 | 12.11 | 11.91 | 12.07 | 10.77 | Y | |
| SN 2013bt | PGC 51271 | — | 19.86 | 16.85 | 14.99 | 14.17 | 13.75 | 13.48 | 13.19 | 12.93 | 13.23 | 10.62 | Y |
| SN 2013cs | ESO 576-17 | — | 16.05 | — | — | — | — | — | 14.57 | 14.07 | 14.14 | 8.52 | Y |
| SN 2013cv | SDSS J162243.02+185733.8 | — | — | 21.86 | 20.05 | 19.93 | 19.74 | 19.44 | — | — | — | 7.48 | Y |
| SN 2013dy | NGC 7250 | — | — | — | — | — | — | — | — | — | — | — | N |
| SN 2013fn | IC 1342 | 17.48 | 16.8 | — | — | — | — | — | 12.54 | 12.33 | 12.43 | 10.48 | Y |
| SN 2015H | NGC 3464 | — | — | — | — | — | — | — | — | — | — | — | N |
| SNF 20080522-000 | SDSS J133647.59+050833.0 | — | 19.36 | 18.59 | 17.45 | 16.95 | 16.65 | 16.54 | — | — | — | 9.48 | N |
| SNF 20080522-011 | SDSS J151959.16+045411.2 | — | — | 24.41 | 22.41 | 21.01 | 20.48 | 20.28 | — | — | — | 7.95 | N |
| IPTF13dgg | NGC 1762 | — | — | — | — | — | — | — | 11.33 | 11.15 | 11.34 | — | Y |
| IPTF13dkl | SDSS J234457.63+032337.9 | 19.8 | 19.37 | 18.75 | 17.47 | 16.93 | 16.65 | 16.4 | — | — | — | 9.41 | N |
| IPTF13dkx | SDSS J012052.56+032023.0 | 19.32 | 19.01 | 18.52 | 17.6 | 17.21 | 17.03 | 16.88 | — | — | — | 8.88 | Y |
| IPTF13ebh | NGC 890 | — | 17.06 | — | — | — | — | — | 10.06 | 9.84 | 10.07 | 10.96 | Y |

^a Units of $\log M_{\odot}$. No errors are reported for this parameter.

Note—The errors on the photometry are hidden here to fit the page but are available in the source code.

Table 4. SN H-band “max_model” and Optical “EBV_model2” μ fits

| Name | t_{max} | $t_{\text{max}}^{\text{err}}$ | MJD | MJD | z_{cmb} | $z_{\text{cmb}}^{\text{err}}$ | H_{max} | $H_{\text{max}}^{\text{err}}$ | N_H | $s_{BV,H}^{\text{err}}$ | $s_{BV,H}^{\text{er}}$ | μ | μ^{er} | N_μ | $s_{BV,\mu}^{\text{er}}$ | $s_{BV,\mu}^{\text{er}}$ | Ref. a | Samp. b |
|-------------------------|------------------|-------------------------------|--------|------------|------------------|-------------------------------|------------------|-------------------------------|-------|-------------------------|------------------------|-------|-------------------|---------|--------------------------|--------------------------|-----------|-----------|
| CSS121006:232854+085452 | 56207.0 | 0.07 | 0.0799 | 0.0008 | 19.945 | 0.168 | 2 | 0.955 | 0.0 | | | | | | | | W18 | W18 |
| CSS121009:011101-172841 | 56220.0 | 0.46 | 0.06 | 0.0006 | 18.162 | 2.079 | 2 | 0.666 | 0.949 | | | | | | | | W18 | W18 |
| CSS121114:090202+101800 | 56252.0 | 0.46 | 0.0419 | 0.0004 | 17.949 | 0.093 | 3 | 1.174 | 0.109 | | | | | | | | W18 | W18 |
| LSQ12ffhs | 56206.0 | 0.07 | 0.0329 | 0.0003 | 17.448 | 0.135 | 4 | 0.918 | 0.048 | | | | | | | | W18 | W18 |
| LSQ12fmx | 56227.0 | 0.46 | 0.0669 | 0.0006 | 19.143 | 0.121 | 4 | 0.880 | 0.050 | | | | | | | | W18 | W18 |
| LSQ13cmct | 56582.0 | 0.0 | 0.0569 | 0.0005 | 18.002 | 0.161 | 3 | 0.684 | 0.200 | | | | | | | | W18 | W18 |
| LSQ13cwp | 56606.0 | 0.07 | 0.0669 | 0.0006 | 18.413 | 0.150 | 3 | 0.911 | 0.048 | 37.053 | 0.091 | 17 | 1.003 | 0.060 | W18 | W18 | W18 | |
| PS1-10w | 55248.0 | 0.0 | 0.0322 | 0.0001 | 17.340 | 0.096 | 10 | 0.915 | 0.013 | | | | | | | | F15 | F15 |
| PS1-13dkh | 56572.0 | 0.07 | 0.0300 | 0.0003 | 17.060 | 0.116 | 3 | 0.938 | 0.041 | 34.973 | 1.407 | 12 | 1.457 | 2.783 | W18 | W18 | W18 | |
| PTF09dc | 55073.0 | 0.0 | 0.0678 | 0.0001 | 18.850 | 0.066 | 4 | 0.748 | 0.049 | | | | | | | | BN12 | BN12 |
| PTF10hdv | 55344.0 | 0.0 | 0.0534 | 0.0001 | 18.591 | 0.024 | 4 | 1.069 | 0.063 | | | | | | | | BN12 | BN12 |
| PTF10ndc | 55390.0 | 0.0 | 0.0818 | 0.0001 | 19.375 | 0.037 | 4 | 1.087 | 0.068 | | | | | | | | BN12 | BN12 |
| PTF10nlg | 55391.0 | 0.0 | 0.0560 | 0.0001 | 18.646 | 0.041 | 5 | 1.107 | 0.083 | | | | | | | | BN12 | BN12 |
| PTF10wnm | 55477.0 | 0.0 | 0.0656 | 0.0001 | 18.943 | 0.010 | 4 | 0.983 | 0.033 | | | | | | | | BN12 | BN12 |
| PTF10wof | 55474.0 | 0.0 | 0.0526 | 0.0001 | 18.547 | 0.026 | 4 | 1.004 | 0.052 | | | | | | | | BN12 | BN12 |
| PTF10xyt | 55493.0 | 0.0 | 0.0496 | 0.0001 | 18.482 | 0.080 | 4 | 1.525 | 0.540 | | | | | | | | BN12 | BN12 |
| PTF11moy | 55824.0 | 0.07 | 0.0600 | 0.0001 | 19.310 | 0.010 | 1 | 0.955 | 0.000 | | | | | | | | W18 | W18 |
| PTF11qmo | 55894.0 | 0.46 | 0.0564 | 0.0001 | 18.345 | 0.073 | 2 | 1.174 | 0.074 | | | | | | | | W18 | W18 |
| PTF11qri | 55897.0 | 0.46 | 0.0550 | 0.0001 | 19.218 | 0.342 | 2 | 1.35 | 0.291 | | | | | | | | W18 | W18 |
| PTF13dad | 56547.0 | 0.07 | 0.0859 | 0.0008 | 19.610 | 0.162 | 3 | 1.174 | 0.125 | | | | | | | | W18 | W18 |
| PTF13ddg | 65545.0 | 0.07 | 0.084 | 0.0008 | 18.574 | 0.027 | 3 | 0.705 | 0.008 | | | | | | | | W18 | W18 |
| SN 1998bu | 50952.0 | 0.0 | 0.0023 | 6.6712e-05 | 11.681 | 0.014 | 19 | 0.977 | 0.003 | 30.328 | 0.011 | 382 | 0.967 | 0.005 | J99,H00 | K+ | K+ | |
| SN 1999ac | 51250.0 | 0.0 | 0.0100 | 3.3356e-05 | 14.587 | 0.030 | 29 | 0.982 | 0.008 | | | | | | | | Ph06 | K+ |
| SN 1999cl | 51342.0 | 0.0 | 0.0031 | 0.0002 | 12.786 | 0.05 | 5 | 0.933 | 0.01 | 31.085 | 0.018 | 175 | 0.922 | 0.011 | K00 | K+ | K+ | |
| SN 1999cp | 51363.0 | 0.0 | 0.0097 | 4.6698e-05 | 14.753 | 0.068 | 2 | 1.000 | 0.009 | 33.139 | 0.013 | 117 | 0.991 | 0.008 | K00 | K+ | K+ | |
| SN 1999ee | 51469.0 | 0.0 | 0.0109 | 5.0034e-05 | 15.037 | 0.021 | 33 | 1.118 | 0.006 | 33.4 | 0.007 | 625 | 1.117 | 0.006 | K04a | K+ | K+ | |
| SN 1999ek | 51481.0 | 0.0 | 0.0173 | 3.3356e-05 | 15.918 | 0.018 | 15 | 0.973 | 0.03 | 34.362 | 0.026 | 56 | 0.948 | 0.014 | K04b | K+ | K+ | |
| SN 1999gp | 51550.0 | 0.07 | 0.027 | 6.0041e-05 | 16.813 | 0.178 | 3 | 1.242 | 0.011 | 35.222 | 0.02 | 150 | 1.128 | 0.022 | K01 | K+ | K+ | |
| SN 2000ce | 51667.0 | 0.46 | 0.0170 | 5.0034e-05 | 16.017 | 0.038 | 5 | 1.041 | 0.033 | 34.708 | 0.070 | 43 | 1.097 | 0.051 | K01 | K+ | K+ | |
| SN 2002bo | 52356.0 | 0.0 | 0.0056 | 6.6712e-05 | 13.834 | 0.036 | 14 | 0.956 | 0.007 | 32.073 | 0.015 | 374 | 0.952 | 0.008 | K04b | K+ | K+ | |
| SN 2002dj | 52450.0 | 0.0 | 0.0096 | 7.3384e-05 | 14.671 | 0.042 | 21 | 0.945 | 0.013 | 32.966 | 0.021 | 166 | 0.944 | 0.015 | P08 | K+ | K+ | |
| SN 2003du | 52766.0 | 0.0 | 0.0073 | 4.6698e-05 | 14.440 | 0.025 | 6 | 1.018 | 0.005 | 32.812 | 0.010 | 279 | 1.016 | 0.006 | S407 | K+ | K+ | |
| SN 2004S | 53038.0 | 0.46 | 0.0086 | 5.3370e-05 | 14.784 | 0.048 | 17 | 1.189 | 0.028 | 33.310 | 0.046 | 120 | 1.111 | 0.04 | K07 | K+ | K+ | |
| SN 2004ef | 53263.0 | 0.46 | 0.0314 | 6.3377e-05 | 17.223 | 0.217 | 4 | 0.897 | 0.009 | 35.535 | 0.009 | 393 | 0.845 | 0.004 | C10 | CSP | CSP | |
| SN 2004eo | 53278.0 | 0.0 | 0.0162 | 5.6705e-05 | 15.668 | 0.047 | 19 | 0.872 | 0.004 | | | | | | | | Pa07b,C10 | K+ |
| SN 2004ey | 53303.0 | 0.0 | 0.0161 | 5.6705e-05 | 15.72 | 0.074 | 9 | 1.116 | 0.017 | 34.105 | 0.008 | 269 | 1.042 | 0.006 | C10 | CSP | CSP | |
| SN 2004gs | 53355.0 | 0.0 | 0.0274 | 0.0001 | 17.152 | 0.138 | 10 | 0.710 | 0.01 | 35.454 | 0.014 | 356 | 0.629 | 0.010 | C10 | CSP | CSP | |

Table 4 continued on next page

Table 4 (continued)

| Name | t_{\max} | t_{\max}^{er} | MJD | z_{cmb} | $z_{\text{cmb}}^{\text{er}}$ | H_{\max} | H_{\max}^{er} | N_H | $s_{BV,H}^{\text{er}}$ | μ | μ^{er} | N_μ | $s_{BV,\mu}^{\text{er}}$ | Ref. a | Samp. b |
|-----------|------------|------------------------|--------|------------------|------------------------------|------------|------------------------|-------|------------------------|--------|-------------------|---------|--------------------------|----------|-----------|
| SN 2004gu | 53361.0 | 0.0 | 0.0478 | 0.0002 | 18.071 | 0.063 | 7 | 1.261 | 0.02 0 | | | | | C10 | CSP |
| SN 2005A | 53379.0 | 0.0 | 0.0188 | 4.0027e-05 | 16.292 | 0.073 | 10 | 0.982 | 0.009 | 34.626 | 0.039 | 196 | 1.108 | 0.030 | C10 |
| SN 2005M | 53405.0 | 0.0 | 0.0274 | 0.0001 | 16.641 | 0.044 | 14 | 1.240 | 0.008 | 35.170 | 0.012 | 476 | 1.220 | 0.008 | C10 |
| SN 2005ag | 53413.0 | 0.0 | 0.0794 | 0.0001 | 19.050 | 0.070 | 9 | 1.148 | 0.012 | | | | | C10 | CSP |
| SN 2005al | 53430.0 | 0.0 | 0.0123 | 6.3377e-05 | 15.63 | 0.047 | 8 | 0.879 | 0.003 | 34.066 | 0.008 | 239 | 0.870 | 0.003 | C10 |
| SN 2005am | 53436.0 | 0.0 | 0.0076 | 0.0001 | 14.033 | 0.052 | 6 | 0.772 | 0.003 | 32.455 | 0.007 | 483 | 0.752 | 0.003 | C10 |
| SN 2005ao | 53439.0 | 0.07 | 0.0394 | 0.0004 | 17.871 | 0.094 | 8 | 1.117 | 0.226 | 36.242 | 0.457 | 27 | 1.116 | 0.213 | F15 |
| SN 2005bl | 53482.0 | 0.0 | 0.0245 | 9.6733e-05 | 16.990 | 0.130 | 13 | 0.364 | 0.007 | | | | | T08,F15 | F15 |
| SN 2005bo | 53479.0 | 0.07 | 0.0140 | 7.3384e-05 | 15.253 | 0.037 | 16 | 0.857 | 0.003 | | | | | F15 | F15 |
| SN 2005cf | 53533.0 | 0.0 | 0.0067 | 3.6692e-05 | 13.912 | 0.041 | 17 | 1.070 | 0.010 | 32.379 | 0.009 | 401 | 0.998 | 0.005 | F15 |
| SN 2005ch | 53535.0 | 0.46 | 0.0269 | 0.0050 | 16.605 | 0.070 | 11 | 0.946 | 0.0490 | | | | | F15 | F15 |
| SN 2005el | 53646.0 | 0.0 | 0.0145 | 2.6685e-05 | 15.578 | 0.026 | 4.9 | 0.876 | 0.004 | 34.096 | 0.010 | 550 | 0.868 | 0.004 | C10,F15 |
| SN 2005eq | 53653.0 | 0.0 | 0.0284 | 8.3391e-05 | 17.042 | 0.028 | 43 | 1.283 | 0.005 | 35.461 | 0.012 | 454 | 1.135 | 0.010 | C10,F15 |
| SN 2005eu | 53659.0 | 0.0 | 0.0350 | 4.6698e-05 | 16.864 | 0.057 | 23 | 1.112 | 0.033 | | | | | F15 | F15 |
| SN 2005hc | 53666.0 | 0.0 | 0.0462 | 0.0001 | 17.961 | 0.137 | 9 | 1.202 | 0.006 | 36.537 | 0.009 | 504 | 1.133 | 0.008 | C10 |
| SN 2005hj | 53674.0 | 0.0 | 0.0580 | 0.0001 | 18.321 | 0.130 | 10 | 1.2 | 0.008 | 36.996 | 0.012 | 247 | 1.194 | 0.009 | S11 |
| SN 2005hk | 53685.0 | 0.0 | 0.0128 | 7.0048e-05 | 15.533 | 0.102 | 25 | 0.522 | 0.015 | | | | | F15 | F15 |
| SN 2005iq | 53687.0 | 0.0 | 0.0336 | 0.0001 | 17.458 | 0.059 | 20 | 0.902 | 0.005 | 35.948 | 0.014 | 207 | 0.899 | 0.007 | C10,F15 |
| SN 2005kc | 53697.0 | 0.0 | 0.0154 | 5.6705e-05 | 15.575 | 0.061 | 8 | 0.922 | 0.012 | 33.965 | 0.024 | 131 | 0.908 | 0.014 | C10 |
| SN 2005ki | 53705.0 | 0.0 | 0.0193 | 6.3377e-05 | 16.260 | 0.031 | 10 | 0.836 | 0.003 | 34.677 | 0.008 | 356 | 0.826 | 0.004 | C10 |
| SN 2005ku | 53693.0 | 0.0 | 0.0454 | 0.0001 | 16.904 | 0.312 | 4 | 1.500 | 0.043 | | | | | S11 | CSP |
| SN 2005ls | 53714.0 | 0.0 | 0.0214 | 0.0001 | 15.653 | 0.041 | 19 | 1.131 | 0.024 | | | | | F15 | F15 |
| SN 2005ma | 53740.0 | 0.46 | 0.0261 | 8.6726e-05 | 16.879 | 0.056 | 16 | 0.973 | 0.018 | | | | | C10,F15 | CSP |
| SN 2006D | 53756.0 | 0.0 | 0.0085 | 6.0041e-05 | 14.553 | 0.045 | 37 | 0.893 | 0.006 | 32.942 | 0.010 | 485 | 0.861 | 0.004 | C10,F15 |
| SN 2006N | 53760.0 | 0.46 | 0.0149 | 9.0062e-05 | 15.170 | 0.078 | 12 | 0.793 | 0.02 | 34.202 | 0.021 | 114 | 0.776 | 0.009 | F15 |
| SN 2006X | 53786.0 | 0.0 | 0.0036 | 6.6712e-05 | 12.926 | 0.017 | 75 | 0.972 | 0.005 | 30.958 | 0.020 | 686 | 0.934 | 0.009 | C10,F15 |
| SN 2006ac | 53781.0 | 0.46 | 0.0237 | 5.6705e-05 | 16.904 | 0.105 | 15 | 0.889 | 0.022 | 34.903 | 0.021 | 164 | 0.871 | 0.008 | F15 |
| SN 2006ax | 53826.0 | 0.0 | 0.0165 | 6.6712e-05 | 15.973 | 0.041 | 31 | 1.090 | 0.014 | 34.334 | 0.009 | 342 | 1.000 | 0.005 | C10,F15 |
| SN 2006bd | 53822.0 | 0.46 | 0.0280 | 0.0001 | 17.275 | 0.117 | 2 | 0.346 | 0.028 | 35.682 | 0.025 | 56 | 0.363 | 0.012 | S11 |
| SN 2006bh | 53823.0 | 0.0 | 0.0102 | 3.3356e-05 | 14.942 | 0.034 | 10 | 0.835 | 0.004 | 33.399 | 0.011 | 176 | 0.824 | 0.006 | C10 |
| SN 2006br | 53849.0 | 0.46 | 0.0250 | 0.0001 | 17.140 | 0.130 | 5 | 0.946 | 0.034 | 35.510 | 0.036 | 60 | 0.950 | 0.024 | S11 |
| SN 2006bt | 53858.0 | 0.0 | 0.0510 | 0.0001 | 16.798 | 0.125 | 5 | 1.189 | 0.012 | | | | | S11 | CSP |
| SN 2006cp | 53897.0 | 0.46 | 0.0227 | 4.6698e-05 | 16.637 | 0.090 | 5 | 1.047 | 0.014 | 34.970 | 0.0260 | 93 | 1.029 | 0.018 | F15 |
| SN 2006cz | 53908.0 | 0.0 | 0.0420 | 0.0002 | 17.848 | 0.636 | 2 | 1.129 | 0.262 | | | | | F15 | F15 |
| SN 2006ej | 53974.0 | 0.0 | 0.0205 | 0.0001 | 16.287 | 0.148 | 3 | 0.902 | 0.022 | 34.734 | 0.018 | 225 | 0.872 | 0.007 | S11 |
| SN 2006eq | 53976.0 | 0.0 | 0.0498 | 8.0055e-05 | 18.080 | 0.280 | 8 | 0.672 | 0.031 | 36.629 | 0.031 | 190 | 0.662 | 0.016 | C10 |
| SN 2006et | 53993.0 | 0.0 | 0.0226 | 0.0001 | 16.354 | 0.034 | 13 | 1.212 | 0.007 | 34.790 | 0.009 | 205 | 1.189 | 0.006 | S11 |
| SN 2006ev | 53987.0 | 0.46 | 0.0292 | 6.0041e-05 | 17.2 | 0.087 | 8 | 0.900 | 0.021 | 35.687 | 0.019 | 106 | 0.898 | 0.008 | S11 |
| SN 2006gj | 53999.0 | 0.0 | 0.0279 | 3.0020e-05 | 17.166 | 0.133 | 4 | 0.718 | 0.010 | 35.628 | 0.017 | 153 | 0.640 | 0.011 | S11 |

Table 4 continued on next page

Table 4 (*continued*)

| Name | t_{\max} | t_{\max}^{err} | MJD | MJD | z_{cmb} | $z_{\text{cmb}}^{\text{err}}$ | H_{\max} | H_{\max}^{err} | N_H | $s_{BV,H}^{\text{err}}$ | μ | μ^{err} | N_μ | $s_{BV,\mu}^{\text{err}}$ | $s_{BV,\mu}^{\text{err}}$ | Ref. <i>a</i> | Samp. <i>b</i> |
|-----------|------------|-------------------------|--------|------------|------------------|-------------------------------|------------|-------------------------|-------|-------------------------|-------|--------------------|---------|---------------------------|---------------------------|---------------|----------------|
| SN 2006gr | 54012.0 | 0.0 | 0.0351 | 7.3384e-05 | 16.920 | 0.160 | 5 | 1.158 | 0.021 | | | | | | | | F15 |
| SN 2006gt | 54003.0 | 0.0 | 0.0446 | 7.6719e-05 | 18.201 | 0.066 | 6 | 0.575 | 0.009 | 36.525 | 0.015 | 108 | 0.567 | 0.008 | C10 | CSP | |
| SN 2006hb | 54004.0 | 0.46 | 0.0146 | 0.0001 | 15.839 | 0.070 | 9 | 0.643 | 0.019 | 34.051 | 0.013 | 270 | 0.652 | 0.007 | S11 | CSP | |
| SN 2006hx | 54021.0 | 0.0 | 0.0453 | 0.0001 | 17.873 | 0.095 | 5 | 0.982 | 0.016 | | | | | | | S11 | CSP |
| SN 2006is | 54009.0 | 0.46 | 0.0313 | 0.0001 | 17.200 | 0.098 | 7 | 1.137 | 0.034 | 35.537 | 0.034 | 206 | 1.132 | 0.022 | S11 | CSP | |
| SN 2006kf | 54041.0 | 0.0 | 0.0210 | 0.0001 | 16.347 | 0.048 | 11 | 0.751 | 0.004 | 34.789 | 0.011 | 194 | 0.708 | 0.006 | S11 | CSP | |
| SN 2006le | 54047.0 | 0.0 | 0.0180 | 4.0027e-05 | 16.232 | 0.042 | 36 | 1.112 | 0.014 | 34.412 | 0.018 | 287 | 1.115 | 0.015 | F15 | F15 | |
| SN 2006lf | 54044.0 | 0.0 | 0.0135 | 3.3356e-05 | 15.107 | 0.052 | 41 | 0.873 | 0.012 | 33.581 | 0.021 | 224 | 0.838 | 0.009 | F15 | F15 | |
| SN 2006lu | 54036.0 | 0.46 | 0.0534 | 0.0001 | 17.743 | 0.133 | 2 | 0.996 | 0.02 | 36.762 | 0.016 | 131 | 0.993 | 0.007 | S11 | CSP | |
| SN 2006ob | 54062.0 | 0.0 | 0.0590 | 0.0001 | 18.457 | 0.337 | 5 | 0.648 | 0.021 | 37.073 | 0.025 | 163 | 0.674 | 0.014 | S11 | CSP | |
| SN 2006os | 54063.0 | 0.46 | 0.0327 | 0.0001 | 17.278 | 0.126 | 5 | 0.951 | 0.023 | 35.583 | 0.027 | 114 | 0.937 | 0.011 | S11 | CSP | |
| SN 2006ot | 54069.0 | 0.0 | 0.0525 | 0.0001 | 18.025 | 0.253 | 7 | 0.683 | 0.032 | 36.370 | 0.055 | 130 | 0.662 | 0.037 | S11 | CSP | |
| SN 2007A | 54112.0 | 0.0 | 0.0176 | 0.0001 | 15.926 | 0.145 | 3 | 1.116 | 0.023 | 34.475 | 0.028 | 74 | 1.090 | 0.025 | S11 | CSP | |
| SN 2007S | 54143.0 | 0.0 | 0.0137 | 6.3377e-05 | 15.534 | 0.026 | 45 | 1.276 | 0.008 | 34.075 | 0.014 | 432 | 1.254 | 0.008 | S11,F15 | F15 | |
| SN 2007af | 54173.0 | 0.0 | 0.0054 | 0.0001 | 13.661 | 0.034 | 24 | 1.086 | 0.010 | 32.006 | 0.005 | 976 | 0.939 | 0.002 | S11 | CSP | |
| SN 2007ai | 54173.0 | 0.0 | 0.0318 | 0.0001 | 17.040 | 0.039 | 6 | 1.220 | 0.007 | 35.749 | 0.031 | 132 | 1.129 | 0.025 | S11 | CSP | |
| SN 2007as | 54180.0 | 0.46 | 0.0167 | 0.0004 | 16.084 | 0.050 | 10 | 0.942 | 0.019 | 34.671 | 0.030 | 141 | 0.934 | 0.012 | S11 | CSP | |
| SN 2007ba | 54197.0 | 0.0 | 0.0383 | 0.0001 | 17.614 | 0.095 | 8 | 0.552 | 0.009 | 35.778 | 0.021 | 134 | 0.568 | 0.011 | S11 | CSP | |
| SN 2007bc | 54199.0 | 0.0 | 0.0207 | 0.0001 | 16.430 | 0.102 | 6 | 0.925 | 0.007 | 34.772 | 0.016 | 183 | 0.896 | 0.006 | S11 | CSP | |
| SN 2007bd | 54206.0 | 0.0 | 0.0306 | 0.0001 | 17.396 | 0.145 | 7 | 0.903 | 0.011 | 35.630 | 0.018 | 131 | 0.897 | 0.008 | S11 | CSP | |
| SN 2007bm | 54223.0 | 0.0 | 0.0066 | 9.6733e-05 | 14.035 | 0.059 | 7 | 0.953 | 0.009 | | | | | | S11 | CSP | |
| SN 2007ca | 54226.0 | 0.0 | 0.0142 | 6.3377e-05 | 15.683 | 0.061 | 25 | 1.121 | 0.021 | 34.379 | 0.020 | 219 | 1.090 | 0.016 | S11,F15 | F15 | |
| SN 2007co | 54265.0 | 0.0 | 0.0278 | 0.0001 | 17.308 | 0.170 | 6 | 0.956 | 0.007 | | | | | | F15 | F15 | |
| SN 2007cq | 54280.0 | 0.0 | 0.0250 | 0.0001 | 16.519 | 0.121 | 6 | 1.018 | 0.008 | | | | | | F15 | F15 | |
| SN 2007fb | 54287.0 | 0.46 | 0.0177 | 6.3377e-05 | 16.145 | 0.169 | 2 | 0.861 | 0.020 | | | | | | F15 | F15 | |
| SN 2007hx | 54354.0 | 0.0 | 0.0797 | 0.0001 | 18.730 | 0.141 | 4 | 1.022 | 0.023 | | | | | | S11 | CSP | |
| SN 2007jg | 54366.0 | 0.0 | 0.0369 | 0.0001 | 17.882 | 0.141 | 5 | 0.944 | 0.005 | 36.174 | 0.016 | 303 | 0.931 | 0.007 | S11 | CSP | |
| SN 2007le | 54398.0 | 0.0 | 0.0066 | 0.0001 | 13.957 | 0.029 | 46 | 1.123 | 0.010 | 32.311 | 0.009 | 500 | 1.053 | 0.006 | S11,F15 | F15 | |
| SN 2007nq | 54397.0 | 0.46 | 0.0448 | 0.0001 | 17.733 | 0.101 | 6 | 0.816 | 0.018 | 36.277 | 0.013 | 238 | 0.793 | 0.006 | S11,F15 | CSP | |
| SN 2007on | 54419.0 | 0.0 | 0.0058 | 3.3356e-05 | 13.295 | 0.027 | 25 | 0.555 | 0.005 | 31.577 | 0.006 | 453 | 0.577 | 0.003 | S11 | CSP | |
| SN 2007rx | 54442.0 | 0.07 | 0.0304 | 6.3377e-05 | 16.186 | 0.088 | 5 | 1.174 | 0.025 | | | | | | F15 | F15 | |
| SN 2007sr | 54446.0 | 0.46 | 0.0058 | 0.0001 | 13.369 | 0.038 | 31 | 1.108 | 0.030 | 31.803 | 0.016 | 405 | 1.174 | 0.011 | F15 | F15 | |
| SN 2008A | 54479.0 | 0.0 | 0.0168 | 5.6705e-05 | 16.106 | 0.138 | 14 | 1.189 | 0.032 | | | | | | F15 | F15 | |
| SN 2008C | 54465.0 | 0.46 | 0.0166 | 2.6685e-05 | 16.085 | 0.059 | 21 | 0.973 | 0.02 | 34.256 | 0.014 | 291 | 0.963 | 0.007 | S11,F15 | CSP | |
| SN 2008R | 54494.0 | 0.0 | 0.0130 | 7.3384e-05 | 15.485 | 0.088 | 5 | 0.626 | 0.010 | 33.791 | 0.016 | 88 | 0.612 | 0.010 | S11 | CSP | |
| SN 2008Z | 54514.0 | 0.0 | 0.0214 | 0.0002 | 16.682 | 0.051 | 44 | 1.249 | 0.011 | 35.283 | 0.024 | 258 | 1.100 | 0.019 | F15 | F15 | |
| SN 2008ae | 54512.0 | 0.0 | 0.0301 | 0.0001 | 17.346 | 0.191 | 23 | 1.189 | 0.047 | 35.702 | 0.065 | 129 | 0.511 | 0.023 | F15 | F15 | |
| SN 2008bc | 54549.0 | 0.0 | 0.0143 | 0.0001 | 15.816 | 0.051 | 11 | 1.091 | 0.013 | 34.069 | 0.014 | 223 | 1.075 | 0.011 | S11 | CSP | |
| SN 2008bq | 54563.0 | 0.0 | 0.0331 | 5.3370e-05 | 17.514 | 0.108 | 4 | 1.078 | 0.007 | 35.658 | 0.016 | 107 | 1.058 | 0.011 | S11 | CSP | |

Table 4 *continued on next page*

Table 4 (continued)

| Name | t_{\max} | t_{\max}^{er} | MJD | z_{cmb} | $z_{\text{cmb}}^{\text{er}}$ | H_{\max} | H_{\max}^{er} | N_H | $s_{BV,H}^{\text{er}}$ | μ | μ^{er} | N_μ | $s_{BV,\mu}^{\text{er}}$ | $\text{Ref. } a$ | Samp. b |
|-----------|------------|------------------------|--------|------------------|------------------------------|------------|------------------------|-------|------------------------|--------|-------------------|---------|--------------------------|------------------|-----------|
| SN 2008fp | 54730.0 | 0.0 | 0.0056 | 0.0001 | 13.545 | 0.016 | 20 | 1.100 | 0.008 | | | | | S11 | CSP |
| SN 2008fr | 54732.0 | 0.46 | 0.0490 | 5.3370e-05 | 18.430 | 0.141 | 6 | 1.098 | 0.027 | 36.174 | 0.020 | 114 | 1.063 | 0.012 | F15 |
| SN 2008fv | 54752.0 | 0.0 | 0.0104 | 5.0034e-05 | 14.977 | 0.088 | 3 | 0.794 | 0.121 | | | | | F15 | F15 |
| SN 2008fx | 54748.0 | 0.0 | 0.0536 | 8.3391e-05 | 18.438 | 0.086 | 5 | 2.846 | 3.637 | | | | | F15 | F15 |
| SN 2008gb | 54746.0 | 0.46 | 0.0374 | 4.3363e-05 | 17.584 | 0.064 | 14 | 1.040 | 0.027 | 36.070 | 0.024 | 108 | 1.025 | 0.014 | F15 |
| SN 2008gl | 54768.0 | 0.0 | 0.0339 | 0.0001 | 17.192 | 0.071 | 12 | 0.862 | 0.009 | 35.816 | 0.016 | 84 | 0.853 | 0.008 | F15 |
| SN 2008gp | 54778.0 | 0.0 | 0.0330 | 0.0001 | 17.488 | 0.144 | 9 | 1.117 | 0.023 | 35.678 | 0.018 | 136 | 1.012 | 0.010 | S11 |
| SN 2008hm | 54804.0 | 0.0 | 0.0194 | 9.6733e-05 | 16.495 | 0.043 | 22 | 1.122 | 0.016 | 34.621 | 0.028 | 166 | 1.060 | 0.019 | F15 |
| SN 2008hs | 54812.0 | 0.0 | 0.0178 | 8.3391e-05 | 16.356 | 0.056 | 21 | 0.563 | 0.012 | 34.712 | 0.019 | 285 | 0.632 | 0.009 | F15 |
| SN 2008hv | 54816.0 | 0.0 | 0.0125 | 0.0001 | 15.523 | 0.048 | 45 | 0.898 | 0.006 | 33.862 | 0.008 | 633 | 0.863 | 0.003 | S11,F15 |
| SN 2008hy | 54800.0 | 0.07 | 0.0094 | 5.3370e-05 | 14.333 | 0.032 | 23 | 0.859 | 0.006 | | | | | F15 | F15 |
| SN 2008ia | 54812.0 | 0.0 | 0.0208 | 0.0001 | 16.329 | 0.052 | 14 | 0.888 | 0.006 | 34.857 | 0.014 | 135 | 0.874 | 0.006 | S11 |
| SN 2009D | 54841.0 | 0.46 | 0.0243 | 4.3363e-05 | 16.645 | 0.023 | 24 | 1.186 | 0.024 | 35.049 | 0.035 | 138 | 1.174 | 0.022 | F15 |
| SN 2009ad | 54886.0 | 0.0 | 0.0280 | 1.6678e-05 | 16.949 | 0.033 | 20 | 1.028 | 0.010 | 35.418 | 0.018 | 150 | 1.025 | 0.010 | F15 |
| SN 2009al | 54896.0 | 0.0 | 0.0237 | 0.0001 | 16.514 | 0.049 | 22 | 1.189 | 0.019 | 34.912 | 0.040 | 146 | 0.953 | 0.024 | F15 |
| SN 2009an | 54898.0 | 0.0 | 0.0103 | 0.0001 | 14.946 | 0.022 | 29 | 0.855 | 0.006 | 33.321 | 0.012 | 205 | 0.846 | 0.006 | F15 |
| SN 2009bv | 54926.0 | 0.0 | 0.0374 | 8.00555e-05 | 17.505 | 0.055 | 13 | 1.118 | 0.029 | 36.328 | 0.036 | 100 | 1.105 | 0.026 | F15 |
| SN 2009do | 54945.0 | 0.46 | 0.0405 | 9.0062e-05 | 17.535 | 0.070 | 9 | 0.944 | 0.025 | 36.123 | 0.026 | 98 | 0.942 | 0.012 | F15 |
| SN 2009ds | 54960.0 | 0.0 | 0.0192 | 7.0048e-05 | 16.327 | 0.127 | 6 | 1.092 | 0.031 | 34.765 | 0.022 | 60 | 1.067 | 0.014 | F15 |
| SN 2009fv | 54995.0 | 0.46 | 0.0308 | 7.3384e-05 | 15.359 | 0.236 | 5 | 0.854 | 0.042 | | | | | F15 | F15 |
| SN 2009ig | 55080.0 | 0.0 | 0.0085 | 3.6692e-05 | 14.254 | 0.115 | 9 | 1.121 | 0.011 | 32.693 | 0.013 | 386 | 1.202 | 0.008 | F15 |
| SN 2009im | 55080.0 | 0.07 | 0.0127 | 0.0001 | 15.248 | 0.097 | 11 | 0.365 | 0.020 | | | | | F15 | F15 |
| SN 2009jr | 55119.0 | 0.0 | 0.0170 | 7.3384e-05 | 16.957 | 0.112 | 14 | 1.122 | 0.041 | | | | | F15 | F15 |
| SN 2009kk | 55126.0 | 0.46 | 0.0124 | 0.0001 | 15.621 | 0.052 | 17 | 0.889 | 0.019 | | | | | F15 | F15 |
| SN 2009kq | 55155.0 | 0.0 | 0.0126 | 6.0041e-05 | 15.316 | 0.051 | 11 | 0.989 | 0.006 | | | | | F15 | F15 |
| SN 2009le | 55165.0 | 0.0 | 0.0172 | 4.6698e-05 | 15.972 | 0.162 | 7 | 0.951 | 0.025 | 34.32 | 0.028 | 57 | 0.984 | 0.019 | F15 |
| SN 2009if | 55148.0 | 0.46 | 0.0450 | 0.0004 | 17.374 | 0.080 | 16 | 0.838 | 0.025 | 35.802 | 0.030 | 98 | 0.841 | 0.014 | F15 |
| SN 2009na | 55201.0 | 0.0 | 0.0225 | 9.6733e-05 | 16.468 | 0.105 | 10 | 0.958 | 0.011 | 34.852 | 0.020 | 90 | 0.937 | 0.012 | F15 |
| SN 2010Y | 55247.0 | 0.0 | 0.0118 | 0.0001 | 15.278 | 0.162 | 10 | 0.560 | 0.012 | 33.794 | 0.018 | 250 | 0.626 | 0.009 | F15 |
| SN 2010ag | 55270.0 | 0.0 | 0.0347 | 0.0001 | 17.584 | 0.069 | 15 | 1.217 | 0.017 | 35.611 | 0.034 | 102 | 1.148 | 0.029 | F15 |
| SN 2010ai | 55277.0 | 0.0 | 0.0203 | 0.0001 | 16.441 | 0.052 | 17 | 0.834 | 0.008 | 35.11 | 0.016 | 135 | 0.826 | 0.007 | F15 |
| SN 2010cr | 55310.0 | 0.07 | 0.0237 | 0.0001 | 17.005 | 0.080 | 12 | 0.705 | 0.030 | 35.317 | 0.049 | 112 | 0.732 | 0.022 | F15 |
| SN 2010dl | 55339.0 | 0.46 | 0.0303 | 0.0001 | 17.168 | 0.158 | 3 | 1.202 | 0.354 | | | | | F15 | F15 |
| SN 2010dm | 55350.0 | 0.46 | 0.0333 | 5.3370e-05 | 17.540 | 0.044 | 6 | 1.262 | 0.037 | | | | | BN12 | BN12 |
| SN 2010dw | 55357.0 | 0.0 | 0.0384 | 0.0001 | 17.659 | 0.111 | 6 | 1.227 | 0.029 | 36.137 | 0.023 | 47 | 1.189 | 0.018 | F15 |
| SN 2010ew | 55381.0 | 0.46 | 0.0267 | 0.0001 | 16.297 | 0.260 | 4 | 0.681 | 0.224 | | | | | F15 | F15 |
| SN 2010ex | 55384.0 | 0.46 | 0.0227 | 7.6719e-05 | 16.664 | 0.363 | 2 | 0.672 | 0.421 | | | | | F15 | F15 |
| SN 2010gn | 55390.0 | 0.0 | 0.0313 | 0.0001 | 17.326 | 0.058 | 8 | 0.743 | 0.032 | 35.814 | 0.067 | 68 | 0.909 | 0.025 | F15, BN12 |
| SN 2010gy | 55426.0 | 0.0 | 0.0660 | 0.0001 | 19.134 | 0.123 | 4 | 0.904 | 0.017 | 37.464 | 0.037 | 88 | 0.904 | 0.014 | BN12 |

Table 4 continued on next page

Table 4 (continued)

| Name | t_{\max} | t_{\max}^{err} | MJD | MJD | z_{cmb} | $z_{\text{err,cmb}}$ | H_{\max} | H_{\max}^{err} | N_H | $s_{BV,H}^{\text{err}}$ | μ | μ^{err} | N_μ | $s_{BV,\mu}^{\text{err}}$ | Ref. <i>a</i> | Samp. <i>b</i> |
|-----------------|------------|-------------------------|--------|------------|------------------|----------------------|------------|-------------------------|-------|-------------------------|-------|--------------------|---------|---------------------------|---------------|----------------|
| SN 2010ho | 55442.0 | 0.0 | 0.0410 | 0.0001 | 18.012 | 0.027 | 4 | 1.039 | 0.067 | | | | | | BN12 | BN12 |
| SN 2010hs | 55454.0 | 0.0 | 0.0770 | 0.0001 | 19.336 | 0.063 | 4 | 2.802 | 1.522 | | | | | | BN12 | BN12 |
| SN 2010iw | 55496.0 | 0.46 | 0.0217 | 4.0027e-05 | 16.248 | 0.052 | 18 | 1.093 | 0.038 | | | | | | F15 | F15 |
| SN 2010ju | 55523.0 | 0.0 | 0.0151 | 1.3342e-05 | 15.583 | 0.036 | 19 | 1.101 | 0.043 | | | | | | F15 | F15 |
| SN 2010jv | 55519.0 | 0.0 | 0.0137 | 8.6726e-05 | 15.341 | 0.034 | 3 | 0.903 | 0.089 | | | | | | F15 | F15 |
| SN 2010kg | 55543.0 | 0.0 | 0.0163 | 3.6692e-05 | 15.85 | 0.033 | 27 | 0.918 | 0.012 | 34.025 | 0.054 | 117 | 0.889 | 0.019 | F15 | F15 |
| SN 2011B | 55583.0 | 0.0 | 0.0058 | 5.3370e-05 | 13.263 | 0.027 | 43 | 0.882 | 0.009 | 31.884 | 0.035 | 222 | 0.871 | 0.012 | F15 | F15 |
| SN 2011K | 55577.0 | 0.0 | 0.0145 | 0.0010 | 15.504 | 0.022 | 16 | 1.174 | 0.016 | | | | | | F15 | F15 |
| SN 2011aa | 55597.0 | 0.46 | 0.0132 | 9.6733e-05 | 14.414 | 0.042 | 28 | 2.391 | 0.075 | | | | | | F15 | F15 |
| SN 2011ae | 55619.0 | 0.46 | 0.0064 | 9.6733e-05 | 13.507 | 0.048 | 31 | 0.940 | 0.026 | | | | | | F15 | F15 |
| SN 2011ao | 55639.0 | 0.0 | 0.0115 | 6.3377e-05 | 14.917 | 0.020 | 29 | 1.010 | 0.012 | 33.531 | 0.039 | 178 | 1.038 | 0.016 | F15 | F15 |
| SN 2011at | 55634.0 | 0.46 | 0.0066 | 8.0055e-05 | 14.021 | 0.046 | 14 | 0.872 | 0.027 | 32.466 | 0.034 | 76 | 0.896 | 0.014 | F15 | F15 |
| SN 2011de | 55711.0 | 0.0 | 0.0302 | 5.0034e-05 | 15.998 | 0.060 | 24 | 1.804 | 0.099 | | | | | | F15 | F15 |
| SN 2011df | 55716.0 | 0.0 | 0.0155 | 0.0001 | 15.581 | 0.019 | 25 | 1.090 | 0.016 | | | | | | F15 | F15 |
| SN 2011fs | 55833.0 | 0.07 | 0.0211 | 0.0001 | 16.127 | 0.036 | 4 | 1.174 | 0.029 | 34.651 | 0.021 | 39 | 1.174 | 0.026 | W18 | W18 |
| SN 2011io | 55894.0 | 0.46 | 0.0396 | 0.0004 | 18.263 | 0.020 | 1 | 0.955 | 0.014 | | | | | | W18 | W18 |
| SN 2012bh | 56016.0 | 0.46 | 0.0267 | 8.3391e-05 | 16.957 | 0.020 | 1 | 0.955 | 0.014 | | | | | | W18 | W18 |
| SN 2012bp | 56013.0 | 0.46 | 0.0282 | 0.0002 | 17.104 | 0.020 | 1 | 0.955 | 0.014 | | | | | | W18 | W18 |
| SN 2012em | 56187.0 | 0.46 | 0.0379 | 0.0003 | 18.120 | 0.020 | 1 | 0.955 | 0.014 | | | | | | W18 | W18 |
| SN 2012fk | 56223.0 | 0.07 | 0.0350 | 0.0003 | 17.467 | 0.046 | 3 | 0.668 | 0.015 | | | | | | W18 | W18 |
| SN 2013bs | 56408.0 | 0.07 | 0.0275 | 0.0002 | 16.78 | 0.122 | 7 | 0.654 | 0.072 | 35.020 | 0.345 | 21 | 0.656 | 0.074 | W18 | W18 |
| SN 2013bt | 56408.0 | 0.0 | 0.0363 | 0.0003 | 17.536 | 0.173 | 5 | 0.891 | 0.121 | | | | | | W18 | W18 |
| SN 2013cs | 56436.0 | 0.0 | 0.0093 | 7.3384e-05 | 14.528 | 0.101 | 4 | 1.081 | 0.022 | 32.727 | 0.043 | 137 | 1.098 | 0.034 | W18 | W18 |
| SN 2013cv | 56429.0 | 0.0 | 0.0350 | 0.0003 | 17.643 | 0.052 | 11 | 1.111 | 0.023 | 36.148 | 0.035 | 159 | 1.114 | 0.026 | W18 | W18 |
| SN 2013fn | 56572.0 | 0.46 | 0.0269 | 0.0002 | 17.106 | 0.054 | 3 | 0.945 | 0.031 | 35.137 | 0.078 | 42 | 0.941 | 0.040 | W18 | W18 |
| SNF20080522-000 | 54621.0 | 0.0 | 0.0471 | 0.0004 | 17.475 | 0.308 | 3 | 1.104 | 0.044 | 36.23 | 0.056 | 58 | 1.174 | 0.050 | F15 | F15 |
| SNF20080522-011 | 54617.0 | 0.46 | 0.0377 | 0.0003 | 17.740 | 0.089 | 9 | 1.074 | 0.033 | 36.113 | 0.034 | 86 | 1.096 | 0.023 | F15 | F15 |
| iPTF13dge | 56558.0 | 0.0 | 0.0156 | 3.3356e-05 | 15.961 | 0.069 | 8 | 0.924 | 0.009 | 33.927 | 0.036 | 452 | 0.880 | 0.011 | W18 | W18 |
| iPTF13dkl | 56566.0 | 0.46 | 0.0400 | 0.0004 | 18.476 | 0.094 | 2 | 0.739 | 0.053 | 36.368 | 0.065 | 12 | 0.886 | 0.032 | W18 | W18 |
| iPTF13lkx | 56568.0 | 0.46 | 0.0300 | 0.0003 | 17.304 | 0.143 | 4 | 0.950 | 0.127 | | | | | | W18 | W18 |
| iPTF13ebh | 56623.0 | 0.0 | 0.0129 | 8.6726e-05 | 15.324 | 0.158 | 3 | 0.623 | 0.013 | 33.395 | 0.028 | 228 | 0.609 | 0.013 | W18 | W18 |

a Reference codes J99: Jha et al. (1999); H00: Hernandez et al. (2000); K00: Krisenciunas et al. (2004a); K04a: Krisenciunas et al. (2004b); Krisenciunas et al. (2006); Ph06: Phillips et al. (2006); Pa07a: Pastorello et al. (2007a); St07: Stanishev et al. (2007); F15: Fransson et al. (2015); C10: Contreras et al. (2010); S11: Stritzinger et al. (2011); BN12: Barone-Nugent et al. (2012); W14; Weyant et al. (2014); F15: Friedman et al. (2015); W18: Weyant et al. (2018)

b Sample name used for the divisions in the analysis. Some SNe Ia were observed by multiple projects. We assign each SNe Ia to a single sample for the purposes of quoting dispersions and distributions in the analysis.

Table 5. SN Sample Mean and Std Deviations

| Sample | SNeIa | residual | wgt residual | χ^2 | χ^2/DoF | stddev | IQR | SEM | Implied σ_H^{int} | Notes |
|--------------|-------|----------|--------------|----------|---------------------|--------|--------|--------|--------------------------|--|
| | | mag | mag | | mag | mag | mag | mag | mag | |
| All | 144 | 0.0330 | -0.0000 | 359.8 | 2.50 | 0.2294 | 0.2106 | 0.0191 | 0.1770 | |
| Light | 40 | 0.0538 | 0.0495 | 60.8 | 1.52 | 0.1868 | 0.2146 | 0.0295 | 0.1276 | $M < 1e+10 M_\odot$ |
| Heavy | 59 | 0.0151 | -0.0314 | 197.5 | 3.35 | 0.2365 | 0.2185 | 0.0308 | 0.1967 | $M \geq 1e+10 M_\odot$ |
| Light | 40 | 0.0538 | 0.0495 | 60.8 | 1.52 | 0.1868 | 0.2146 | 0.0295 | 0.1276 | $M < 1e+10 M_\odot$, $\Delta H_{\max} > -0.5 \text{ mag}$ |
| Heavy | 57 | 0.0427 | 0.0363 | 69.0 | 1.21 | 0.1869 | 0.2074 | 0.0248 | 0.1061 | $M \geq 1e+10 M_\odot$, $\Delta H_{\max} > -0.5 \text{ mag}$ |
| Hubble Flow | 80 | -0.0176 | -0.0318 | 292.8 | 3.66 | 0.2344 | 0.2260 | 0.0262 | 0.2090 | $z > 0.02$ |
| Hubble Light | 25 | 0.0415 | 0.0499 | 53.3 | 2.13 | 0.1951 | 0.2113 | 0.0390 | 0.1614 | $z > 0.02, M < 1e+10 M_\odot$ |
| Hubble Heavy | 31 | -0.0381 | -0.0782 | 164.9 | 5.32 | 0.2452 | 0.1992 | 0.0440 | 0.2333 | $z > 0.02, M \geq 1e+10 M_\odot$ |

Table 6. SN Sample Mean and Std Deviations - Optical

| Sample | SNeIa | residual | wgt residual | χ^2 | χ^2/DoF | stddev | IQR | SEM | Implied σ_μ^{int} | Notes |
|--------|-------|----------|--------------|----------|---------------------|--------|--------|--------|----------------------------|------------------------|
| | | mag | mag | | mag | mag | mag | mag | mag | |
| All | 104 | 0.0338 | 0.0000 | 242.9 | 2.34 | 0.2094 | 0.2063 | 0.0205 | 0.1622 | |
| Light | 23 | 0.1116 | 0.0523 | 81.1 | 3.53 | 0.2278 | 0.2021 | 0.0475 | 0.2145 | $M < 1e+10 M_\odot$ |
| Heavy | 48 | 0.0063 | -0.0170 | 102.9 | 2.14 | 0.1993 | 0.1499 | 0.0288 | 0.1500 | $M \geq 1e+10 M_\odot$ |

Table 7. Information Criteria Results for Different Models

| Residual | Fit ^a | ΔAIC_c | ΔBIC |
|------------|--------------------------|-----------------------|---------------------|
| H_{\max} | Constant | 0.00 | 0.00 |
| | Linear | -4.52 | -2.01 |
| | Step: 10.00 | -0.92 | 1.60 |
| | Step: 10.44 | -9.84 | -4.87 |
| | Modified Logistic: 10.38 | -4.25 | 3.15 |
| | Modified Logistic: 10.00 | -3.31 | 1.67 |
| | Generalized Logistic | 10.88 | 22.97 |
| μ | Constant | 0.00 | 0.00 |
| | Linear | -3.48 | -1.33 |
| | Step: 10.00 | -1.50 | 0.64 |
| | Step: 10.44 | -9.51 | -5.28 |
| | Modified Logistic: 11.60 | -0.68 | 5.56 |
| | Modified Logistic: 10.00 | -2.00 | 2.23 |
| | Generalized Logistic | 6.12 | 16.17 |

^aIf the fit is followed by a number, the number is the location of either the best fit break (step function) or the midpoint (logistic function) in units of $\log M_{\odot}$.

Table 8. Significance of Linear and Step Function Fits

| Residual | Fit | Constant | σ_{Constant} | Slope Step | $\sigma_{\text{Slope Step}}$ | Units |
|------------|-------------|----------|----------------------------|------------|------------------------------|-------------------------------------|
| H_{\max} | Constant | 0.03 | 0.02 | | | mag |
| | Linear | 0.79 | 0.29 | -0.08 | 0.03 | $\text{mag } (\log M_{\odot})^{-1}$ |
| | Step: 10.00 | 0.07 | 0.03 | -0.07 | 0.04 | mag |
| | Step: 10.44 | 0.07 | 0.02 | -0.18 | 0.05 | mag |
| μ | Constant | 0.05 | 0.02 | | | mag |
| | Linear | 0.94 | 0.37 | -0.09 | 0.04 | $\text{mag } (\log M_{\odot})^{-1}$ |
| | Step: 10.00 | 0.11 | 0.04 | -0.10 | 0.05 | mag |
| | Step: 10.44 | 0.12 | 0.03 | -0.17 | 0.05 | mag |

Table 9. SN Sample Mean and Std Deviations - Surveys

| Residual | Pec. Vel. | Sample | SNeIa | residual | wgt residual | χ^2 | χ^2/DoF | stddev | IQR | SEM | Implied σ^{int} |
|------------------|-----------|--------------------|-------|----------|--------------|----------|---------------------|--------|-------|-------|-------------------------------|
| | | km s ⁻¹ | | mag | mag | | | mag | mag | mag | mag |
| H_{max} | 300 | All | 144 | 0.033 | 0.000 | 359.8 | 2.50 | 0.229 | 0.211 | 0.019 | 0.177 |
| | | K+ | 11 | 0.173 | 0.073 | 6.9 | 0.63 | 0.209 | 0.258 | 0.063 | ... |
| | | W18 | 18 | -0.066 | -0.133 | 133.0 | 7.39 | 0.301 | 0.219 | 0.071 | 0.288 |
| | | F15 | 56 | 0.010 | -0.022 | 128.6 | 2.30 | 0.234 | 0.232 | 0.031 | 0.180 |
| | | CSP | 47 | 0.045 | 0.014 | 69.9 | 1.49 | 0.195 | 0.214 | 0.029 | 0.131 |
| | | BN12 | 12 | 0.111 | 0.102 | 21.4 | 1.79 | 0.097 | 0.073 | 0.028 | 0.124 |
| H_{max} | 150 | All | 144 | 0.016 | 0.000 | 492.5 | 3.42 | 0.229 | 0.211 | 0.019 | 0.200 |
| | | K+ | 11 | 0.157 | 0.089 | 18.7 | 1.70 | 0.209 | 0.258 | 0.063 | 0.166 |
| | | W18 | 18 | -0.083 | -0.123 | 151.1 | 8.40 | 0.301 | 0.219 | 0.071 | 0.295 |
| | | F15 | 56 | -0.007 | -0.021 | 197.8 | 3.53 | 0.234 | 0.232 | 0.031 | 0.208 |
| | | CSP | 47 | 0.028 | 0.016 | 103.8 | 2.21 | 0.195 | 0.214 | 0.029 | 0.161 |
| | | BN12 | 12 | 0.094 | 0.089 | 20.9 | 1.74 | 0.097 | 0.073 | 0.028 | 0.117 |
| μ | 300 | All | 104 | 0.034 | 0.000 | 242.9 | 2.34 | 0.209 | 0.206 | 0.021 | 0.162 |
| | | K+ | 11 | 0.181 | 0.074 | 11.8 | 1.08 | 0.205 | 0.251 | 0.062 | 0.095 |
| | | W18 | 8 | -0.133 | -0.067 | 22.1 | 2.76 | 0.201 | 0.165 | 0.071 | 0.200 |
| | | F15 | 39 | 0.039 | -0.007 | 133.5 | 3.42 | 0.225 | 0.195 | 0.036 | 0.199 |
| | | CSP | 44 | 0.018 | -0.000 | 72.2 | 1.64 | 0.173 | 0.157 | 0.026 | 0.125 |
| | | BN12 | 2 | 0.136 | 0.134 | 3.1 | 1.57 | 0.013 | 0.010 | 0.009 | 0.114 |
| μ | 150 | All | 104 | 0.018 | 0.000 | 390.5 | 3.76 | 0.209 | 0.206 | 0.021 | 0.189 |
| | | K+ | 11 | 0.165 | 0.079 | 26.4 | 2.40 | 0.205 | 0.251 | 0.062 | 0.193 |
| | | W18 | 8 | -0.150 | -0.110 | 36.7 | 4.58 | 0.201 | 0.165 | 0.071 | 0.234 |
| | | F15 | 39 | 0.023 | 0.008 | 203.8 | 5.22 | 0.225 | 0.195 | 0.036 | 0.216 |
| | | CSP | 44 | 0.002 | -0.005 | 120.9 | 2.75 | 0.173 | 0.157 | 0.026 | 0.154 |
| | | BN12 | 2 | 0.120 | 0.118 | 2.9 | 1.45 | 0.013 | 0.010 | 0.009 | 0.104 |

^aThe K+ sample does not return an implied σ_H^{int} . σ^{int} is determined by setting χ^2/DoF equal to one and solving for the intrinsic dispersion. The K+ χ^2/DoF is less than one which would result in an imaginary intrinsic dispersion.

Table 10. Number of SNeIa for Different Sections

| Section | Type | # H_{max} | Step H_{max} | BF Step Loc H_{max} | # μ | Step μ | BF Step Loc μ |
|---------|------------|--------------------|-----------------------|------------------------------|---------|-------------------|-------------------|
| | | mag | log10 M_{\odot} | | mag | log10 M_{\odot} | |
| 4.2.3 | Original | 99 | 0.18 ± 0.05 | 10.44 | 71 | 0.17 ± 0.05 | 10.44 |
| 5.2 | No Outlier | 97 | 0.10 ± 0.04 | 10.44 | 70 | 0.17 ± 0.05 | 10.44 |
| 5.3 | Joint | 66 | 0.11 ± 0.05 | 10.44 | 66 | 0.18 ± 0.05 | 10.44 |
| 5.4 | Add Int | 99 | 0.11 ± 0.05 | 10.44 | 71 | 0.14 ± 0.05 | 10.44 |

Table 11. Optical versus H Hubble Residuals

| Sample | # SNeIa | Mean | Wgt Mean | SEM | Std. Dev. | Pearson's r |
|------------|---------|------|----------|------|-----------|---------------|
| | | mag | mag | mag | mag | |
| All | 99 | 0.03 | 0.05 | 0.02 | 0.19 | 0.63 |
| $z < 0.02$ | 51 | 0.04 | 0.05 | 0.03 | 0.19 | 0.61 |
| $z > 0.02$ | 48 | 0.02 | 0.05 | 0.03 | 0.19 | 0.60 |